

1 **Structures of three MORN repeat proteins and a re-evaluation of the**
2 **proposed lipid-binding properties of MORN repeats.**

3
4 Sara Sajko* (1), Irina Grishkovskaya* (1), Julius Kostan* (1), Melissa Graewert (2), Kim
5 Setiawan (3), Linda Trübestein (1), Korbinian Niedermüller (3), Charlotte Gehin (4), Antonio
6 Sponga (1), Martin Puchinger (1), Anne-Claude Gavin (4), Dimitri Svergun (2), Tom Leonard
7 (1), Terry K. Smith (5), Brooke Morriswood (3), Kristina Djjinovic-Carugo (1, 6)

8
9 * = equal contribution

10
11 Authors for correspondence:

12 Brooke Morriswood (brooke.morriswood@uni-wuerzburg.de)

13 Kristina Djjinovic-Carugo (kristina.djjinovic@univie.ac.at)

14
15
16 **Affiliations:**

17 ¹Department of Structural and Computational Biology, Max Perutz Labs, University of Vienna,
18 Campus Vienna Biocenter 5, A-1030 Vienna, Austria

19
20 ²European Molecular Biology Laboratory, Hamburg Unit, c/o DESY, Notkestrasse 85, 22607
21 Hamburg, Germany

22
23 ³Department of Cell and Developmental Biology, Biocenter, University of Würzburg, 97074
24 Würzburg, Germany.

25
26 ⁴European Molecular Biology Laboratory, Meyerhofstraße 1, 69117 Heidelberg, Germany.

27
28 ⁵School of Biology, BSRC, University of St. Andrews, North Haugh, St. Andrews, Fife KY16
29 9ST, UK

30
31 ⁶Department of Biochemistry, Faculty of Chemistry and Chemical Technology, University of
32 Ljubljana, Večna pot 113, SI-1000 Ljubljana, Slovenia

33
34
35
36 **Keywords:** MORN repeat, MORN1, structure, phospholipids, *Trypanosoma*, Apicomplexa.

37

38 ABSTRACT

39 MORN (membrane occupation and recognition nexus) repeat proteins have a wide taxonomic
40 distribution, being found in both prokaryotes and eukaryotes. Despite this ubiquity, they remain
41 poorly characterised at both a structural and a functional level compared to other common
42 repeat motifs such as leucine-rich repeats, armadillo repeats, WD40 repeats, and ankyrin
43 repeats. In functional terms, they are often assumed to be lipid-binding modules that mediate
44 membrane targeting, but direct evidence for this role is actually lacking. This putative activity
45 was addressed by focusing on a protein composed solely of MORN repeats - *Trypanosoma*
46 *brucei* MORN1. No evidence for binding to membranes or lipid vesicles by TbMORN1 either
47 in vivo or in vitro could be obtained. TbMORN1 did interact with individual phospholipids, but
48 it remains unclear if this was physiological or an artefact. High- and low-resolution structures
49 of the MORN1 protein from *Trypanosoma brucei* and homologous proteins from the parasites
50 *Toxoplasma gondii* and *Plasmodium falciparum* were obtained using a combination of
51 macromolecular crystallography, small-angle X-ray scattering, and electron microscopy. The
52 structures indicated that MORN repeats can mediate homotypic interactions, and can function
53 as both dimerisation and oligomerisation devices.

54

55 INTRODUCTION

56 MORN (Membrane Occupation and Recognition Nexus) repeats were first discovered in 2000,
57 following a screen for proteins present in the triad junctions of skeletal muscle (Takeshima et
58 al., 2000). The junctophilins, the protein family identified in this screen, were observed to have
59 8 repeat motifs present in their N-terminal regions. The repeats were given the name MORN
60 based on a proposed role in mediating plasma membrane association of the N-terminal
61 domain of the junctophilins. The MORN repeats were initially classified as being 14 amino
62 acids in length, with an approximate consensus sequence of YEGEWxNGKxHGYP
63 (Takeshima, Komazaki et al., 2000). A bioinformatics analysis at the time indicated that
64 assemblies of 8 consecutive MORN repeats were also present in a putative junctophilin
65 orthologue in a nematode (*Caenorhabditis elegans*), a family of plant (*Arabidopsis thaliana*)
66 lipid kinases, and a bacterial (*Cyanobacterium*) protein (Takeshima et al., 2000). Later
67 genome-era bioinformatics has shown that MORN repeat proteins are in fact found
68 ubiquitously, being present in both eukaryotes and prokaryotes (El-Gebali, Mistry et al., 2019).

69
70 The number of MORN repeat proteins in any given protein can vary greatly, from two to over
71 20, and they are found in combination with a wide range of other domains and protein repeat
72 motifs. Most published work now favours a 23-amino acid length for a single MORN repeat,
73 with the highly-conserved GxG motif at positions 12-14. A 14-amino acid length is still favoured
74 by some groups, however (Habicht, Woehle et al., 2015). Notable mammalian MORN repeat
75 proteins besides the junctophilins include ALS2/alsin, at least two radial spoke proteins
76 (RSPH10B, RSPH1/meichoacidin), the histone methyltransferase SETD7, and
77 retinophilin/MORN4 (Tsuchida, Nishina et al., 1998, Wilson, Jing et al., 2002, Otomo, Hadano
78 et al., 2003, Mecklenburg, 2007).

79
80 MORN repeats are generally assumed to be lipid-binding modules, but direct evidence for this
81 function is actually lacking. In junctophilins, there is good evidence that the N-terminal region
82 containing the MORN repeats mediates plasma membrane targeting (Takeshima et al., 2000,
83 Nakada, Kashihara et al., 2018, Rossi, Scarcella et al., 2019). It has not been demonstrated
84 whether the MORN repeats or the other sequences in the N-terminal region are responsible
85 for this however, or if this targeting is due to protein-lipid or protein-protein interactions.

86
87 Similarly, although there is good evidence that the N-terminal region (amino acids 1-452) of
88 junctophilin-2 can directly bind lipids, it has not specifically been shown that the MORN repeats
89 are responsible. Binding could potentially be mediated by other nearby sequences, especially
90 the run of over 100 amino acids that occurs between repeats 6 and 7 (Bennett, Davenport et
91 al., 2013). Work on the family of plant phosphatidylinositol(4)phosphate 5-kinases (PIPKs) that
92 contain MORN repeats has led to suggestions that the repeats might regulate the activity of
93 the kinase domain, bind to phospholipids, or mediate protein-protein interactions (Ma, Lou et
94 al., 2006, Im, Davis et al., 2007, Camacho, Smertenko et al., 2009). It therefore remains
95 unclear what role(s) this ubiquitous class of repeat motifs actually have (Mikami, Saavedra et
96 al., 2010).

97
98 Coupled to this lack of unambiguous functional data is a lack of high-resolution structural
99 information, exemplified by the ongoing lack of consensus as to whether a single repeat is 14

100 or 23 amino acids. This contrasts sharply with the considerable amount of information
101 available on other classes of protein repeat motifs such as ankyrin repeats, leucine-rich
102 repeats, or WD40 repeats (Andrade, Perez-Iratxeta et al., 2001). Until very recently, the
103 structure of the SETD7 histone methyltransferase was the sole representative of the MORN
104 repeat protein family in the protein data bank (PDB) (Jacobs, Harp et al., 2002, Wilson et al.,
105 2002, Xiao, Jing et al., 2003). Even here, the structure of the N-terminal domain containing
106 the repeats is incomplete, and the level of sequence similarity of the repeats to those of
107 junctophilins and other family members makes assignment difficult. Each repeat appears to
108 form a β -hairpin with an acidic surface, but it remains unclear if this is a general property of
109 MORN repeats. The SETD7 structure has not been analysed in this context, with more work
110 focusing on its catalytic methyltransferase domain. In 2019, and while this manuscript was in
111 preparation, Li et al. published the first high-resolution structure of a canonical MORN repeat
112 protein, specifically the MORN4/retinophilin protein in complex with its Myo3a binding partner
113 (Li, Liu et al., 2019). This structure contains four MORN repeats. More structural analysis of
114 MORN repeat proteins is still needed however, in particular for providing a structure-based
115 definition of the repeat class itself.

116

117 To address this, and additionally to tackle the question of putative lipid binding, it would
118 obviously be advantageous to utilise a protein that is composed solely of MORN repeats. In
119 this way, the contribution of other sequences or domains could be discounted. The MORN1
120 protein from the early-branching eukaryote *Trypanosoma brucei* is an ideal candidate in this
121 regard, and has the advantage of also being well-characterised at a cell biology level
122 (Morriswood, He et al., 2009, Esson, Morriswood et al., 2012, Morriswood, Havlicek et al.,
123 2013, Morriswood & Schmidt, 2015).

124

125 TbMORN1 consists of 15 consecutive 23-amino acid MORN repeats, with barely any
126 intervening sequence whatsoever (Fig. 1A). In *T. brucei*, TbMORN1 is localised to an $\sim 2 \mu\text{m}$
127 long cytoskeleton-associated complex (the hook complex) that is found just below the inner
128 leaflet of the plasma membrane. The hook complex encircles the neck of a small invagination
129 of the plasma membrane that contains the root of the cell's single flagellum (Lacomble,
130 Vaughan et al., 2009). This invagination, termed the flagellar pocket, is the sole site of endo-
131 and exocytosis in trypanosome cells and is thought to be analogous to the ciliary pocket that
132 is found at the base of some mammalian primary cilia (Grunfelder, Engstler et al., 2003,
133 Engstler, Thilo et al., 2004, Molla-Herman, Ghossoub et al., 2010).

134

135 Previous work on TbMORN1 demonstrated by fluorescence recovery after photobleaching
136 (FRAP) that it is a stable component of the hook complex, and a list of its binding partners and
137 near neighbours has been obtained using proximity-dependent biotin identification (BioID)
138 (Esson et al., 2012, Morriswood et al., 2013). In functional terms, depletion of TbMORN1 by
139 RNAi in the mammalian-infective form of the parasite resulted in a lethal phenotype
140 (Morriswood et al., 2009). Functional analysis indicated that the protein might be involved in
141 endocytosis, as well as regulating the flow of macromolecular cargo through the neck of the
142 flagellar pocket (Morriswood & Schmidt, 2015).

143

144 In this study, a detailed biochemical, structural, and functional analysis of the TbMORN1
145 protein was carried out. A truncated form missing the first MORN repeat that was best suited

146 for in vitro work was found not to bind to phospholipid vesicles under any conditions, although
147 there are indications that it might be able to associate with individual lipid molecules. In
148 addition, high-resolution crystal structures of a truncated form of the TbMORN1 protein and
149 its homologues from the parasites *Toxoplasma gondii* (TgMORN1) and *Plasmodium*
150 *falciparum* (PfMORN1) structures enabled a first structure-based definition of the MORN
151 repeat itself, and provided confirmation that MORN repeats can mediate homotypic
152 interactions - a function that may unify previous observations relating to MORN repeats.
153
154

155 RESULTS

156

157 TbMORN1 forms tail-to-tail dimers via its C-terminus

158

159 TbMORN1 is composed of 15 consecutive 23-amino acid MORN repeats, with a 5-amino acid
160 extension after the 6th repeat (Fig. 1A). An alignment of the repeats in TbMORN1 revealed
161 several highly conserved glycine residues, with a rough consensus of
162 YxGEWx₂Gx₃GxGx₃Yx₂Gx₂ (Fig. 1A, sequence logo). Bioinformatic analysis of TbMORN1
163 predicted an all- β secondary structure, with each repeat expected to form a β -hairpin (strand-
164 loop-strand) pattern (Fig. 1A).
165

165

166 To determine which TbMORN1 constructs were amenable for biochemical and structural
167 studies, limited proteolysis assays were carried out. These assays used a series of proteases
168 with different cleavage specificities (proteinase K, trypsin, and chymotrypsin) (Fig. S1A). The
169 resulting proteolytic fragments were analysed by mass spectrometry (Fig. S1B). Comparison
170 of the proteolytic fragments obtained at different dilutions suggested progressive digestion
171 occurring from the N-terminus (Fig. S1B, compare K1 and K2, T1/T2/T3). The C-terminus of
172 the molecule (repeats 13-15) seemed to be fairly stable, with no proteolytic digestion observed
173 at this end. In addition, the pattern of fragments generally suggested that the assignment of
174 repeat boundaries based on bioinformatic analysis was accurate.
175

175

176 Consequently, a panel of different truncations were cloned according to the MORN repeat
177 boundaries predicted by the alignment (Fig. 1A). These truncations were named according to
178 the number of repeats they contained - for example, TbMORN1(1-15) denotes full-length
179 protein. These truncations were expressed in bacteria and purified using a two-step protocol
180 combining affinity purification and size exclusion chromatography (Fig. S1C).
181

181

182 The oligomeric state and polydispersity of the purified proteins were investigated using size
183 exclusion chromatography coupled to multi-angle light scattering (SEC-MALS). SEC-MALS
184 analysis of TbMORN1(1-15) elution profiles suggested the formation of either aggregates or
185 higher-order assemblies (Fig. 1B). The yields of TbMORN1(1-15) were always very low,
186 making this construct not generally suitable for in vitro assays. By contrast, TbMORN1(2-15)
187 displayed a well-defined monodisperse peak in SEC-MALS, with a molecular weight
188 corresponding to a dimer (Fig. 1B). This strongly suggested that the first MORN repeat
189 mediated oligomerisation. Further successive truncations from the N-terminus (TbMORN1(7-

190 15) and TbMORN1(10-15)) also eluted as monodisperse dimers, suggesting that dimerisation
191 of TbMORN1 is mediated by the C-terminus (Fig. S1D). Consistent with this conclusion,
192 removal of the last MORN repeat in the construct TbMORN1(1-14) resulted in the elution of a
193 mixture of monomers, dimers, and higher-order structures (Fig. 1B). This demonstrated that
194 the C-terminal repeats play an important role in dimer stabilisation.

195
196 Circular dichroism (CD) measurements taken of TbMORN1(1-15), TbMORN1(2-15), and
197 TbMORN1(7-15) indicated β -strand character in all cases, with >30% antiparallel β -strand
198 content for each construct (Fig. S1E). Therefore, the secondary structure content of
199 TbMORN1 was in good agreement with a priori bioinformatic predictions (Fig. 1A).
200 Thermostability measurements of TbMORN1(1-15), TbMORN1(2-15) and TbMORN1(7-15)
201 using CD returned values in $^{\circ}\text{C}$ of 45.6 +/- 0.1, 43.5+/-0.1, and 42.2+/-0.1 respectively. The
202 relative similarity of these values indicated that there had been no significant destabilisation
203 of the protein resulting from truncation, consistent with the suggested repeat motif boundaries
204 obtained using limited proteolysis (Fig. S1B).

205
206 To map which residues were likely mediating dimerisation, cross-linking mass spectrometry
207 (XL-MS) was used to analyse TbMORN1(1-15). Two different chemical cross-linkers were
208 used: EDC (1-ethyl-3-(3-dimethylaminopropyl)carbodiimide), which has a zero-length spacer
209 arm and forms bonds between carboxyl groups and primary amines, and BS³
210 (bis(sulphosuccinimidyl)suberate), which has an 11.4 Å spacer arm and cross-links primary
211 amines. For both chemicals, most cross-links were observed to form between repeats 13, 14,
212 and 15, especially via repeat 14 (Table S1). These data were consistent with those obtained
213 by SEC-MALS (Fig. 1B, Fig. S1D), suggesting that TbMORN1 molecules in solution form tail-
214 to-tail dimers via their C-termini. It remained unclear whether the polypeptide chains in these
215 tail-to-tail dimers were in a parallel or antiparallel orientation, however.

216

217 **TbMORN1 can bind lipid side chains but not phospholipid liposomes**

218

219 As a first test of the hypothesis that MORN repeats can directly interact with phospholipids,
220 protein-lipid overlay assays were carried out using PIP strips. Purified TbMORN1(1-15) was
221 found to interact with a number of different phosphoinositide species on the PIP strips,
222 principally PI(3)P, PI(4)P, and PI(5)P, but also PI(3,4)P₂, PI(3,5)P₂, PI(4,5)P₂, and
223 phosphatidic acid (PA) (Fig. 2A). This same trend, with a stronger interaction observed with
224 monophosphate PIPs than diphosphate PIPs, has also been seen in protein-lipid overlay
225 assays using purified junctophilin-2. This might be due to a lower solubility of the
226 monophosphate PIPs, however (Bennett et al., 2013). As a positive control, the PIP strips
227 were incubated with the pleckstrin homology (PH) domain of phospholipase C delta (PLC δ).
228 Strong binding was observed to PI(4,5)P₂ only, as expected (Fig. 2B).

229

230 Of these candidates, the most intriguing was PI(4,5)P₂. It is a known endocytic effector, is
231 enriched in the flagellar pocket membrane of trypanosomes, and depletion of TbMORN1 by
232 RNAi resulted in a phenotype suggestive of an endocytosis defect (Demmel, Schmidt et al.,
233 2014, Morriswood & Schmidt, 2015). Furthermore, a PI(4)P 5-kinase, TbPIPKA, has been

234 shown to have a strongly overlapping distribution with TbMORN1 in vivo (Demmel et al.,
235 2014).

236

237 To confirm that TbMORN1 could interact with PI(4,5)P₂, fluorescence anisotropy was used as
238 a second independent and quantitative approach. In this method, the tumbling of a
239 fluorescently-labelled lipid in solution is reduced upon binding to a larger protein molecule,
240 and the change in the polarisation of the emitted light can be measured. TbMORN1(2-15)
241 showed excellent binding to BODIPY TMR-labelled PI(4,5)P₂, with a K_d of approximately 7.5
242 +/- 4.1 μM (Fig. 2C). To narrow down the PI(4,5)P₂ binding site(s) on TbMORN1, truncation
243 constructs were again used. Both TbMORN1(7-15) and TbMORN1(10-15) showed strong
244 binding to PI(4,5)P₂, with K_d values of 7.7 +/- 2.6 and 1.0 +/- 0.1 μM respectively, indicating
245 that the interaction was occurring in the C-terminal portion of TbMORN1 (Fig. 2C).

246

247 Curiously, while the anisotropy signal for TbMORN1(7-15) was lower than that of
248 TbMORN1(2-15), the highest anisotropy signal of all was obtained for TbMORN1(10-15) (Fig.
249 2C). This was surprising, as one would usually expect the largest construct containing the
250 binding site to give the highest anisotropy signal - the larger protein means less tumbling of
251 the fluorophore-conjugated lipid, resulting in greater polarisation of the emitted light and a
252 higher anisotropy signal.

253

254 As an additional test, native gel electrophoresis assays were carried out. In these assays,
255 interaction between a protein and a fluorescently-labelled lipid is detected by co-migration of
256 the lipid with the protein. Both TbMORN1(2-15) and TbMORN1(10-15) produced a band shift
257 of BODIPY TMR-labelled PI(4,5)P₂. In contrast to the PIP strip data, no band shift was seen
258 for BODIPY TMR-labelled PI(4)P (Fig. S2A, B). This too was surprising as this lipid had given
259 the strongest signal in the overlay assays (Fig. 2A). Of note, all of the assays to this point -
260 overlay assays, fluorescence anisotropy, native gel electrophoresis - had looked at the binding
261 of TbMORN1 to isolated lipids below their critical micelle concentration. This situation is
262 somewhat artificial, and so for better physiological relevance the binding of TbMORN1 to
263 phospholipid membranes was investigated using liposome pelleting assays.

264

265 The assays were carried out with liposomes of roughly 100 nm diameter, and containing 0-
266 20% PI(4,5)P₂. Varying the amount of PI(4,5)P₂ from 0-20% did not result in any increase in
267 the amount of TbMORN1(2-15) present in the pellet (P) fraction, while strong concentration-
268 dependent co-sedimentation was observed with the positive control Doc2B (Fig. 2D).
269 Quantification of the amount of protein in the pellet relative to the 0% PI(4,5)P₂ condition
270 showed that the amount of TbMORN1(2-15) was within roughly 10% of the control condition
271 at all times (Fig. 2E).

272

273 Additional assays were carried out using liposomes of differing diameters (100 and 400 nm)
274 in order to vary curvature, and different cholesterol contents (0 and 40%) in order to
275 concentrate PI(4,5)P₂ into microdomains. Neither approach produced an increase in
276 TbMORN1(2-15) association (Fig. S3A). Therefore, TbMORN1 appeared to bind to isolated
277 molecules of PI(4,5)P₂ but not to liposomes, in agreement with the fluorescence anisotropy
278 assays with isolated lipids which had suggested a binding site in the C-terminal region of
279 TbMORN1.

280

281 The TbMORN1 primary structure was next examined for putative PI(4,5)P₂-binding sites,
282 based on similarity to known PI(4,5)P₂-binding sites in the PH, PLC-δ1, CALM-N, ENTH,
283 FERM, PTB, and I3P-RBC domains (Franzot, Sjoblom et al., 2005). Two candidate sites were
284 identified in the C-terminus of TbMORN1: one in repeat 13, and one in repeat 14. The location
285 of these sites was in agreement with the fluorescence anisotropy assays, which had
286 suggested binding to the C-terminal region of TbMORN1 (Fig. 2C).

287

288 Site-directed mutagenesis was carried out on these sites in the TbMORN1(2-15)-encoding
289 construct either singly or in combination. These single or double mutants of TbMORN1(2-15)
290 were then expressed, purified, and biophysically characterised. Thermostability of the purified
291 proteins was assessed using differential scanning fluorimetry (DSF), and indicated that
292 mutagenesis of the site in repeat 14 and the double mutant both resulted in slightly decreased
293 stability (i.e. a lower T_m) than TbMORN1(2-15) (Table S2).

294

295 SEC-MALS analysis showed that while mutagenesis of the site in repeat 13 did not alter the
296 dimeric state of TbMORN1(2-15), mutagenesis of the site in repeat 14 resulted in a mixture of
297 monomers and dimers, while mutagenesis of both sites resulted in a monomeric protein (Fig.
298 S3B). This supported the conclusion from the SEC-MALS studies that the dimerisation site
299 also resides in the C-terminal segment (Fig. 1B, Fig. S1D). CD analyses indicated that the
300 constructs retained an all-β secondary structure (Fig. S3C).

301

302 Despite these changes, all three TbMORN1(2-15) mutant constructs showed unimpaired
303 binding to PI(4,5)P₂ in fluorescence anisotropy assays (Fig. S3D). Furthermore, all three
304 mutants actually had stronger binding affinities for PI(4,5)P₂ than the wild-type TbMORN1(2-
305 15) construct, with K_d values of ~ 1 μM. Although these results might indicate that
306 TbMORN1(2-15) utilises a non-canonical PI(4,5)P₂ binding site, a more parsimonious
307 explanation was that the data reflected a nonspecific interaction. Subsequent experiments
308 favoured this latter interpretation.

309

310 All fluorescence anisotropy assays had been carried out using labelled PI(4,5)P₂ with 16-
311 carbon aliphatic chains. When the assays were repeated using a version of PI(4,5)P₂ with 6-
312 carbon aliphatic chains, no binding was seen (Fig. S4A). A range of lipids (PI, PI(4)P,
313 PI(3,4)P₂, PI(3,5)P₂) with 6-carbon aliphatic chains were then tested for interaction with
314 TbMORN1(2-15) by fluorescence anisotropy, and no binding to any was seen (Fig. S4A).

315

316 Furthermore, it was observed that TbMORN1(2-15) could also bind to PI(3,4,5)P₃ - which had
317 not given a positive result in the overlay assays (Fig. 2A) - if the lipid had 16-carbon aliphatic
318 chains (Fig. S4B). This interaction with 16-carbon PI(4,5)P₂ and PI(3,4,5)P₃ was seen using
319 BODIPY-fluorescein-labelled lipids instead of BODIPY TMR-labelled ones (Fig. S4B). The
320 binding of TbMORN1(2-15) to 16-carbon versions of either PI(4,5)P₂ or PI(3,4,5)P₃ was
321 comparable to that seen for positive controls (Fig. S4C).

322

323 These results strongly suggested that the observed binding of TbMORN1(2-15) to PI(4,5)P₂
324 by both fluorescence anisotropy and native gel electrophoresis was in fact due to interaction

325 with the 16-carbon aliphatic chains and not with the lipid headgroup. An inability to interact
326 with the lipid headgroup was also consistent with the observed lack of interaction of
327 TbMORN1(2-15) with phospholipid membranes in the liposome pelleting assays (Fig. 2D,E,
328 Fig. S3A).

329

330 In conclusion, while protein overlay assays indicated that TbMORN1(1-15) and TbMORN1(2-
331 15) could interact with phospholipid species, subsequent fluorescence anisotropy and native
332 gel electrophoresis assays strongly suggested that this interaction was actually with the
333 aliphatic chains. No evidence for TbMORN1(2-15) binding to phospholipid liposomes in vitro
334 was obtained.

335

336

337 TbMORN1 co-purifies with PE but does not bind to lipid vesicles in vitro

338

339 A caveat to the previous conclusion was that the purified recombinant TbMORN1 was
340 obtained via mechanical lysis of bacterial cells in the absence of detergent (see Materials and
341 Methods). It was therefore possible that TbMORN1 was associating with bacterial lipids that
342 might be occupying the binding sites.

343

344 To test this, purified recombinant TbMORN1(1-15) and TbMORN1(10-15) were treated
345 according to a de-lipidation protocol, and the resulting supernatants were analysed by mass
346 spectrometry. Interestingly, large amounts of phosphatidylethanolamine (PE) were found to
347 have been bound to TbMORN1(1-15) (Fig. 3A). The co-purifying PE displayed a narrow
348 window of molecular moieties differing in the length of the aliphatic chain. No significant PE
349 presence was detected in supernatants obtained following de-lipidation of TbMORN1(10-15)
350 (Fig 3B). Given that TbMORN1(10-15) showed robust binding to the 16-carbon chain PI(4,5)P₂
351 (Fig. 2C), this suggested that PE was not occluding the binding site.

352

353 To remove co-purifying lipids, recombinant TbMORN1(1-15) was purified using hydrophobic
354 interaction chromatography - in this regime, almost no lipids were detected in the elutions.
355 Triton X-100 treatment was also found to efficiently remove bound lipids.

356

357 Co-purification of PE with TbMORN1(1-15) is not evidence of physiological interaction, as PE
358 is highly abundant in bacteria and carries a net neutral charge (Cronan, 2003). As such, PE
359 might simply have associated with the recombinant protein following lysis of the bacteria prior
360 to purification. To investigate this, mass spectrometry analysis of whole-cell lipids from
361 bacteria expressing recombinant TbMORN1(1-15) or TbMORN1(10-15) was carried out.
362 Curiously, bacterial cells expressing TbMORN1(1-15) showed elevated levels of PE (Fig. 3C).
363 This effect was not seen in bacterial cells expressing TbMORN1(10-15), which had
364 approximately normal levels of PE (Fig. 3D).

365

366 In summary, TbMORN1(1-15) but not TbMORN1(10-15) was found to have co-purifying PE,
367 and bacterial cells expressing TbMORN1(1-15) appeared to have elevated levels of PE. This
368 suggested that PE might be a plausible candidate for a physiological interaction partner of
369 TbMORN1.

370

371 To test the possibility of PE binding, and also to check whether the presence of co-purifying
372 PE was affecting possible PI(4,5)P₂ binding, pelleting assays using sucrose-loaded vesicles
373 (SLVs) were carried out. Sucrose loading increases the vesicle mass and enables much lower
374 centrifugation forces to be used for pelleting, thereby reducing the risk of false positives due
375 to protein aggregates pelleting independently of vesicle association. Three types of SLVs were
376 used: PE-enriched SLVs, PI(4,5)P₂-enriched SLVs, and SLVs reconstituted from purified
377 trypanosome whole-cell lipids. These were incubated with TbMORN1(2-15) purified either in
378 the absence or presence of Triton X-100, i.e. either without or with co-purifying bacterial lipids.

379

380 As expected, in the absence of Triton X-100 treatment to remove bound lipids, purified
381 recombinant TbMORN1(2-15) did not co-sediment with any of the liposome preparations (Fig.
382 4A). Even after purified recombinant TbMORN1(2-15) was treated with Triton X-100 to remove
383 bound lipids, no association with the liposomes was seen (Fig 4B). As a positive control for
384 pelleting, the PH domain of PLC γ was used. This showed robust and specific pelleting in
385 presence of PI(4,5)P₂-containing liposomes, but in no other conditions (Fig4C, arrow). At this
386 point, the candidate approach to TbMORN1 lipid binding was discontinued.

387

388 As an unbiased and high-throughput approach, TbMORN1 was next tested in a liposome
389 microarray assay (LiMA). LiMA enables sampling of a wide range of liposome compositions
390 and curvatures in a single experiment. Readout is via the detection of two fluorophores - one
391 on a carrier lipid in the liposomes, and one on the protein of interest (Saliba, Vonkova et al.,
392 2014, Saliba, Vonkova et al., 2016). Colocalised signals are regarded as positive hits. For
393 these assays EGFP-TbMORN1(2-15) was expressed and purified. The EGFP-TbMORN1(2-
394 15) protein showed no significant preference or affinity for liposomes across the whole range
395 of conditions tested (Fig. 4D,E). Each lipid was tested at three different concentrations. Of
396 note, no binding was seen to either phosphoinositide lipids or PE. In contrast, the PH domain
397 of PLC δ , which was again used as a positive control, showed a strong and specific binding to
398 PI(4,5)P₂ liposomes and, to a lesser extent, SM-enriched ones (Fig. 4F, note difference in y-
399 axis scale compared to panels D, E).

400

401 In summary, purified recombinant TbMORN1(2-15) showed no binding to liposomes under
402 any conditions assayed (Fig. 2D,E, Fig. S3A, Fig. 4A-F). TbMORN1(2-15) showed robust
403 binding to PI(4,5)P₂ and PI(3,4,5)P₃ molecules in fluorescence anisotropy assays, but only
404 when lipid reporters with 16-carbon aliphatic chains were used (Fig. 2C, Fig. S3D, Fig. S4A,
405 B). TbMORN1(1-15) was found to co-purify with PE. Taken together, these data suggest that
406 TbMORN1 requires large hydrophobic chains of the lipid for binding, which would explain the
407 negative results in the liposome-based assays.

408

409

410 TbMORN1 does not associate with membranes in vivo

411

412 At this point, the only remaining positive indicators of an interaction of TbMORN1 with lipid
413 came from the PIP strips (Fig. 2A), and the bacterial mass spectrometry data (Fig. 3A, C). The
414 latter data showed that TbMORN1(1-15) but not TbMORN1(10-15) co-purified with PE, and

415 that bacteria expressing TbMORN1(1-15) had elevated PE levels. These elevated cellular PE
416 levels might represent upregulated synthesis to compensate for something binding and
417 sequestering the lipid (Fig. 3A, C).

418

419 Notably, all these positive pieces of evidence related to TbMORN1(1-15), which was
420 polydisperse in vitro and formed large oligomers (Fig. 1B). The membrane-binding activity of
421 these polydisperse oligomers was not possible to test in vitro, as the purification yields of
422 TbMORN1(1-15) were always low. As an alternative, the possible membrane association of
423 full-length TbMORN1 protein was examined in vivo.

424

425 For these experiments, cell lines of bloodstream form *T. brucei* were generated that inducibly
426 expressed full-length TbMORN1(1-15) with an N-terminal Ty1 epitope tag. The presence of
427 the ectopic gene in the genomes of the transfected cells was confirmed by PCR analysis of
428 genomic DNA. Induction of Ty1-TbMORN1(1-15) overexpression using tetracycline (Tet)
429 produced a strong growth defect in all three *T. brucei* clones tested (Fig. 5A). A rise in the
430 number of so-called "BigEye" cells with grossly enlarged flagellar pockets was seen in the
431 same time 96-hour window (Fig. 5B). Such a phenotype had previously been seen following
432 depletion of TbMORN1 (Morriswood & Schmidt, 2015). The BigEye phenotype is thought to
433 result from perturbations to membrane traffic, especially endocytosis (Allen, Goulding et al.,
434 2003).

435

436 Immunoblotting with anti-TbMORN1 antibodies confirmed tight and inducible expression of
437 the ectopic Ty1-TbMORN1 protein (Fig. 5C, left panel). The presence of the Ty1 epitope tag
438 in the ectopic protein was confirmed by blotting with anti-Ty1 antibodies (Fig. 5C, right panel).
439 Quantification of the immunoblots indicated only around 2-fold overexpression of Ty1-
440 TbMORN1 relative to endogenous TbMORN1 protein (Fig. 5D).

441

442 These strong negative effects were unexpected, and could potentially be due either to the
443 overexpression of the MORN1 protein, or to the presence of the Ty1 tag. To check the first
444 point, cells that inducibly overexpressed untagged TbMORN1 from an ectopic locus were
445 generated. The presence of the ectopic gene in the genomes of assayed clones was
446 confirmed by PCR. Induction of ectopic gene expression by addition of tetracycline resulted in
447 overexpression of TbMORN1 in immunoblots (Fig. S5A). Quantification of overexpression
448 indicated that approximately 7 times more TbMORN1 protein was present in induced cells
449 relative to controls (Fig. S5B). Cells overexpressing untagged TbMORN1 exhibited a very
450 strong growth defect, stronger than that seen for overexpression of Ty1-TbMORN1 (Fig. S5C).
451 Therefore, TbMORN1 protein levels alone were capable of producing a negative effect on
452 growth in the absence of the Ty1 tag.

453

454 It was however not possible to obtain cells that solely expressed Ty1-TbMORN1 by
455 endogenous replacement, despite repeated attempts. This indicated that Ty1-TbMORN1
456 cannot functionally compensate for the loss of the endogenous protein.

457

458 Immunofluorescence microscopy analysis of whole cells labelled with anti-TbMORN1
459 antibodies showed that Ty1-TbMORN1-overexpressing cells displayed a whole-cell labelling
460 pattern, unlike controls (Fig. 5E, left panels). Although no sign of protein aggregation was

461 observed, this suggested that perhaps the Ty1-TbMORN1 protein might not localise correctly.
462 Immunofluorescence microscopy analysis of detergent-extracted cytoskeletons labelled using
463 anti-Ty1 antibodies confirmed that Ty1-TbMORN1 was able to target correctly, however; as
464 expected, no labelling was seen in controls. (Fig. 5E, right panels).

465

466 To confirm the immunofluorescence microscopy observations, one-step biochemical
467 fractionation using the non-ionic detergent IGEPAL was used. The detergent-soluble
468 cytoplasmic fraction (SN) was separated from the detergent-insoluble cytoskeleton pellet (P)
469 by centrifugation (Fig. 5F). In control cells, endogenous TbMORN1 associated almost entirely
470 with the cytoskeletal (P) fraction (Fig. 5G). Blotting fractions from Ty1-TbMORN1-
471 overexpressing cells with anti-TbMORN1 antibodies showed that the overexpressed Ty1-
472 TbMORN1 was mostly extracted by the detergent (Fig. 5G, arrow 1). However, a small amount
473 did associate with the cytoskeleton (P) fraction. This association was accompanied by a
474 displacement of some of the endogenous protein into the cytoplasmic SN fraction (Fig. 5G,
475 arrows 2).

476

477 Quantification of fractionation data from multiple experiments supported the qualitative
478 analysis (Fig. 5H). Summing the signals of Ty1-TbMORN1 and TbMORN1 present in the
479 cytoskeletal fraction in overexpressing cells indicated that the total amount of cytoskeleton-
480 associated protein was approximately the same as in controls (Fig 5H, grey bar). This
481 suggested that there are a finite number of Ty1-TbMORN1 molecules that can associate with
482 the cytoskeleton. As the total amount of endogenous and ectopic TbMORN1 associated with
483 the cytoskeleton is roughly the same in both overexpressing cells and controls, this suggested
484 also that the dominant negative cellular effects are primarily due to the endogenous and
485 ectopic TbMORN1 in the cytoplasmic fraction.

486

487 To determine if the cytoplasmic fraction of endogenous and ectopic TbMORN1 in the
488 overexpressing cells was membrane-associated or cytosolic, two-step fractionations were
489 carried out. These assays involved a first extraction with digitonin, then a second extraction
490 with IGEPAL. Digitonin has an affinity for cholesterol and other lipids enriched in the plasma
491 membrane, so at the right concentration it should enable the extraction of cytosol while leaving
492 organelles relatively intact (Adam, Marr et al., 1990).

493

494 To optimise the conditions for digitonin extraction, a cell line expressing cytosolic GFP as a
495 marker was used (Batram, Jones et al., 2014). These cells were extracted with varying
496 concentrations of digitonin, using 1% IGEPAL as a positive control for full extraction, and
497 fractions were separated by centrifugation (Fig. S6A). The supernatant and pellet fractions
498 were immunoblotted with antibodies against GFP and the ER luminal chaperone BiP (Fig.
499 S6B), and the results quantified (Fig. S6C). At 40 µg/ml, good extraction of GFP was obtained
500 with only minimal extraction of BiP (Fig. S6B, arrow 1). A timecourse of extraction using 40
501 µg/ml digitonin was then carried out (Fig. S6D). Increasing the incubation time over a range
502 of 15-30 min did not appear to increase the amount of GFP extraction (Fig. S6E,F). As a result,
503 a 25 min incubation time was used in the subsequent experiments.

504

505 A two-step extraction using first digitonin and then IGEPAL was then carried out (Fig. 6A). The
506 digitonin supernatant (SN1) was enriched for cytosol, while the membrane/organelle fraction

507 present in the pellet (P1) was subsequently extracted using IGEPAL and partitioned into SN2.
508 Cells expressing cytosolic GFP were spiked in alongside Ty1-TbMORN1-overexpressing cells
509 in order to use GFP as a cytosolic marker.

510

511 Analysing equal fractions by immunoblotting showed that the Ty1-TbMORN1 and TbMORN1
512 proteins not associated with the cytoskeleton were predominantly cytosolic (Fig. 6B). The GFP
513 cytosolic marker was almost wholly extracted by the digitonin, and accompanied by the
514 majority of the cytoplasmic Ty1-TbMORN1 and TbMORN1 (Fig. 6B, arrows 1).

515

516 The Ty1-TbMORN1 and TbMORN1 that were not extracted by digitonin and therefore present
517 in P1 were not strongly extracted by IGEPAL and barely present in the second supernatant
518 (SN2), while the ER marker BiP was (Fig. 6B, arrows 2). Almost all the Ty1-TbMORN1 and
519 TbMORN1 present in P1 partitioned into the second pellet, P2. Quantification of multiple
520 independent experiments using the three separate clones produced results consistent with
521 the exemplary blot shown (Fig. 6C,D). The presence of the overexpressed Ty1-TbMORN1
522 and displaced endogenous TbMORN1 in the digitonin supernatant (SN1) indicated that they
523 are predominantly cytosolic. This indicated that TbMORN1 does not associate with
524 membranes *in vivo*.

525

526 In conclusion, the extensive studies conducted on TbMORN1 here provide no evidence
527 whatsoever that its MORN repeats are able to associate with phospholipid membranes *in vivo*
528 or directly interact with phospholipid vesicles *in vitro*. TbMORN1 was able to bind to individual
529 lipid molecules, notably PE. This interaction does not appear to be mediated by lipid
530 headgroups however, and it is very hard to imagine how it would occur under physiological
531 conditions unless TbMORN1 is a carrier and not a membrane-binding protein.

532

533 If MORN repeats do not bind membranes, then this raises the question of what they really do,
534 and whether this other function might unify the various observations made about MORN
535 repeat proteins to date. ALS2 has been suggested to use its MORN repeats to form an
536 antiparallel dimer (Kunita, Otomo et al., 2004), and the evidence obtained here showed that
537 TbMORN1 molecules also formed tail-to-tail dimers via their C-termini (Figs. 1, S1).
538 Mammalian PI(4)P 5-kinases are also dimers, implying that the MORN repeats found at the
539 N-termini of the family of plant PIPKs might function to mediate homotypic interactions (Rao,
540 Misra et al., 1998). To investigate how the MORN1 dimers were being formed, high-resolution
541 structural studies were used.

542

543

544 High-resolution crystal structures of three MORN repeat proteins

545

546 Crystallisation trials were initially performed with TbMORN1(2-15) and TbMORN1(7-15).
547 Diffraction data were obtained for TbMORN1(7-15) in two different crystal forms (P2₁ and C2),
548 but attempts to solve the phase problem using experimental phasing approaches (multiple
549 isomorphous replacement, multiple anomalous scattering exploiting selenium and sulphur
550 atom signals) and molecular replacement failed due to low reproducibility of crystals,
551 anisotropy of diffraction data, and absence of sufficient homology of TbMORN1 to other

552 MORN repeat-containing proteins of known structure. At that point, the only MORN repeat-
553 containing protein for which the crystal structure was solved was SETD7, a histone
554 methyltransferase. SETD7 is predicted to contain up to 6 MORN repeats at its N-terminus, but
555 they display low sequence homology to both the MORN repeats of TbMORN1 and the
556 consensus MORN repeat sequence obtained by Pfam. This prevented successful use of
557 molecular replacement as an approach.

558
559 As a new tactic, the MORN1 proteins from the apicomplexan parasites *Plasmodium falciparum*
560 (PfMORN1) and *Toxoplasma gondii* (TgMORN1) were analysed. Despite their evolutionary
561 distance, they share high (57% and 54%, respectively) sequence identity with TbMORN1 (Fig.
562 S7A,B). CD measurements of purified recombinant protein indicated that TgMORN1,
563 TgMORN1(7-15), PfMORN1, PfMORN1(2-15) and PfMORN1(7-15) all had an overall β -
564 structure (Fig. S7C,D). This agrees with bioinformatic predictions and is consistent with the
565 data obtained for TbMORN1 (Fig. S1E).

566
567 Diffracting crystals of selenomethionine-labelled PfMORN1(7-15) were obtained and its
568 crystal structure was determined to 2.14 Å resolution using the single-wavelength anomalous
569 dispersion (SAD) method. The structures of TgMORN1(7-15) and both P2₁ and C2 crystal
570 forms of TbMORN1(7-15) were subsequently determined to 2.90, 2.35 and 2.53 Å resolution,
571 respectively, with the PfMORN1(7-15) structure used as a search model for the molecular
572 replacement (Fig. 7A-C). The structures of PfMORN1(7-15), TgMORN1(7-15), and both P2₁
573 and C2 forms of TbMORN1(7-15) were refined to an R_{work}/R_{free} of 23.0%/26.4%, 28.3%/32.2%,
574 23.2%/25.6% and 22.5%/28.2%, respectively (Table 1). TbMORN1(7-15) P2₁ (Fig. 7A), C2
575 (Fig. S8A) and TgMORN1(7-15) (Fig. 7B) crystallised with one dimer in the asymmetric unit,
576 while PfMORN1(7-15) (Fig. 7C) crystallised with one subunit in the asymmetric unit, and the
577 functional dimer was formed via crystallographic symmetry axis.

578
579 All MORN1(7-15) crystal structures showed subunit interaction via the C-terminal regions to
580 form antiparallel tail-to-tail dimers, with variable inter-subunit angles and dimerisation
581 interfaces (Fig. 7A-C, Fig. S8A). The two subunits in the TbMORN1(7-15) C2 crystal form and
582 the TgMORN1(7-15) dimer made a rather straight assembly, while in the P2₁ form they
583 displayed a bend of about 30° (Fig. S8A). The TbMORN1(7-15) and TgMORN1(7-15) dimers
584 thus appeared as rod-shaped particles. This dimer architecture is consistent with the limited
585 proteolysis data, which had indicated that the N-terminal regions of the molecule are more
586 exposed (Fig. S1A,B). Interestingly, PfMORN1(7-15) displays a V-shaped dimer with an inter-
587 subunit angle of about 45°, and incorporated a structural Zn²⁺ ion at the dimer interface (Fig.
588 7C). One crystal form of TgMORN1(7-15) also adopts the same V-shape seen for
589 PfMORN1(7-15) (Fig. S9B). Here too, a Zn²⁺ ion is also found at the dimer interface.

590
591 Superimposing the TbMORN1(7-15) P2₁ subunit with the structures of the TgMORN1(7-15)
592 and PfMORN1(7-15) subunits over 202 C α atoms yielded rmsd values of 1.0 and 1.1 Å,
593 respectively, revealing high structural similarity between the three proteins. The common
594 structural feature of all three subunits is an elongated and twisted β -sheet. The curved shape
595 of each constituent MORN repeat forms a groove laterally delimited by a rim. An individual
596 MORN1(7-15) subunit is approximately 80 Å in length and displays a longitudinal groove of
597 about 16 Å in depth (Fig. 7A).

598

599 Comparison of a single TbMORN1(7-15) subunit with known three-dimensional structures was
600 carried out using the DALI server (Holm & Rosenstrom, 2010, Holm & Laakso, 2016). This
601 revealed closest similarity with the G-box domain at the C-terminus of the human CPAP
602 protein. CPAP is a centriolar protein essential for microtubule recruitment. The G-box
603 comprises a single elongated β -sheet with all residues being solvent-exposed, and is capable
604 of forming supramolecular assemblies [PDB entry 4LZF, (Hatzopoulos, Erat et al., 2013)].
605 Despite the low sequence identity (10%) between TbMORN1(7-15) and CPAP, the Z-score
606 calculated by DALI suggested a significant similarity between the two structures (rmsd over
607 155 superimposed C_{α} atoms = 3.9 Å, Z-score = 12).

608

609 A structure-based redefinition of the MORN repeat

610

611 The crystal structures confirmed that each 23-amino acid MORN repeat is composed of a β -
612 hairpin followed by a 6-residue loop that connects to the next MORN repeat. Each β -hairpin
613 is composed of two 6-residue β -strands connected by a 5-residue loop. The MORN repeats
614 from all three crystal structures could be readily superimposed, showing a high level of
615 structural conservation (Fig. 7D). Based on this high level of conservation, a revised sequence
616 alignment of the TbMORN1 repeats was constructed that better reflects the structural
617 architecture of the protein (Fig. 7E, compare with Fig. 1A). The alignment of repeats 7-15 was
618 obtained directly from structural superpositions and used to bootstrap the alignment of the
619 upper part (repeats 1-6).

620

621 The new consensus MORN repeat sequence displays three highly-conserved features: a GxG
622 motif at the start, a conserved glycine (G) at position 10, and a YEGEW motif at positions 13-
623 17 (Fig. 7E). A slightly less conserved LxY motif is at positions 5-7. The GxG motif is at the
624 beginning of the first β -strand, while the YEGEW motif comprises most of the second β -strand.

625

626 The glycine residues at position 10 are in a β -hairpin of type I, where the most commonly-
627 observed residue at this position is a glycine (Hutchinson & Thornton, 1994). The GxG motif
628 is strictly conserved because the first G residue adopts a main chain conformation mapping
629 to the lower right corner of the Ramachandran plot, which is exclusively allowed for glycines.
630 The conformation of this glycine is stabilised via a main-chain hydrogen bond with the
631 tryptophan (W) residue of the YEGEW motif (Fig. 7F). The high conservation of the second
632 glycine residue in the GxG motif is to accommodate the highly conserved neighbouring
633 aromatic residues from the YEGEW and LxY motifs, as any larger side chain would create
634 steric clashes. The tyrosine and tryptophan side chains of the YEGEW and LxY motifs provide
635 a textbook example of aromatic stacking, filling up the groove and stabilising the tertiary
636 structure of the TbMORN1 subunit (Fig. 7F, G). The highly conserved tyrosine of the YEGEW
637 motif is sandwiched in a T-shaped π -stacking interaction between the highly conserved
638 tryptophan residue from its own motif and the tryptophan residue in the next YEGEW motif
639 (Fig. 7F). The tyrosine of the LxY motif is stabilised via hydrophobic or aromatic interactions
640 with the leucine residues in its own and the subsequent LxY motif.

641

642 Three MORN repeats of SETD7 can be aligned with TbMORN1 repeat 7 over 22-23 aligned
643 C α atoms with an rmsd of 2.3, 1.5 and 1.9 Å respectively (Fig. S8B). The first glycine residue
644 in the SETD7 MORN repeats is conserved with that in TbMORN1, while tyrosine,
645 phenylalanine, and valine replace the tryptophan of the YEGEW motif (Fig. S8C).

646

647

648 TbMORN1 displays an overall negative charge

649

650 The TbMORN1(7-15) antiparallel dimer displays a two-fold symmetry perpendicular to the
651 longitudinal axis of the assembly (Fig. 7A). Analysis of amino acid conservation derived from
652 a sequence alignment of representative MORN repeat-containing proteins showed a well
653 conserved stretch of residues in the groove (Fig. 8A). Due to the twofold symmetric nature of
654 the quaternary structure assembly, surface properties are displayed on opposite sides of the
655 elongated dimeric particle and perpetuated symmetrically along the rims (Fig. 8A-C).

656

657 Each TbMORN1 subunit displays a negative electrostatic potential. The most prominent
658 feature of each subunit is the negatively charged groove, which contributes to the highly
659 negative electrostatic potential of the dimer. This groove is flanked by a larger non-charged
660 area with a central positively-charged pocket (Fig. 8B, left-hand side, 8C middle). The
661 negatively-charged patch is formed by residues residing on loops of MORN repeats 9–13, and
662 several of them display high sequence conservation throughout the structural alignment (Fig.
663 8A,B, left-hand side).

664

665 The positive charge of the pocket closer to the dimer interface is contributed by the universally
666 conserved Lys316 residue, which is positioned on a loop connecting MORN repeats 13 and
667 14, and which is juxtaposed with Arg293 from the loop connecting MORN repeats 12 and 13.
668 The Arg293 residue is additionally involved in aromatic stacking interactions with the residues
669 Tyr278, Trp288 and Phe311, the latter forming a large surrounding non-charged area.

670

671 The rest of the subunit surface towards the N-terminus of each TbMORN1 subunit displays a
672 non-charged and partially hydrophobic character (Fig. 8C), while the opposite side of the
673 subunit displays a fairly uniform distribution of negative charges (Fig. 8B, right-hand side). The
674 overall negative charge of TbMORN1(7-15) and the lack of pronounced positive patches that
675 could serve as binding sites for negatively-charged phospholipid polar heads is in line with the
676 negative binding data.

677

678

679 TbMORN1 forms an extended antiparallel dimer

680

681 The dimer interface is built from residues in MORN repeats 12-15, which connect the two
682 subunits in an antiparallel, tail-to-tail orientation (Fig. 7A-C). The tightest overlap between the
683 two subunits occurs at the site of MORN repeats 14 and 15. In the P2₁ and C2 TbMORN1(7-
684 15) crystal forms, the dimer interfaces occupy surface areas of 747 Å² and 966 Å²,
685 respectively. Calculations of gain in solvation free energy (ΔG) upon dimer formation for
686 TbMORN1(7-15) C2 and P2₁ performed with the PDBePISA package (Krissinel & Henrick,

687 2007) yielded values of -20.1 kcal/mol and -11.3 kcal/mol, respectively, with corresponding p-
688 values of interface specificity 0.01 and 0.08. Δ^iG values lower than -10 to -15 kcal/mol and p-
689 values lower than 0.5 are significant for stable protein dimers, indicating highly specific
690 dimerisation interfaces (Krissinel & Henrick, 2007).

691

692 In both crystal forms of TbMORN1(7-15), the central core of the dimer interface is the same
693 (Fig. 9A, Fig. S9A). Due to the twofold symmetry, the majority of the stabilising interactions
694 are duplicated and build up an extended dimer interface. A series of hydrophobic and aromatic
695 π -stacking interactions between residues from repeats 14 and 15, together with hydrogen
696 bonds across the edges, stabilise the dimer (Fig. 9A, Fig. S9A).

697

698 Furthermore, the very negatively-charged C-terminal region of one TbMORN1 subunit forms
699 an arch above the positively-charged platform contributed by Lys316 and Arg293 (Fig. 8B).
700 Two residues from MORN repeat 14 - Lys325 (subunit A) and Asp326 (subunit B) - form a salt
701 bridge, which further stabilises the dimer interface.

702

703 In the C2 crystal form, the dimer is additionally stabilised by two disulphide bridges formed
704 between Cys351 at the C-terminus of repeat 15, and Cys282 from the β -hairpin loop of repeat
705 12 (Fig. S9A). In the P2₁ crystal structure, the position of the loop differs from that in the C2
706 dimer, and keeps the C $_{\alpha}$ atoms of Cys351 and Cys282 at a distance of 11.7 Å, preventing
707 disulphide bond formation. Here, the side chain of Cys351 is engaged in a polar interaction
708 with Asp303 (Fig. 9A, Fig. S9A).

709

710 A retroactive validation of the dimer interface came from the earlier PI(4,5)P₂-binding work.
711 Mutagenesis of repeat 14 had unexpectedly produced a mixture of monomers and dimers,
712 while the simultaneous mutagenesis of two candidate sites in repeats 13 and 14 had resulted
713 in a pure monomer population (Fig. S3B). Analysis of the interaction and electrostatic maps
714 of TbMORN1(7-15) and its mutagenised variants clearly showed that Arg293 and Lys316,
715 residing in repeats 13 and 14 respectively, are crucial for maintaining TbMORN1 in a stable
716 dimeric state through electrostatic interactions (Fig. 9C). Lys315 (in MORN repeat 14) does
717 not appear to be directly involved in the dimerisation interface, but could peripherally
718 contribute to the stabilisation of the C-terminal region of TbMORN1 through its electrostatic
719 potential. Residues Arg292, Lys296 (both in MORN repeat 13), and Arg321, Lys325 (both in
720 MORN repeat 14) were mapped to the outer surface of the dimer and therefore do not take
721 part in the dimerisation interface (Fig. 9A, Fig. S9A).

722

723 The transition of TbMORN1(2-15)^{Mut14} from a dimeric to a mixed monomer/dimer population is
724 therefore a direct consequence of the single point mutation K316A, whereas the complete
725 abrogation of dimerisation observed for the TbMORN1(2-15) double mutant can be attributed
726 to a synergistic effect of both R293A and K316A point mutations (Fig. S3B, Fig. 9C).

727

728

729 The V-shaped and extended dimer forms of apicomplexan MORN1 proteins

730

731 Unlike the extended dimers of TbMORN1(7-15) and TgMORN1(7-15), the V-shaped
732 PfMORN1(7-15) is mainly stabilised by a single Zn²⁺ ion incorporated into the core of its dimer

733 interface, spanning over 665 Å² (Fig. 7C, Fig 9B). One Cys306 and one Asp309 from each
734 respective subunit tetrahedrally coordinate Zn²⁺ with the expected coordination distances
735 (2.32 Å for Zn²⁺-S and 1.94 Å for Zn²⁺-O). In addition, residues from repeats 13-15 are involved
736 in stabilising the dimer via a combination of hydrophobic, polar, and electrostatic interactions
737 across the subunits.

738
739 In comparison to the TbMORN1(7-15) C2 crystal form, the extended TgMORN1(7-15)
740 structure has an approximately 1.5-times smaller dimer interface (601 Å²), which is contributed
741 solely by residues from MORN repeats 13-15 (Fig. 7B, Fig. S9C). This is closer in size to the
742 747 Å² interface of the P2₁ crystal form of TbMORN1(7-15). The final C-terminal part of the
743 protein seems to be flexible and does not engage in the stabilisation of the dimer. In
744 comparison to TbMORN1(7-15), the dimer interface of TgMORN1(7-15) is not built around
745 aromatic stacking, but instead employs hydrophobic interactions between Phe350 and
746 neighbouring small hydrophobic residues, such as Leu335 and Leu327 (Fig. S9C).

747
748 Although TgMORN1(7-15) was predominantly found as an extended dimer (Fig. 7B), a V-
749 shaped form similar to that of PfMORN1(7-15) was sporadically observed in the crystal lattice
750 (Fig. S9B). The two V-shaped dimers share the same coordination sphere of a Zn²⁺ ion, which
751 in TgMORN1(7-15) is provided by the Cys305 and Asp308 residues (Fig. S9D). The latter
752 residue in turn interacts with the Ser310 residue from the other subunit. While the salt bridge
753 and anion π -interactions are also conserved between the two V-shaped dimers, the aromatic
754 stacking present in the core of the PfMORN1(7-15) dimer interface is functionally replaced in
755 the TgMORN1(7-15) V-shaped dimer by a series of aromatic stacking interactions at its vertex.
756 Although Asp residues 303 (TbMORN1), 308 (TgMORN1) and 309 (PfMORN1) are conserved
757 in all the three proteins, the coordination of a Zn²⁺ ion clearly demands the presence of both
758 cysteine and aspartate residues. Such pairs are present in PfMORN1 and TgMORN1, but not
759 in TbMORN1, where the cysteine residue at the corresponding position is replaced by Leu301.
760 The coordination residues map to the β -hairpin of MORN repeat 13, which in TgMORN1 and
761 PfMORN1, but not TbMORN1, contains an insertion of a glutamate residue - Glu307 and
762 Glu308, respectively. Taking part in an anion π -interaction with a phenylalanine residue
763 (Phe303 and Phe304, respectively), the resulting Glu-Phe pairs effectively stabilise the
764 TgMORN1 and PfMORN1 dimers in their V-shaped form. Moreover, these very same
765 glutamate residues further stabilise the two V-shaped dimers by being involved in a salt bridge
766 with lysine residues (Lys321 in TgMORN1 and Lys322 in PfMORN1). At the equivalent
767 position in TbMORN1, Lys316 does not participate in a salt bridge, but rather points towards
768 the negative patch at the C-terminal part of the other subunit and stabilises the extended dimer
769 via electrostatic interactions.

770
771 To see whether it was possible to predict if a MORN repeat protein formed either extended or
772 V-shaped dimers, or both, a comparative sequence analysis was carried out. The sequences
773 of 15 selected MORN repeat proteins from various protist lineages were aligned with the C-
774 terminal parts of TbMORN1, TgMORN1 and PfMORN1 encompassing repeats 12-15 (Fig.
775 S10). The residues in the crystal structures of TgMORN1(7-15) and PfMORN1(7-15) forming
776 the Zn²⁺-coordination sphere and anion π -interaction were taken as a fingerprint for a V-
777 shaped dimer. All sequences of MORN repeat proteins from kinetoplastids contain a leucine
778 residue (Leu301 in the case of *T. brucei*) at the position of the coordinating Cys residue, and

779 lack the Phe-Glu either side of it forming the anion π -interaction pair - as these residues are
780 essential for V-shape dimerisation, the kinetoplastid proteins are all thus predicted to form
781 extended dimers only. Conversely, all protein sequences in the dataset from apicomplexans
782 (*Toxoplasma gondii*, *Plasmodium falciparum*, *Gregarina niphandrodes*, *Babesia microti*,
783 *Cryptosporidium parvum*, *Eimeria acervulina*, *Theileria equi*) contained these cysteine,
784 phenylalanine, and glutamate residues. This suggests that all these apicomplexan proteins -
785 probably MORN1 homologues - can adopt both extended and V-shaped forms. In addition,
786 the sequences from the alveolates *Symbiodinium microadriaticum* and *Perkinsus marinus*,
787 and the stramenopile *Aureococcus anophagefferens* also contain these three residues,
788 implying that they too might adopt both extended and V-shaped conformations.
789 Apicomplexans belong to the Alveolata clade, and both alveolates and stramenopiles are in
790 the SAR supergroup (Adl, Bass et al., 2019). This suggests that the ability to adopt two
791 conformations might have arisen within this specific clade, and possibly explains its absence
792 from the kinetoplastid sequences, as kinetoplastids are excavates.

793

794 MORN1 proteins adopt extended conformations in solution

795

796 The crystal structures were all consistent with the earlier results of the cross-linking mass
797 spectrometry experiments carried out on TbMORN1 in solution, which had indicated close
798 proximity between repeats 13-15 (Table S1). To confirm the presence of V-shaped and
799 extended dimers in solution, all three MORN1 proteins were structurally analysed using small-
800 angle X-ray scattering (SAXS). SAXS analysis of TbMORN1(7-15) and TgMORN1(7-15)
801 indicated an extended dimer in solution, and the crystal structures could be docked into the
802 calculated molecular envelopes without difficulty (Fig. 10A, B, Fig. S9E). The SAXS analysis
803 of PfMORN1(7-15) indicated an extended structure, similar to that seen for TbMORN1(7-15)
804 and TgMORN1(7-15) (Fig. 10C). This supported the prediction that TgMORN1 and PfMORN1
805 are capable of adopting two different conformations. Subsequent SAXS analysis of
806 TbMORN1(2-15) produced a molecular envelope for the almost-full-length protein, into which
807 an extrapolated version of the model of TbMORN1(7-15) could be docked (Fig. 10D, Fig. S9E).

808

809 Rotary shadowing EM on TbMORN1(2-15) produced results consistent with the SAXS
810 analysis, showing small kinked rods approximately 25 nm in length (Fig. 10E). The population
811 was homogeneous, consistent with the monodispersity of this construct observed by SLS (Fig.
812 1B). Comparison of the maximal dimer dimension (D_{\max}) for TbMORN1(2-15) obtained from
813 SAXS and EM showed a very good agreement between the two values of 250-260 Å. Rotary
814 shadowing EM was also carried out on the small amount of TbMORN1(1-15) that eluted from
815 the SEC column. Full-length TbMORN1 was far more heterogeneous than TbMORN1(2-15),
816 consistent with the polydispersity observed by SLS (Fig. 1B). In addition to single kinked rods,
817 longer filamentous assemblies of varying length were occasionally observed (Fig. 10F).
818 Rarely, much larger meshlike assemblies of full-length TbMORN1 could be observed (Fig.
819 10G), offering a tantalising clue into the higher-order assembly properties of the protein. These
820 properties will be investigated in future work.

821

822

823

824

825 DISCUSSION

826

827 MORN repeat proteins are found ubiquitously in the tree of life, but the function of MORN
828 repeats themselves has remained unclear and supported by very limited structural information
829 to date. MORN repeats were first named almost 20 years ago, in a paper identifying the
830 junctophilin protein family (Takeshima et al., 2000).

831

832 While there is abundant evidence that junctophilins associate with the plasma membrane, and
833 that the MORN repeat-containing region is likely to mediate this, there is to the authors'
834 knowledge no paper demonstrating that the junctophilin MORN repeats directly interact with
835 lipids (Takeshima et al., 2000, Munro, Jayasinghe et al., 2016, Woo, Srikanth et al., 2016,
836 Perni, Lavorato et al., 2017, Jayasinghe, Clowsley et al., 2018, Nakada et al., 2018, Rossi et
837 al., 2019). Despite this, the evidence that the MORN repeat-containing region mediates
838 plasma membrane targeting has been repeatedly cited as evidence that MORN repeats
839 directly bind lipids. MORN repeats are thus widely assumed to be lipid-binding modules,
840 despite there actually being no evidence for direct membrane binding. Warnings that the
841 function of MORN repeats has not really been elucidated, and that extant data are frequently
842 contradictory, have been largely overlooked (Mikami et al., 2010).

843

844 This study set out to provide a test of the lipid-binding hypothesis by using a protein composed
845 exclusively of MORN repeats, TbMORN1. The data provide something of a cautionary tale.

846

847 At first, the evidence obtained using overlay assays and fluorescence anisotropy indicated an
848 ability to bind specific phospholipids (Fig. 2A, C). This binding appears to be mediated
849 primarily by the aliphatic chains of the phospholipids however, as no binding was ever seen
850 in the anisotropy assays when small (6-carbon) lipids were used.

851

852 Purified recombinant TbMORN1(1-15) was at least found to co-purify with PE. Bacteria
853 expressing TbMORN1(1-15) showed elevated levels of PE, which might additionally suggest
854 that something was binding and sequestering the lipid, requiring them to upregulate synthesis
855 (Fig. 3A, C). Almost no PE was found to co-purify with TbMORN1(10-15), and none was
856 detected with the apicomplexan MORN1 proteins. This suggests that the N-terminal part of
857 TbMORN1 is a major interaction area.

858

859 It is worth noting that neither PE nor any other lipids were observed in the crystal structure of
860 TbMORN1(7-15). This might again be due to the fact that TbMORN1(7-15) does not contain
861 the N-terminal part of the molecule, or possibly because the lysine methylation step used to
862 enhance crystallisation altered its surface-exposed lysine residues, making them unavailable
863 for electrostatic interactions with lipid molecules due to the loss of positive charge. Despite
864 this evidence for binding to PE, no sign of direct binding by TbMORN1 to lipid vesicles in vitro
865 (Fig. 2D,E, Fig. 4) or in vivo (Fig. 6) could be obtained.

866

867 A remaining question then is whether this ability to bind fatty acid chains greater than 6-carbon
868 length is physiological, or an artefact. Given that TbMORN1 is a cytoskeleton-associated

869 protein, it is hard to imagine how it would be able to get access to the hydrophobic chains of
870 membrane-embedded phospholipids in vivo, although it is localised directly under the
871 cytoplasmic leaflet of the plasma membrane. The electrostatic profile of TbMORN1(7-15) is
872 also not suggestive of membrane binding, with a strong overall negative charge profile (Fig
873 8B). Consequently, a physiological interaction with phospholipid membranes seems very
874 unlikely.

875
876 It is important to note that phospholipid binding and membrane binding are two separate
877 things. Not interacting with membranes might not preclude the TbMORN1 proteins taking
878 some PE or other phospholipids out of membranes without stably interacting with the
879 membranes themselves. A similar hypothesis would be that TbMORN1 functions as a
880 carrier/transporter of lipids with aliphatic chains within a certain length, but it is difficult to
881 envisage what the corresponding physiological role would be in the context of the flagellar
882 pocket. For now, the simplest interpretation remains that there is no interaction of TbMORN1
883 with lipid membranes, and consequently no physiological interaction with membrane-
884 embedded phospholipids either.

885
886 Due to the twofold symmetry of both extended and V-shaped MORN1 dimers – the dimeric
887 particle displays the conserved groove on opposite sides of the dimer, therefore excluding this
888 region for interaction with the membranes and leaving as an option the rims lining the groove
889 (Fig. 8A-B). In the extended dimers, the two rims display a concave and a convex curvature,
890 suggestive of membrane sculpting BAR domain proteins which interact with membranes
891 mainly via non-specific electrostatic interactions (Salzer, Kostan et al., 2017, Carman &
892 Dominguez, 2018). These curved surfaces nevertheless do not display a pronounced positive
893 charge, nor the typical membrane insertion motifs characteristic for BAR domain proteins,
894 refuting thus the hypothesis for membrane binding via non-specific electrostatic interactions.
895 In conclusion, the quaternary structure architecture together with surface properties of the
896 MORN1 dimers do not support membrane binding.

897
898 There are however a small number of caveats that might still allow a lipid-binding activity to
899 be present. In vitro, the best indications for lipid binding came from the full-length protein,
900 TbMORN1(1-15). TbMORN1(1-15) gave positive result on lipid blots (Fig. 2A), co-purified with
901 PE (Fig. 3A), and its expression correlated with increased PE levels in bacteria (Fig. 3C). No
902 co-purification of PE was seen with the apicomplexan MORN1 proteins despite 57% identity
903 at an amino acid level. This lipid-binding activity therefore seems specific to TbMORN1. The
904 elevation of PE levels seen in bacteria expressing TbMORN1(1-15) is highly unusual, and the
905 authors do not currently have a good explanation for it that does not invoke lipid sequestration.
906 If the PE co-purifying with recombinant TbMORN1(1-15) was just carry-over, then the lipid
907 profile should resemble that of total bacterial cellular lipids, which is not the case. Furthermore,
908 the bound PEs display a narrow range of aliphatic chains, suggesting specificity of
909 binding/recognition.

910
911 Lipids in trypanosomes have, in general, much longer aliphatic chains than those in bacteria.
912 In *T. brucei*, PE accounts for around 10-20% of total lipid, with aliphatic chains of 36:0 being
913 the dominant isoform (Richmond, Gibellini et al., 2010). In *E. coli*, PE is the predominant
914 zwitterionic lipid and accounts for around 80% of total lipid (Epanand & Epanand, 2009). As the

915 length of the side chains in bacterial lipids is predominantly 14 and 16 carbon atoms (Pramanik
916 & Keasling, 1997), PE molecules with 16 carbon atoms chains are the most common. Notably,
917 TbMORN1(1-15) overexpressed in *E. coli* co-purified with PE species of much greater length
918 (30:0 – 36:2) (Fig. 3A), which was also reflected in increased production of these PE species
919 in overexpressing bacteria (Fig. 3C). Taken together, these data strongly suggest the
920 specificity of TbMORN1(1-15) towards PE species with aliphatic chains of a length
921 characteristic for *T. brucei*.

922

923 Similarly, *in vivo*, it remains a possibility that the cytoskeleton-associated fraction is associated
924 with the plasma membrane, potentially indirectly by binding to membrane-embedded partners.
925 in some way. The data presented here show only that TbMORN1 and Ty1-TbMORN1, when
926 not associated with cytoskeleton, are cytosolic rather than associated with the
927 membrane/organelle fraction. The cause of the negative phenotypic effects resulting from
928 overexpression of either untagged or Ty1-tagged TbMORN1 remains unclear.

929

930 As a final possibility, it might also be the case that a post-translational modification of
931 TbMORN1 is essential for lipid binding, and is either not added in bacteria or lost during
932 purification. Testing the activity of TbMORN1 expressed in a eukaryotic expression system or
933 translated *in vitro* would be means of exploring this.

934

935 These data have clear implications for other MORN repeat proteins. Junctophilins do appear
936 to bind lipids, but it is not clear if the MORN repeats are mediating this or just within the
937 region/domain involved (Bennett et al., 2013). There is again evidence for the role of the N-
938 terminal part of junctophilins mediating plasma membrane localisation, but this does not rule
939 out an indirect association via protein-protein interactions being the primary driver (Takeshima
940 et al., 2000). It now also appears that palmitoylation may play a significant role in junctophilin
941 association with the plasma membrane (Jiang, Hu et al., 2019), Another recent paper on
942 junctophilin-2 showed that upon cleavage by an endogenous protease, the N-terminal region
943 translocates to the nucleus via a nuclear localisation signal and functions there as a
944 transcription factor (Guo, Wang et al., 2018). The original paper on the junctophilin family
945 noted the nuclear localisation of some truncations of junctophilin-1, but the significance of this
946 was not appreciated at the time (Takeshima et al., 2000).

947

948 It is difficult to say whether this translocation and nuclear function is easier or harder to explain
949 if the MORN repeats in the N-terminus are dedicated lipid-binding modules. Lipid-binding is
950 known to cause conformational changes in junctophilin-2, and such conformational changes
951 in reverse may well drive the protease-mediated dissociation, but again it is not clear if these
952 changes are in any way due to the MORN repeats themselves. Additionally, it has been
953 observed that the MORN repeats of ALS2 are not required for targeting to endosomes,
954 although the exact domain mediating correct targeting is not agreed upon (Yamanaka, Vande
955 Velde et al., 2003, Kunita et al., 2004).

956

957 In summary, the presence of MORN repeats in a protein should not be taken as indicative of
958 lipid binding or lipid membrane binding without experimental evidence. Equally, evidence of
959 binding from PIP strips alone should be interpreted with caution, given that the phospholipids
960 are being presented to the protein in a non-physiological setting.

961

962 If MORN repeats are not lipid membrane modules by default, this raises the question of what
963 they might actually be doing. The structural studies presented here make a case that one
964 conserved function of MORN repeats is in homotypic interactions, and possibly also in higher-
965 order assembly.

966

967 The three high-resolution structures described in this work are amongst the first canonical
968 MORN repeat proteins to be detailed. Given that the structures are from representatives of
969 two of the five eukaryotic supergroups - the excavates, and the SAR (stramenopiles,
970 alveolates, Rhizaria) clade - this demonstrates how the fundamental structure of the MORN
971 repeat has been conserved over evolutionary time.

972

973 All three MORN1 proteins analysed here formed tail-to-tail dimers via their C-termini with the
974 polypeptide chains aligned in an antiparallel arrangement. The all- β structure of the proteins
975 produces a twisting elongated structure, with a groove lined with aromatic side chains running
976 longitudinally through it. While this manuscript was in preparation, Li et al. published a high-
977 resolution structure of the MORN4/retinophilin protein in complex with the myosin 3a tail.
978 Binding was mediated by this central groove, showing that it can be used for very high-affinity
979 protein-protein interactions (Li et al., 2019).

980

981 The three high-resolution MORN1 crystal structures were consistent with the lower-resolution
982 SAXS data obtained on the same proteins in solution (Fig. 10, Table S1). The apicomplexan
983 MORN1 proteins appear capable of forming both extended and V-shaped conformations. The
984 key residues mediating the dimer interface in the V-shaped form were defined, and shown to
985 be conserved throughout the Apicomplexa. It thus seems likely that all apicomplexan MORN1
986 proteins can adopt these two conformations.

987

988 MORN1 proteins in Apicomplexa have been shown to be a key component of the basal
989 complex, which undergoes a constriction event at the end of the cell division cycle (Gubbels,
990 Vaishnav et al., 2006, Hu, 2008). It is therefore tempting to speculate that these extended
991 and V-shaped conformations represent the pre- and post-constriction states of the MORN1
992 proteins in the basal complex. If so, this would constitute a remarkable rearrangement of the
993 molecules in the dimer, which would move through about 145° (Supplementary Video 1).

994

995 The high-resolution structures also enabled a new structure-based consensus sequence for
996 a MORN repeat to be defined (Fig. 7E). A single MORN repeat forms a β -hairpin, one of the
997 conserved building blocks of structural biology, with a long loop attached. The structural basis
998 for the conservation of individual residues within the MORN repeat has been defined (Fig. 7E,
999 F). These structures strongly argue that an individual MORN repeat is longer than the 14
1000 amino acids sometimes suggested. Despite the lower level of sequence conservation in the
1001 loop following the hairpin, a 23-amino acid length seems the most parsimonious definition from
1002 a structural perspective.

1003

1004 One interesting consequence of this redefinition of the repeat is that it suggests that full-length
1005 TbMORN1 begins with an incomplete repeat, a feature also noted in the MORN4/retinophilin

1006 structure (Li et al., 2019). The (M)IYSEGE residues at the very N-terminus are predicted to
1007 form only a single β -strand rather than a complete hairpin (Fig. 7E). Li et al. suggested that
1008 this incomplete repeat could function as a capping element, but given that the first repeat in
1009 MORN1 is critical for oligomerisation, an alternative explanation is possible: the N-terminus of
1010 a second TbMORN1 molecule (itself encoding a single β -strand) could complete this hairpin
1011 through intermolecular interactions. Oligomerisation would thus be driven by a "split-MORN"
1012 mechanism where a complete hairpin is formed by the interaction of the N-termini of two
1013 proteins. Further work will be needed to test this hypothesis. The concluding data presented
1014 here suggest that TbMORN1 utilises this oligomerisation capacity to build mesh-like
1015 assemblies, which can reach considerable size in vitro (Fig. 10G). The biophysical properties
1016 of these meshworks, in particular their tensile strength, are likely to be another fruitful avenue
1017 of investigation.

1018
1019
1020

1021 MATERIALS AND METHODS:

1022

1023 **Antibodies and other reagents**

1024 All custom antibodies have been described previously. The rabbit anti-TbMORN1 were made
1025 for a previous project (Morriswood et al., 2013). The mouse monoclonal anti-Ty1 (BB2)
1026 antibodies were a gift from Cynthia He (University of Singapore) (Bastin, Bagherzadeh et al.,
1027 1996). The mouse monoclonal anti-PFR1,2 antibodies (L13D6) were a gift from Keith Gull
1028 (University of Oxford) (Kohl, Sherwin et al., 1999). The anti-BiP antibodies were a gift from Jay
1029 Bangs (University at Buffalo) (Bangs, Uyetake et al., 1993). The rabbit anti-GFP antibodies
1030 were a gift from Graham Warren (MRC Laboratory for Molecular Cell Biology) (Pelletier, Stern
1031 et al., 2002). The following antibodies were obtained from commercial sources: anti-strep tag
1032 StrepMAB-Classic (iba), HRP-conjugated anti-mouse (ThermoFisher Scientific), anti-GST
1033 (Santa Cruz Biotechnology). Defatted BSA was purchased from Sigma-Aldrich.

1034

1035

1036 **Cloning and mutagenesis of expression constructs**

1037 The 1077 bp TbMORN1 open reading frame (ORF) (UniProt accession no. Q587D3;
1038 TriTrypDB database accession no. Tb927.6.4670) was amplified by PCR from genomic DNA
1039 obtained from *Trypanosoma brucei brucei* strain Lister 427 and ligated into vector pETM-13
1040 encoding a Strep-tag at the 3' end of the insert. TbMORN1 truncations were generated using
1041 this construct as a template by ligase-independent cloning (Doyle, 2005). The sequences for
1042 TbMORN1(2-15) and TbMORN1(1-14) were additionally ligated into the pCoofy12 vector
1043 encoding a 3C protease-cleavable N-terminal Twin-Strep-tag (Scholz, Besir et al., 2013) by
1044 sequence and ligation-independent cloning (Li & Elledge, 2012). Mutagenesis constructs were
1045 generated by standard methods using the pre-existing pCoofy12_TbMORN1(2-15) construct
1046 as the template (Hemsley, Arnheim et al., 1989). All primer sequences are available upon
1047 request. For LiMA experiments, the construct encoding the EGFP-TbMORN1(2-15) was
1048 cloned in a two-step procedure by sequence and ligation-independent cloning followed by
1049 Gibson assembly using pCoofy12_TbMORN1(2-15) and the pEGFP-C1 vector (Gibson,

1050 Young et al., 2009). The 1092 bp TgMORN1 (UniProt accession no. Q3S2E8) and 1095 bp
1051 PfMORN1 (UniProt accession no. Q8IJ93) ORFs were amplified by PCR from genomic DNA.
1052 Truncations of the TgMORN1 and PfMORN1 constructs were generated using ligase-
1053 independent cloning. The TgMORN1 constructs were additionally ligated into the pET14
1054 vector encoding a 3C protease-cleavable N-terminal His10-tag. The PfMORN1 constructs
1055 were additionally ligated into the pCoofy32 encoding a 3C protease-cleavable N-terminal
1056 His10-tag and C-terminal OneStrep-tag.

1057

1058

1059 **Recombinant protein expression and purification**

1060 Rosetta 2 (DE3)pLysS bacterial cells transformed with the required expression plasmids were
1061 grown at 37 °C with shaking in the presence of the appropriate antibiotics. Large scale
1062 expression was carried out either in Luria-Broth or in auto-induction (ZY) medium (Studier,
1063 2005), with 500 ml media being inoculated with 3-5 ml of pre-cultured cells. Cells in Luria-
1064 Broth were grown to an OD₆₀₀ ~ 0.8 – 1.0, after which 50 µM IPTG was added to induce
1065 recombinant protein expression. The cells were then incubated at lower temperature
1066 (overnight, 20 °C). The cells were then harvested by centrifugation (5000 x g, 30 min), and
1067 either lysed immediately or stored at -80 °C. For purification, the cells were resuspended in
1068 lysis buffer (50 mM Tris-HCl pH 8.5, 200 mM NaCl, 5% (w/v) glycerol, 1 mM DTT, protease
1069 inhibitor cocktail, benzonase). The pellet emulsions were first homogenised by mixing on ice
1070 using a T 10 basic Ultra-Turrax dispersing instrument (IKA), and lysis was accomplished using
1071 a single cycle in a cell disruptor (Constant systems Ltd), with the pressure set to 1.35 kPa.
1072 Lysates were clarified by centrifugation (18,000 x g, 45 min, 4 °C), and a two-step fast protein
1073 liquid chromatography (FPLC) purification protocol using an ÄKTA Protein Purification System
1074 (GE Healthcare Life Sciences) at 8 °C was then followed to obtain the recombinant protein.
1075 The supernatants were applied to two connected Strep-Trap HP 5 ml columns packed with
1076 Strep-Tactin ligand immobilized in an agarose matrix (GE Healthcare Life Sciences) (GE
1077 Healthcare Life Sciences) previously equilibrated with equilibration buffer (50 mM Tris-HCl pH
1078 8.5, 200 mM NaCl, 2% (w/v) glycerol, 1 mM DTT). Flow speed was adjusted to 2.5 ml/min.
1079 When 100% step gradient of elution buffer (equilibration buffer plus 2.5 mM D-desthiobiotin)
1080 was applied, the bound proteins were eluted in a single chromatographic peak. Selected peak
1081 fractions were examined by SDS-PAGE for protein content and purity, pooled accordingly,
1082 and concentrated in Amicon Ultra centrifugal filter units (MerckMillipore, various pore sizes)
1083 according to the manufacturer's instructions. These affinity-purified protein concentrates were
1084 then applied to a previously equilibrated HiLoad 16/600 Superdex 200 pg column (GE
1085 Healthcare Life Sciences) packed with dextran covalently bound to highly cross-linked
1086 agarose, enabling separation of proteins with MW in the range of 10 – 600 kDa. Flow speed
1087 was adjusted to 1 ml/min and fractions of 1.5 ml were collected. Fractions corresponding to
1088 the targeted chromatographic peak were examined for protein content by SDS-PAGE, pooled
1089 accordingly to their purity, concentrated, and stored at -80 °C until use.

1090

1091

1092 **Limited proteolysis**

1093 Purified recombinant His-TbMORN1(1-15) at 1 mg/ml was separately incubated with three
1094 proteases (α -chymotrypsin, trypsin, and proteinase K) in 20 mM Tris-HCl pH 8.5, 200 mM
1095 NaCl, 2% glycerol, 0.2 mM CaCl₂ (15 min, RT). The proteases were used at dilutions of 1:100

1096 - 1:2000. The reactions were stopped by the addition of SDS-Coomassie sample loading
1097 buffer for analysis by gel electrophoresis. The indicated protein bands were extracted from the
1098 gel and subjected to mass spectrometry analysis.

1099

1100

1101 **Size-exclusion chromatography coupled to multi-angle light scattering (SEC MALS)**

1102 The MW and oligomeric state of purified proteins were verified by size exclusion
1103 chromatography (SEC) coupled to multi-angle light scattering (MALS), using a Superdex 200
1104 Increase 10/300 GL column (GE Healthcare Life Sciences). Up to five protein samples of 100
1105 μl were dialysed against 2x 1 L of freshly-prepared, degassed gel filtration buffer (20 mM Tris-
1106 HCl pH 8.5, 200 mM NaCl, 2% (w/v) glycerol, 0.5 mM DTT) (overnight, 4 °C). Gel filtration
1107 buffer was also used for overnight equilibration of the column and in the subsequent
1108 measurements. Protein samples were clarified by centrifugation using a TLA-55 rotor in an
1109 Optima MAX-XP table top ultracentrifuge (Beckman Coulter) (90,720 x g, 30 min, 4 °C). 100
1110 μl of 2 – 4 mg/ml protein samples were applied to a column using the 1260 Infinity HPLC
1111 system (Agilent Technologies) coupled to a MiniDawn Treos detector (Wyatt Technologies)
1112 with a laser emitting at 690 nm. An RI-101 detector (Shodex) was used for refractive index
1113 determination and the Astra 7 software package (Wyatt Technologies) for data analysis. No
1114 correction of refractive index was necessary due to the 2% (w/v) glycerol content in the buffer.

1115

1116

1117 **Circular dichroism (CD)**

1118 Far-UV CD was used both for measurement of secondary structure and for validation of the
1119 thermostability of TbMORN1 constructs. To avoid the absorption of Tris and NaCl below 180
1120 nm (Kelly, Jess et al., 2005), three protein samples of 100 μl were first dialysed against 2x 1
1121 L of dialysis buffer (20 mM NaH_2PO_4 , 20 mM Na_2HPO_4 , 200 mM NaF) (overnight, 4 °C). The
1122 pH 8.0 was adjusted by mixing the mono- and dibasic sodium phosphate solutions. The
1123 dialysed proteins were clarified by centrifugation in an Optima MAX-XP tabletop
1124 ultracentrifuge (Beckman Coulter Life Sciences) (90,720 x g, 30 min, 4 °C). The concentration
1125 of protein samples was adjusted to 0.25 mg/ml. CD measurements were carried out in a quartz
1126 cuvette with an optical path length of 0.5 mm (Stana Scientific Ltd) using a Chirascan Plus
1127 spectrophotometer (Applied Photophysics) equipped with the Chirascan-plus DMS software
1128 package. The CD profiles for secondary structure calculations were obtained at RT in the
1129 range of 190 – 260 nm. Further analysis was carried out using the BeStSel server, which is
1130 specialised in the analysis of CD data from proteins rich in β -strands (Micsonai, Wien et al.,
1131 2015, Micsonai, Wien et al., 2018). Data were converted to $\Delta\epsilon$ ($\text{M}^{-1}\text{cm}^{-1}$) and uploaded to the
1132 BeStSel online server. Melting experiments were performed in the range of 190 – 260 nm, 20
1133 – 80 °C, with a temperature ramp of 0.8 °C/min. Data were analysed with Global 3 software
1134 package.

1135

1136

1137 **Chemical cross-linking coupled to mass spectrometry (XL-MS)**

1138 For chemical cross-linking with EDC (1-ethyl-3-(3-dimethylaminopropyl)carbodiimide
1139 hydrochloride) or BS³ (bis(sulfosuccinimidyl)suberate), 200-300 μl of approximately 30 μM
1140 TbMORN1 sample was dialysed twice against 1 L of EDC buffer (20 mM MES-NaOH pH 6.8,
1141 200 mM NaCl) or BS³ buffer (20 mM HEPES-NaOH pH 8.0, 200 mM NaCl) (overnight, 4 °C).

1142 Following dialysis, the protein was clarified by centrifugation (90,720 x g, 30 min, 4 °C) using
1143 a TLA-55 rotor in an Optima MAX-XP tabletop ultracentrifuge (Beckman Coulter Life
1144 Sciences). EDC (ThermoFischer Scientific) was first equilibrated to RT and then a stock
1145 solution in EDC buffer was prepared. 1.3 μM TbMORN1 previously dialysed in EDC buffer
1146 was mixed with 0, 200, and 400 μM EDC (all final concentrations) in a total volume of 40 μl .
1147 After a 30 min incubation at RT, 10 μl of SDS loading buffer was added and the mixtures were
1148 further denatured by heating (95 °C, 10 min). The experiments with BS³ were carried out
1149 identically except that BS³ buffer and 3.4 μM TbMORN1 were used, and the incubation time
1150 was 120 min. Samples were separated by SDS-PAGE, stained with Coomassie dye, and
1151 selected bands corresponding to monomers and dimers cross-linked with 400 μM cross-linker
1152 were excised and subjected to enzymatic digestion and subsequent mass spectrometry
1153 analysis. Coomassie Brilliant Blue-stained excised bands were destained with a mixture of
1154 acetonitrile and 50 mM ammonium bicarbonate (ambic), in two consecutive steps (each 10
1155 min, RT). The proteins were reduced using 10 mM DTT in 50 mM ambic for (30 min, 56 °C),
1156 alkylated with 50 mM iodoacetamide in 30 mM ambic in the dark (30 min, RT), and digested
1157 with trypsin (Promega, mass spectroscopy grade) (overnight, 37 °C). The reaction was
1158 stopped using 10% (v/v) formic acid and extracted peptides were desalted using C18
1159 Stagetips (Rappsilber, Mann et al., 2007). Peptides were analysed on an UltiMate 3000 HPLC
1160 RSLCnano system coupled to a Q Exactive HF mass spectrometer, equipped with a
1161 Nanospray Flex ion source (all Thermo Fisher Scientific). Peptides were loaded onto a trap
1162 PepMap 300 C18 column of dimensions 5 mm x 300 μm i.d., packed with 5 μm particles with
1163 a pore size of 100 Å (Thermo Fisher Scientific, cat. no. 164718) and separated on an analytical
1164 C18 100 column of dimensions 500 mm x 75 μm i.d., packed with 2 μm particles with a pore
1165 size of 100 Å (Thermo Fisher Scientific, cat. no. 164942), applying a linear gradient from 2%
1166 to 40% solvent B (80% acetonitrile, 0.1% formic acid) at a flow rate of 230 nl/min over 120
1167 min. The mass spectrometer was operated in a data-dependent mode at high resolution of
1168 both MS1 and MS2 level. Peptides with a charge of +1, +2 or of a higher than +7, were
1169 excluded from fragmentation. To identify cross-linked peptides, the spectra were searched
1170 using pLink software v1.23 (Yang, Wu et al., 2012). Q Exactive HF raw-files were pre-
1171 processed and converted to mgf-files using pParse (Yuan, Liu et al., 2012). The MaxQuant
1172 database (Tyanova, Temu et al., 2016) was used to search the spectra for the most abundant
1173 protein hits. Carbamidomethylation of cysteine and oxidation of methionine residues were set
1174 as variable modifications. Trypsin was set as an enzyme specificity, and EDC or BS³ was set
1175 as a cross-linking chemistry. In case of EDC, aspartic and glutamic acid residues, as well as
1176 C-termini of proteins, were allowed to be linked with lysine residues. In the case of BS³, lysine
1177 residues and N-termini of proteins were allowed to be linked with lysine residues, N-termini of
1178 proteins, as well as to serine, threonine and tyrosine residues. Search results were filtered for
1179 1% FDR (false discovery rate) on the PSM (number of peptide-spectrum matches) level and
1180 a maximum allowed precursor mass deviation of 5 ppm. To remove low quality PSMs, an
1181 additional e-Value cutoff of < 0.001 was applied. In order to distinguish intra- from inter-
1182 molecular chemical cross-links, results from monomers and dimers were compared. A
1183 potential inter-molecular cross-link must have shown the following criteria: (1) minimally 3
1184 peptide PSMs in dimer and (2) minimally 3-times more PSMs in dimer than in monomer.

1185

1186

1187 **Protein-lipid overlay assays (PIP strips)**

1188 PIP strips were purchased from Echelon Biosciences (cat. no. P-6001). PBS-T (PBS, 0.1%
1189 TWEEN-20) was used as a general buffer. Purified recombinant TbMORN1(1-15) was clarified
1190 by centrifugation (20,817 x g, 20 min, 4 °C) prior to use. The PIP strips were blocked using
1191 blocking buffer (3% (w/v) defatted BSA, PBS-T) (60 min, RT) and then incubated with 5 µg/ml
1192 of TbMORN1 in 10 ml of blocking solution (60 min, RT). After three washes with PBS-T, the
1193 membranes were overlaid with anti-strep antibodies diluted in blocking solution (60 min, RT).
1194 After a further three PBS-T washes, the membranes were overlaid with HRP-conjugated
1195 secondary antibodies (60 min, RT). The membranes were then washed three times with PBS-
1196 T and visualised by ECL (Western Blotting substrate, Thermo Fisher) using a Fusion FX
1197 imager (Vilber Lourmat). All binding and wash steps were carried out with gentle agitation of
1198 the membranes. For the positive control, the PIP strip was overlaid with GST-tagged PLC-δ1
1199 PH domain (Echelon Biosciences) and mouse monoclonal anti-GST antibodies (Santa Cruz
1200 Biotechnology) were used.

1201

1202

1203 **Fluorescence anisotropy**

1204 Stocks of BODIPY TMR-labelled PI C6, PI(4)P C6, PI(3,4)P₂ C6, PI(3,5)P₂ C6, PI(4,5)P₂ C6
1205 and PI(4,5)P₂ C16 were sonicated (5 min, RT) in a sonication bath, and in parallel with purified
1206 recombinant TbMORN1(2-15), TbMORN1(7-15), TbMORN1(10-15), were clarified by
1207 centrifugation (20,817 x g, 20 min, 4 °C). The concentrations of lipid stocks were determined
1208 with a Hitachi U-3501 UV-VIS spectrophotometer, using quartz absorbance cuvettes and an
1209 optical path length of 10 mm (Hellma Analytics). For this purpose, the maximum absorbance
1210 of BODIPY TMR dye at λ = 544 nm was measured; its extinction coefficient ε = 60,000 cm⁻¹
1211 M⁻¹. The total volume of each respective sample was 110 µl. The concentration of selected
1212 TbMORN1 constructs was varied from 0 to 35 µM (or more), while the concentration of added
1213 lipid was kept constant at 0.1 µM. Measurements were performed on a Perkin Elmer LS50B
1214 fluorimeter in quartz cuvettes with an optical path length of 10 x 2 mm (Hellma Analytics). To
1215 ensure a constant temperature of 20 °C in the measured sample, the measurement cell was
1216 connected to a water bath. The parameters for fluorescence anisotropy (r) measurements
1217 were: λ_{ex} = 544 nm and aperture of excitation slit = 15 nm; λ_{em} = 574 nm and aperture of
1218 emission wavelength = 20 nm; time of integration = 1 s and T = 20 °C. The grating factor (G
1219 factor), which provides grating correction for the optical system, was determined on samples
1220 with exclusively 0.1 µM lipid and kept constant during measurement of each concentration
1221 series. Triplicates of each protein concentration point were measured and afterwards
1222 averaged using Excel software. Graphs were drawn and fitted in SigmaPlot ver. 13.0. The
1223 equation used for fitting was a four parameters logistic curve where:

1224

$$1225 \quad y = \min + \frac{(\max - \min)}{1 + \left(\frac{x}{EC50}\right)^{-Hillslope}},$$

1226

1227 Options were set to default; initial parameters values, as well as parameters min, max, EC50,
1228 Hillslope, were selected automatically, parameter constraints were max > min and EC50 > 0,
1229 number of iterations was 200, and tolerance was kept at 1e⁻¹⁰. The reduced chi-square method
1230 was used to compute parameters' standard errors. Experimental r values of respective 0.1 µM
1231 BODIPY TMR-lipid and protein-TMR BODIPY-lipid mixtures were compared with theoretical
1232 values obtained by Perrin equation.

1233

1234

1235 **Mass spectrometry analysis of extracted lipids**

1236 Lipid extractions from purified recombinant full length and truncated TbMORN1 were achieved
1237 by three successive vigorous extractions with ethanol (90% v/v) according to a published
1238 protocol (Fyffe, Alphey et al., 2006). The pooled extracts were dried using N₂ gas in a glass
1239 vial and re-extracted using a modified Bligh and Dyer method (Richmond et al., 2010). For
1240 whole *E. coli* lipid extracts, cells were washed with PBS and extracted following the modified
1241 Bligh and Dyer method. All extracts were dried under N₂ gas in glass vials and stored at 4 °C.
1242 Extracts were dissolved in 15 µl of chloroform:methanol (1:2) and 15 µl of acetonitrile:propan-
1243 2-ol:water (6:7:2) and analysed with an Absceix 4000 QTrap, a triple quadrupole mass
1244 spectrometer equipped with a nano-electrospray source. Samples were delivered using a
1245 Nanomate interface in direct infusion mode (~125 nl/min). Lipid extracts were analysed in
1246 both positive and negative ion modes using a capillary voltage of 1.25 kV. MS/MS scanning
1247 (daughter, precursor and neutral loss scans) were performed using nitrogen as the collision
1248 gas with collision energies between 35-90 V, allowing lipid structure assignments.

1249

1250

1251 **Preparation of sucrose-loaded vesicles (SLVs) and pelleting assay**

1252 To generate synthetic SLVs, lipids reconstituted in CHCl₃ were mixed in the following ratio:
1253 30% DOPC; 35% DOPE; 15% DOPS; 20% cholesterol. 5 mol % PI(4,5)P₂ was added in place
1254 of 5 mol% DOPE in the PI(4,5)P₂-containing liposomes. Lipids were extracted from
1255 bloodstream from *T. brucei* according to an established protocol (Bligh & Dyer, 1959). Briefly,
1256 mid-log phase cells were harvested by centrifugation (750 x g, 10 min, RT), washed once with
1257 PBS, then resuspended in 100 µl PBS and transferred to a glass tube. 375 µl of 1:2 (v/v)
1258 CHCl₃:MeOH was added and the mixture was vortexed (20 s) and then incubated with
1259 continuous agitation (15 min, RT). A further 125 µl CHCl₃ was then added to make the mixture
1260 biphasic, and following brief vortexing 125 µl ddH₂O was added. The mixture was vortexed
1261 again and then separated by centrifugation (1000 x g, 5 min, RT). The lower organic layer was
1262 then transferred to a new glass vial, dried under a nitrogen stream, and kept at 4 °C until use.
1263 For the preparation of SLVs from trypanosomal lipids the lyophilized lipids (extract from 8x10⁷
1264 cell equivalents) were reconstituted in 50 µl CHCl₃. 6 µM Rhodamine B dihexadecanoyl
1265 phosphoethanolamine (Rh-DHPE) was added to all lipid mixtures to facilitate the visualisation
1266 of the SLVs. The lipid mixtures were dried under a nitrogen stream, and the lipid films hydrated
1267 in 20 mM HEPES pH 7.4, 0.3 M sucrose. The lipid mixtures were subjected to 4 cycles of
1268 freezing in liquid nitrogen followed by thawing in a sonicating water bath at RT. The vesicles
1269 were pelleted by centrifugation (250,000 x g, 30 min, RT) and resuspended in 20 mM HEPES
1270 pH 7.4, 100 mM KCl to a total lipid concentration of 1 mM. SLVs were incubated with 1.5 µM
1271 purified TbMORN1(2-15) at a 1:1 ratio (30 min, RT). To separate soluble and SLV-bound
1272 TbMORN1(2-15), the vesicles were pelleted by centrifugation (8,700 x g, 30 min, RT), and
1273 equal volumes of supernatant and resuspended pellet were separated by SDS-PAGE and
1274 analysed by Coomassie staining.

1275

1276

1277 **Liposome microarray assay (LiMA)**

1278 LiMA (Saliba et al., 2014) was performed in the lab of Anne-Claude Gavin (EMBL Heidelberg,
1279 Germany) according to the standard protocol (Saliba et al., 2016). TbMORN1(2-15) tagged N-
1280 terminally with EGFP and two positive controls, PLC δ 1-PH and Lactadherin-C2, both fused to
1281 superfolder GFP (sfGFP), were applied to microarrays printed with different signalling lipids.
1282 In brief, lipids of interest were combined with the carrier lipid DOPC, PEGylated PE, and PE
1283 labelled with Atto 647 dye (PE-Atto 647, 0.1 mol%). Lipid mixtures containing 2, 5, and 10
1284 mol% of the signalling lipid were spotted onto a thin agarose layer (TAL). The agarose layers
1285 were hydrated using buffer A (20 mM Tris-HCl pH 8.5, 200 mM NaCl) and vesicles formed
1286 spontaneously. Efficiency of liposome formation was verified by fluorescence microscopy. The
1287 protein was diluted to 7 μ M in buffer A and 40 μ l was applied to each array. Microarrays were
1288 incubated (20 min, RT) and subsequently washed three times with 40 μ l of buffer A. Chips
1289 were analysed by automated fluorescence microscopy. Positions of liposomes were
1290 determined by tracking the fluorescence of PE-Atto 647 and images were taken for 3 ms and
1291 5 ms exposure times. In parallel, the fluorescence of EGFP was determined for 1, 5, 10, 30,
1292 75, 100, 200 and 300 ms exposures. Images were processed using CellProfiler and
1293 CPAnalyst. Only EGFP signals that overlapped with Atto 647 signals were taken into account.
1294 Normalised binding intensity (NBI) was calculated as the ratio between EGFP and Atto 647
1295 fluorescence, normalised by exposure time. Three microarrays were examined, carrying
1296 liposomes with the following signalling lipids; PIP-chip: DOPA, DOPE, DOPI, DOPS, DODAG,
1297 cardiolipin, BMP, DOPI(4,5)P₂, DOPG; GLP-chip: ceramide C16, ceramide(1)P C16,
1298 ceramide(1)P C18, S(1)P, S, SM, DOPI(4,5)P₂, DOPS; SL-chip: DOPI(3)P, brain PI(4)P,
1299 DOPI(5)P, DOPI(3,4)P₂, DOPI(3,5)P₂, brain PI(4,5)P₂, DOPI(3,4,5)P₃, DOPS and cholesterol.
1300 Each microarray was performed in triplicate.

1301

1302

1303 **Cell culture and cell line generation**

1304 Bloodstream form *T. brucei* cells were maintained in HMI-9 media supplemented with 10%
1305 foetal bovine serum (Sigma-Aldrich, St. Louis, USA) at 37 °C and 5% CO₂ in cell culture flasks
1306 with filter lids (Greiner). For overexpression studies, 427 strain "single marker" cells - which
1307 express T7 RNA polymerase and the Tetracycline repressor protein, both maintained under
1308 2.5 μ g/ml G418 selection - were used (Wirtz, Leal et al., 1999). For optimisation of digitonin
1309 extraction conditions, the GFP^{ESPro}-221^{ES}.121^{tet} cell line, which constitutively expresses GFP
1310 from the VSG expression site, was used (Batram et al., 2014). Constructs for overexpression
1311 of Ty1-tagged TbMORN1 and untagged TbMORN1 were obtained by cloning the required
1312 ORFs into the pLEW100v5-HYG plasmid; the identity of the inserts was verified by DNA
1313 sequencing followed by BLAST analysis against the TbMORN1 ORF (Tb927.6.4670). The
1314 plasmids were linearised by NotI digestion, and plasmid DNA was purified by ethanol
1315 precipitation. Linearisation was verified using agarose gel electrophoresis. Stable cell lines
1316 were generated by using 20 μ g of the linearised plasmids to transfect $\sim 3 \times 10^7$ "single marker"
1317 cells in transfection buffer (90 mM Na₂PO₄, 5 mM KCl, 0.15 mM CaCl₂, 50 mM HEPES pH
1318 7.3) using the X-001 program of an Amaxa Nucleofector II (Lonza, Switzerland) ((Burkard,
1319 Fragoso et al., 2007, Schumann Burkard, Jutzi et al., 2011). Clones were obtained from the
1320 transfected cells by limiting dilution under 5 μ g/ml hygromycin selection. Clones were verified
1321 as described in the manuscript text.

1322

1323

1324 **Growth curves and BigEye cell counts**

1325 22 ml cells at a defined starting concentration were divided into two flasks of 10 ml each, and
1326 overexpression of the ectopic transgene was initiated in one flask by the addition of
1327 tetracycline to a final concentration of 1 µg/ml. For overexpression of Ty1-TbMORN1, a
1328 starting concentration of 1×10^4 cells/ml was used, and the cells were split and reseeded at this
1329 concentration after 48 h. For overexpression of untagged TbMORN1, a starting concentration
1330 of 1×10^3 cells/ml was used with no reseeded. Tetracycline was refreshed every 24 h in both
1331 cases. Population density was measured using a Z2 Coulter Counter (Beckman Coulter,
1332 Krefeld, Germany) at the indicated timepoints. For quantification of BigEye cell incidence at
1333 the indicated timepoints, the cultures were briefly agitated to mix the cells, which were then
1334 allowed to settle for 30 min. The culture flasks were then examined directly using an inverted
1335 phase contrast microscope (Leitz Labovert) and a 10x objective lens. Three fields of view were
1336 chosen at random for each flask and the number of normal and BigEye cells manually
1337 quantified, using higher magnification where necessary. Given the low magnification used, the
1338 numbers presented are likely to be underestimates of the true incidence.

1339

1340

1341 **Immunoblotting**

1342 To obtain whole cell lysates, cell concentration was measured using a Z2 Coulter Counter,
1343 and a defined volume was then transferred to 15 ml Falcon tubes. The cells were pelleted by
1344 centrifugation (750 x g, 10 min, RT), resuspended in 1 ml PBS, and transferred to microfuge
1345 tubes. The cells were again pelleted (1800 x g, 2 min, RT), and the cell pellet then directly
1346 resuspended in SDS loading buffer to a final concentration of 2×10^5 cells/µl. The lysates were
1347 heated (95 °C, 10 min) before use. Lysates were separated by SDS-PAGE (1.4×10^6 cells/lane
1348 in a 15-well gel of 1.0 mm thickness), and the proteins then transferred to nitrocellulose
1349 membranes. The membranes were blocked in blocking buffer (10% milk, PBS, 0.3% TWEEN-
1350 20) (30 min, RT), and then incubated with the indicated primary antibodies in blocking buffer
1351 (1 h, RT). The membranes were washed three times in PBS-T (PBS, 0.3% TWEEN-20), and
1352 were then incubated with IRDye-conjugated secondary antibodies in PBS-T (1 h, RT). After a
1353 further three washes in PBS-T the membranes were briefly dried between sheets of filter paper
1354 and then imaged using an Odyssey CLx (LI-COR Biosciences, Bad Homburg, Germany).
1355 Processing and quantification was carried out using ImageStudioLite software (LI-COR
1356 Biosciences).

1357

1358

1359 **Immunofluorescence microscopy**

1360 Cell concentration was measured using a Z2 Coulter Counter, and 10^6 cells per coverslip were
1361 taken. The cells were transferred to 15 ml Falcon tubes, and fixed directly in media by the
1362 addition of paraformaldehyde solution to a final concentration of 4% (37 °C, 20 min). 10 ml
1363 trypanosome dilution buffer (TDB; 20 mM Na_2HPO_4 , 2 mM NaH_2PO_4 , 5 mM KCl, 80 mM NaCl,
1364 1 mM MgSO_4 , 20 mM glucose) was then added, and the cells were pelleted by centrifugation
1365 (750 x g, 10 min, RT). The supernatant was removed, the cell pellet was resuspended in 500
1366 µl TDB, and the cells were transferred to poly-L-lysine-coated coverslips in a 24-well plate.
1367 The cells were attached to the coverslips by centrifugation (750 x g, 4 min, RT), and the cells

1368 were permeabilised using a solution of 0.25% TritonX-100 in PBS (5 min, RT). The cells were
1369 washed with PBS, blocked using a solution of 3% BSA in PBS (30 min, RT), and sequentially
1370 incubated with primary and secondary antibodies diluted in PBS (1 h, RT for each) with three
1371 PBS wash steps after each incubation. After the final wash, the coverslips were rinsed in
1372 ddH₂O, excess fluid removed by wicking, and mounted on glass slides using Fluoromount-
1373 DAPI (Southern Biotech). For analysis of detergent-extracted cytoskeletons, cells were
1374 washed using TDB and attached to poly-L-lysine coverslips as described above. The cells
1375 were detergent-extracted using extraction buffer (0.5% IGEPAL, 0.1 M PIPES-NaOH pH 6.9,
1376 2 mM EGTA, 1 mM MgSO₄, 0.1 mM EDTA, cOmplete protease inhibitors [Roche]) (5 min, RT),
1377 washed three times with extraction buffer, and then fixed with ice-cold MeOH (-20 °C, 30 min).
1378 Blocking, antibody incubation steps, and mounting were as described above. All liquid
1379 handling was carried out using a P1000 micropipette, and pipetting was done as gently as
1380 possible to minimise shear forces. The coverslips were imaged using a Leica DMI6000B
1381 inverted microscope equipped with a Leica DFC365 camera and a 100x oil objective lens
1382 (NA1.4) and running Leica Application Suite X software. The same exposure times were used
1383 for acquisition of +/-Tet samples, and 40 z-slices of 0.21 µm thickness were taken per field of
1384 view. Image processing was carried out using ImageJ. Maximum intensity z-projections are
1385 shown.

1386

1387

1388 **Fractionation**

1389 Cell concentration was measured using a Z2 Coulter Counter, and an equal number of cells
1390 (~2.5x10⁷ per experiment) was taken from the control (-Tet) and overexpression (+Tet)
1391 samples and transferred to 50 ml Falcon tubes. The cells were pelleted by centrifugation (750
1392 x g, 10 min, 4 °C), and the cell pellets then resuspended in 1 ml TDB and transferred to
1393 microfuge tubes. The cells were pelleted by centrifugation (1800 x g, 2 min, 4 °C), and then
1394 resuspended in 200 µl extraction buffer (see Immunofluorescence microscopy section for
1395 composition). After a short incubation (15 min, RT, orbital mixer), a 5% (10 µl) input sample
1396 was taken, and the mixtures separated by centrifugation (3400 x g, 2 min, 4 °C) into detergent-
1397 soluble (cytoplasmic) supernatant and detergent-insoluble (cytoskeleton) pellet fractions. The
1398 supernatant was transferred to a fresh microfuge tube, its exact volume noted, and a 5%
1399 sample taken. The tube containing the pellet was centrifuged a second time (3400 x g, 2 min,
1400 4 °C) in order to bring down material sticking to the tube wall; this second supernatant was
1401 discarded. The pellet was resuspended in 200 µl extraction buffer and a 5% sample (10 µl)
1402 taken. SDS loading buffer was added to the input, supernatant, and pellet samples to a final
1403 volume of 20 µl, and denaturation assisted by heating (95 °C, 10 min). Equal fractions were
1404 loaded onto polyacrylamide gels, separated by SDS-PAGE, and analysed by immunoblotting.
1405 In the exemplary blot shown (Fig. 5G, each sample is a 4.5% fraction, equivalent to ~10⁶ cells
1406 in the Input fraction). For optimisation of extraction conditions using digitonin, essentially the
1407 same protocol was followed except that ultra-pure digitonin (Calbiochem) in TDB buffer was
1408 used and incubations were carried out at 24 °C in a heating block. For the two-step
1409 digitonin/IGEPAL fractionations (Fig. 8), cells were pelleted by centrifugation (750 x g, 10 min,
1410 RT), resuspended in 1 ml TDB, transferred to microfuge tubes, and pelleted again (750 x g, 3
1411 min, RT). The cell pellet was resuspended in 400 µl of 40 µg/ml digitonin in TDB and extracted
1412 (25 min, 24 °C), after which a 5% input sample was taken. The mixture was then separated

1413 by centrifugation (750 x g, 5 min, RT) and 320 μ l of the cytosolic fraction (SN1) transferred to
1414 a fresh tube and a 5% sample was taken. The cell pellet was then resuspended with 1 ml TDB
1415 and the extracted cells again pelleted by centrifugation (750 x g, 5 min, RT). The extracted
1416 cells were then resuspended in 400 μ l extraction buffer (see Immunofluorescence section
1417 above for composition) and incubated (24 °C, 15 min, heating block with shaker). After the
1418 incubation, a 5% sample (P1) was taken, and the extracted cells pelleted by centrifugation
1419 (3400 x g, 2 min, RT). 320 μ l of the supernatant (SN2) was transferred to a fresh microfuge
1420 tube and a 5% sample was taken. The pellet was resuspended in 1 ml TDB and centrifuged
1421 again (750 x g, 5 min, RT). The pellet (P2) was then resuspended in 400 μ l extraction buffer.
1422 SDS loading buffer was added to the 5% samples (I, SN1, SN2, P1, P2) to a final volume of
1423 40 μ l. Samples were analysed by immunoblotting as detailed above.

1424

1425

1426 **Crystallisation**

1427 Crystallisation of TbMORN1(7-15), TgMORN1(7-15) and PfMORN1(7-15) was performed at
1428 22 °C using a sitting-drop vapour diffusion technique and micro-dispensing liquid handling
1429 robots (Phoenix RE (Art Robbins Instruments) and Mosquito (TTP labtech)). In the case of
1430 TbMORN1(7-15), crystals only appeared from reductively methylated protein, using a
1431 standard protocol (Walter, Meier et al., 2006). The best diffracting crystals of TbMORN1(7-15)
1432 were grown at a protein concentration of 3.5 mg/ml in the following conditions: 0.166 M Tris-
1433 HCl pH 8.8, 0.15 M MgCl₂, 0.45 M KI, 24% PEG 2000 MME, and 4% glycerol. The tetragonal
1434 crystals of TgMORN1(7-15) were obtained at a protein concentration of 10 mg/ml in the
1435 following conditions: 0.1 M Tris-HCl pH 8.2, 15% PEG 3350, 0.2 M NaCl. The diffracting
1436 crystals of both selenomethionine-containing crystals and native crystals of PfMORN1(7-15)
1437 were obtained at a protein concentration of 8 mg/ml in the conditions “B11” from the Morpheus
1438 II crystallisation screen (Molecular Dimensions): 2 mM divalents mix (0.5 mM MnCl₃, 0.5 mM
1439 CoCl₂, 0.5 mM NiCl₂, 0.5 mM Zn(OAc)₂, 0.1 M Buffer System 6, pH 8.5 (Gly-Gly, AMPD), and
1440 50% precipitation Mix 7 (20 % PEG 8000, 40% 1,5-Pentenediol). The crystals were flash
1441 cooled in liquid nitrogen prior to data collection.

1442

1443

1444 **X-ray diffraction data collection and crystal structure determination**

1445 Initially, the structure of PfMORN1(7-15) was determined using the single-wavelength
1446 anomalous diffraction (SAD) method. The selenomethionine dataset was collected at the
1447 beamline ID29 (ESRF, Grenoble) at 100K at the peak of selenium using a wavelength of 0.979
1448 Å. The data frames were processed using the XDS package (Kabsch, 2010), and converted
1449 to mtz format with the program AIMLESS (Winn, Ballard et al., 2011). The apo-PfMORN1(7-
1450 15) structure was solved using single anomalous diffraction with AUTOSOL software from the
1451 PHENIX package. The structures of TgMORN1(7-15) and TbMORN1(7-15) were then solved
1452 using the molecular replacement program PHASER (McCoy, Grosse-Kunstleve et al., 2007)
1453 with the atomic coordinates of PfMORN1(7-15) as a search model. The structures were then
1454 refined with REFMAC and Phenix Refine and rebuilt using Coot (Murshudov, Vagin et al.,
1455 1997, Emsley & Cowtan, 2004, Adams, Afonine et al., 2010). The structures were validated
1456 and corrected using the PDB_REDO server (Joosten, Long et al., 2014). The figures were
1457 produced using Pymol and Chimera software. Coordinates have been deposited in the protein

1458 data bank (accession codes 6T4D, 6T4R, 6T68, 6T69, 6T6Q). Data collection and refinement
1459 statistics are reported in Table 3.

1460

1461

1462 **Small angle X-ray scattering (SAXS)**

1463 Synchrotron radiation X-ray scattering from various MORN constructs in solution were
1464 collected at different synchrotron facilities (Table S3). TgMORN1(7-15), TbMORN1(7-15) as
1465 well as PfMORN1(7-15) were collected at the EMBL P12 beamline of the storage ring PETRA
1466 III (DESY, Hamburg, Germany) (Blanchet, Spilotros et al., 2015). Images were recorded using
1467 a photon counting Pilatus-2M detector at a sample to detector distance of 3.1 m and a
1468 wavelength (λ) of 1.2 Å covering the range of momentum transfer $0.01 < s < 0.5 \text{ \AA}^{-1}$; with $s =$
1469 $4\pi \sin\theta/\lambda$, where 2θ is the scattering angle. To obtain data from a monodisperse sample from
1470 TgMORN1(7-15) and TbMORN1(7-15), a size exclusion chromatography column directly
1471 coupled to the scattering experiment (SEC-SAXS) was employed. The parallel collection of
1472 UV and light scattering data allowed the protein to be monitored while it eluted from the column
1473 (Graewert, Franke et al., 2015). Throughout the complete chromatography process, 1 s
1474 sample exposures were recorded. As mobile phase, the various buffers were used:
1475 TbMORN1(7-15): 20mM Tris-HCl pH 8.5, 200 mM NaCl, 2% (v/v) glycerol, 1 mM DTT.
1476 TgMORN1(7-15): 20 mM Tris-HCl pH 7.5, 100 mM NaCl. 100 μ l of purified sample (3.8 mg/mL
1477 TbMORN1(7-15) and 2.6 mg/ml TgMORN1(7-15)) were injected onto a Superdex 200 10/300
1478 (GE Healthcare) column and the flow rate was set to 0.5 ml/min. SAXS data were recorded
1479 from macromolecular free fractions corresponding to the matched solvent blank. PfMORN1(7-
1480 15) was measured in batch mode from a concentration series spanning 1-8 mg/ml. 20 mM
1481 Tris-HCl pH 7.5, 100 mM NaCl buffer was measured for background subtraction. As a
1482 concentration dependent increase in size was detectable further analysis were based solely
1483 on the data collected at 1 mg/ml. In a similar manner as described above, TbMORN1(2-15)
1484 data were collected at ESRF BM29 beamline (Pernot, Round et al., 2013) in SEC-SAXS mode
1485 with the setup described in by Brennich et al. (Brennich, Round et al., 2017). SAXS data from
1486 the run were collected at a wavelength of 0.99 Å using a sample-to-detector (PILATUS 1 M,
1487 DECTRIS) distance of 2.867 m. Here too, a Superdex 200 10/300 (GE Healthcare) column
1488 was used as well as 20 mM Tris-HCl pH 7.5, 100 mM NaCl as mobile phase. 100 μ l of 5.8
1489 mg/ml TbMORN1(2-15) were injected. Data reduction to produce final scattering profiles of
1490 dimeric MORN1 constructs were performed using standard methods. Briefly, 2D-to-1D radial
1491 averaging was performed using the SASFLOW pipeline (Franke, Petoukhov et al., 2017). For
1492 data collected at ESRF EDNA pipeline (Brennich, Kieffer et al., 2016) was used. CHROMIXS
1493 was used for the visualisation and reduction of the SEC-SAXS datasets (Panjkovich &
1494 Svergun, 2018). Aided by the integrated prediction algorithms in CHROMIXS the optimal
1495 frames within the elution peak and the buffer regions were selected. Single buffer frames were
1496 then subtracted from sample frames one by one, scaled and averaged to produce the final
1497 subtracted curve. The indirect inverse Fourier transform of the SAXS data and the
1498 corresponding probable real space-scattering pair distance distribution ($p(r)$ versus r profile)
1499 of the various MORN1 constructs were calculated using GNOM (Svergun, 1992), from which
1500 the R_g and D_{max} were determined. The $p(r)$ versus r profile were also used for *ab initio* bead
1501 modelling of selected MORN1 constructs. For this, 20 independent runs of DAMMIF (Franke
1502 & Svergun, 2009) in the case of TbMORN1(2-15) and DAMMIN (Svergun, 1999) in case of
1503 the shorter MORN1(7-15) constructs were performed. From these the most probable models

1504 were selected by DAMAVER (Volkov & Svergun, 2003). The ab initio modelling was performed
1505 with and without symmetry constraints (p2 symmetry to reflect the dimeric state of the protein).
1506 Comparison with theoretical curves calculated from the X-tal structures described here was
1507 performed with Crysol (Svergun, Barberato et al., 1995). Due to the elongated nature of the
1508 molecules, fits were improved by increasing LM (maximum order of harmonics) to 50. The
1509 molecular mass (MM) was evaluated based on concentration independent methods according
1510 to Porod (Porod, 1951) and as implemented in the ATSAS package. Dimensionless Kratky
1511 plots were constructed according to (Receveur-Brechot & Durand, 2012) and the reference
1512 point for globular proteins at $\sqrt{3}$, 1.1 indicated. Graphical representation was produced using
1513 Pymol Molecular Graphics System (Schrödinger, LLC.). The SAXS data (Table S3) and ab
1514 initio bead models as well as fits to the crystal structures described within this work have been
1515 deposited into the Small-Angle Scattering Biological Data Bank (SASBDB) (Valentini, Kikhney
1516 et al., 2015) under the accession codes SASDG97, SASDGA7, SASDGB7, SASDGC7.

1517
1518

1519 **Transmission electron microscopy (EM) with rotary shadowing**

1520 TbMORN1 and TbMORN1(2-15) were purified according to the two-step procedure detailed
1521 above. They were then diluted in spraying buffer (100 mM $\text{NH}_4\text{CH}_3\text{CO}_2$ -NaOH pH 8.5, 30%
1522 (v/v) glycerol) to a final concentration of 50 – 100 $\mu\text{g}/\text{ml}$. Diluted samples were sprayed onto
1523 freshly cleaved mica chips (Christine Gröpl) and immediately transferred into a MED020 high
1524 vacuum evaporator (BAL-TEC) equipped with electron guns. While rotating, samples were
1525 coated with 0.6 nm of Platinum (BAL TIC) at an angle of 4° , followed by 6 nm of Carbon
1526 (Oerlicon) at 90° . The obtained replicas were floated off the mica chips, transferred to 400
1527 mesh Cu/Pd grids (Agar Scientific), and examined using a Morgagni 268D transmission
1528 electron microscope (FEI) operated at 80 kV. Images were acquired using an 11 megapixel
1529 Morada CCD camera (Olympus-SIS).

1530
1531

1532 **ACKNOWLEDGEMENTS**

1533 Financial support was from Austrian Science Fund (FWF) grants P22265-B12 FWF (to
1534 Graham Warren) P27016-B21 (to Brooke Morriswood and Kristina Djinovic-Carugo), P28135
1535 and P30584 (both to Tom Leonard). Kristina Djinovic-Carugo's research was additionally
1536 supported by Austrian Science Fund (FWF) Projects I525 and I1593, P22276, P19060 and
1537 W1221, Federal Ministry of Economy, Family and Youth through the initiative “Laura Bassi
1538 Centres of Expertise”, funding the Centre of Optimized Structural Studies, N°253275, by the
1539 Wellcome Trust Collaborative Award (201543/Z/16), COST action BM1405 - Non-globular
1540 proteins - from sequence to structure, function and application in molecular physiopathology
1541 (NGP-NET), WWTF (Vienna Science and Technology Fund) Chemical Biology project LS17-
1542 008, and by the University of Vienna. Funding also came from Medical Research Council grant
1543 MR/Mo20118/1 (to Terry Smith). We are indebted to Graham Warren (MRC Laboratory for
1544 Molecular Cell Biology, University College London), for comments and support. Valeria
1545 Stefania carried out the SAXS measurements. The Martens lab at the Max Perutz Labs Vienna
1546 provided the Doc2B protein; Iva Lucic in the Leonard group supplied the Akt protein. Euripedes
1547 Almeida Ribeiro advised on fluorescence anisotropy measurements. Markus Engstler

1548 (University of Würzburg) provided the bloodstream form GFP cells as well as lab space and
1549 support. Susanne Fenz (University of Würzburg) assisted with the purification of trypanosome
1550 lipids. The authors thank the staff of MX and SAXS beamlines at ESRF in Grenoble and
1551 EMBL-Hamburg for their excellent support. EM data were recorded at the EM Facility of the
1552 Vienna BioCenter Core Facilities GmbH (VBCF), a member of the Vienna BioCenter (VBC),
1553 Austria. Proteomics analyses were performed by the Mass Spectrometry Facility at Max
1554 Perutz Labs Vienna using the VBCF instrument pool.
1555
1556
1557
1558

1559 References

- 1560 Adam SA, Marr RS, Gerace L (1990) Nuclear protein import in permeabilized mammalian
1561 cells requires soluble cytoplasmic factors. *J Cell Biol* 111: 807-16
- 1562 Adams PD, Afonine PV, Bunkoczi G, Chen VB, Davis IW, Echols N, Headd JJ, Hung LW,
1563 Kapral GJ, Grosse-Kunstleve RW, McCoy AJ, Moriarty NW, Oeffner R, Read RJ,
1564 Richardson DC, Richardson JS, Terwilliger TC, Zwart PH (2010) PHENIX: a comprehensive
1565 Python-based system for macromolecular structure solution. *Acta Crystallogr D Biol*
1566 *Crystallogr* 66: 213-21
- 1567 Adl SM, Bass D, Lane CE, Lukes J, Schoch CL, Smirnov A, Agatha S, Berney C, Brown
1568 MW, Burki F, Cardenas P, Cepicka I, Chistyakova L, Del Campo J, Dunthorn M, Edvardsen
1569 B, Eglit Y, Guillou L, Hampl V, Heiss AA et al. (2019) Revisions to the Classification,
1570 Nomenclature, and Diversity of Eukaryotes. *J Eukaryot Microbiol* 66: 4-119
- 1571 Allen CL, Goulding D, Field MC (2003) Clathrin-mediated endocytosis is essential in
1572 *Trypanosoma brucei*. *Embo J* 22: 4991-5002
- 1573 Andrade MA, Perez-Iratxeta C, Ponting CP (2001) Protein repeats: structures, functions, and
1574 evolution. *J Struct Biol* 134: 117-31
- 1575 Bangs JD, Uyetake L, Brickman MJ, Balber AE, Boothroyd JC (1993) Molecular cloning and
1576 cellular localization of a BiP homologue in *Trypanosoma brucei*. Divergent ER retention
1577 signals in a lower eukaryote. *J Cell Sci* 105 (Pt 4): 1101-13
- 1578 Bastin P, Bagherzadeh Z, Matthews KR, Gull K (1996) A novel epitope tag system to study
1579 protein targeting and organelle biogenesis in *Trypanosoma brucei*. *Mol Biochem Parasitol*
1580 77: 235-9
- 1581 Batram C, Jones NG, Janzen CJ, Markert SM, Engstler M (2014) Expression site
1582 attenuation mechanistically links antigenic variation and development in *Trypanosoma*
1583 *brucei*. *Elife* 3: e02324
- 1584 Bennett HJ, Davenport JB, Collins RF, Trafford AW, Pinali C, Kitmitto A (2013) Human
1585 junctophilin-2 undergoes a structural rearrangement upon binding PtdIns(3,4,5)P3 and the
1586 S101R mutation identified in hypertrophic cardiomyopathy obviates this response. *Biochem*
1587 *J* 456: 205-17

- 1588 Blanchet CE, Spilotros A, Schwemmer F, Graewert MA, Kikhney A, Jeffries CM, Franke D,
1589 Mark D, Zengerle R, Cipriani F, Fiedler S, Roessle M, Svergun DI (2015) Versatile sample
1590 environments and automation for biological solution X-ray scattering experiments at the P12
1591 beamline (PETRA III, DESY). *J Appl Crystallogr* 48: 431-443
- 1592 Bligh EG, Dyer WJ (1959) A rapid method of total lipid extraction and purification. *Can J*
1593 *Biochem Physiol* 37: 911-7
- 1594 Brennich ME, Kieffer J, Bonamis G, Antolinos AD, Hutin S, Pernot P, Round A (2016) Online
1595 data analysis at the ESRF bioSAXS beamline, BM29. *Journal of Applied Crystallography* 49:
1596 203-212
- 1597 Brennich ME, Round AR, Hutin S (2017) Online Size-exclusion and Ion-exchange
1598 Chromatography on a SAXS Beamline. *J Vis Exp*
- 1599 Burkard G, Fragoso CM, Roditi I (2007) Highly efficient stable transformation of bloodstream
1600 forms of *Trypanosoma brucei*. *Mol Biochem Parasitol* 153: 220-3
- 1601 Camacho L, Smertenko AP, Perez-Gomez J, Hussey PJ, Moore I (2009) Arabidopsis Rab-E
1602 GTPases exhibit a novel interaction with a plasma-membrane phosphatidylinositol-4-
1603 phosphate 5-kinase. *J Cell Sci* 122: 4383-92
- 1604 Carman PJ, Dominguez R (2018) BAR domain proteins-a linkage between cellular
1605 membranes, signaling pathways, and the actin cytoskeleton. *Biophys Rev* 10: 1587-1604
- 1606 Cronan JE (2003) Bacterial membrane lipids: where do we stand? *Annu Rev Microbiol* 57:
1607 203-24
- 1608 Demmel L, Schmidt K, Lucast L, Havlicek K, Zankel A, Koestler T, Reithofer V, de Camilli P,
1609 Warren G (2014) The endocytic activity of the flagellar pocket in *Trypanosoma brucei* is
1610 regulated by an adjacent phosphatidylinositol phosphate kinase. *Journal of cell science* 127:
1611 2351-64
- 1612 Doyle SA (2005) High-throughput cloning for proteomics research. *Methods Mol Biol* 310:
1613 107-13
- 1614 El-Gebali S, Mistry J, Bateman A, Eddy SR, Luciani A, Potter SC, Qureshi M, Richardson
1615 LJ, Salazar GA, Smart A, Sonnhammer ELL, Hirsh L, Paladin L, Piovesan D, Tosatto SCE,
1616 Finn RD (2019) The Pfam protein families database in 2019. *Nucleic Acids Res* 47: D427-
1617 D432
- 1618 Emsley P, Cowtan K (2004) Coot: model-building tools for molecular graphics. *Acta*
1619 *Crystallogr D Biol Crystallogr* 60: 2126-32
- 1620 Engstler M, Thilo L, Weise F, Grunfelder CG, Schwarz H, Boshart M, Overath P (2004)
1621 Kinetics of endocytosis and recycling of the GPI-anchored variant surface glycoprotein in
1622 *Trypanosoma brucei*. *Journal of cell science* 117: 1105-15
- 1623 Epand RM, Epand RF (2009) Lipid domains in bacterial membranes and the action of
1624 antimicrobial agents. *Biochim Biophys Acta* 1788: 289-94
- 1625 Esson HJ, Morriswood B, Yavuz S, Vidilaseris K, Dong G, Warren G (2012) Morphology of
1626 the trypanosome bilobe, a novel cytoskeletal structure. *Eukaryot Cell* 11: 761-72

- 1627 Franke D, Petoukhov MV, Konarev PV, Panjkovich A, Tuukkanen A, Mertens HDT, Kikhney
1628 AG, Hajizadeh NR, Franklin JM, Jeffries CM, Svergun DI (2017) ATSAS 2.8: a
1629 comprehensive data analysis suite for small-angle scattering from macromolecular solutions.
1630 *J Appl Crystallogr* 50: 1212-1225
- 1631 Franke D, Svergun DI (2009) DAMMIF, a program for rapid ab-initio shape determination in
1632 small-angle scattering. *J Appl Crystallogr* 42: 342-346
- 1633 Franzot G, Sjoblom B, Gautel M, Djinovic Carugo K (2005) The crystal structure of the actin
1634 binding domain from alpha-actinin in its closed conformation: structural insight into
1635 phospholipid regulation of alpha-actinin. *J Mol Biol* 348: 151-65
- 1636 Fyffe SA, Alphey MS, Buetow L, Smith TK, Ferguson MA, Sorensen MD, Bjorkling F, Hunter
1637 WN (2006) Reevaluation of the PPAR-beta/delta ligand binding domain model reveals why it
1638 exhibits the activated form. *Mol Cell* 21: 1-2
- 1639 Gibson DG, Young L, Chuang RY, Venter JC, Hutchison CA, 3rd, Smith HO (2009)
1640 Enzymatic assembly of DNA molecules up to several hundred kilobases. *Nat Methods* 6:
1641 343-5
- 1642 Graewert MA, Franke D, Jeffries CM, Blanchet CE, Ruskule D, Kuhle K, Flieger A, Schafer
1643 B, Tartsch B, Meijers R, Svergun DI (2015) Automated pipeline for purification, biophysical
1644 and x-ray analysis of biomacromolecular solutions. *Sci Rep* 5: 10734
- 1645 Grunfelder CG, Engstler M, Weise F, Schwarz H, Stierhof YD, Morgan GW, Field MC,
1646 Overath P (2003) Endocytosis of a glycosylphosphatidylinositol-anchored protein via
1647 clathrin-coated vesicles, sorting by default in endosomes, and exocytosis via RAB11-positive
1648 carriers. *Mol Biol Cell* 14: 2029-40
- 1649 Gubbels MJ, Vaishnav S, Boot N, Dubremetz JF, Striepen B (2006) A MORN-repeat
1650 protein is a dynamic component of the *Toxoplasma gondii* cell division apparatus. *J Cell Sci*
1651 119: 2236-45
- 1652 Guo A, Wang Y, Chen B, Wang Y, Yuan J, Zhang L, Hall D, Wu J, Shi Y, Zhu Q, Chen C,
1653 Thiel WH, Zhan X, Weiss RM, Zhan F, Musselman CA, Pufall M, Zhu W, Au KF, Hong J et
1654 al. (2018) E-C coupling structural protein junctophilin-2 encodes a stress-adaptive
1655 transcription regulator. *Science* 362
- 1656 Habicht J, Woehle C, Gould SB (2015) *Tetrahymena* Expresses More than a Hundred
1657 Proteins with Lipid-binding MORN Motifs that can Differ in their Subcellular Localisations. *J*
1658 *Eukaryot Microbiol* 62: 694-700
- 1659 Hatzopoulos GN, Erat MC, Cutts E, Rogala KB, Slater LM, Stansfeld PJ, Vakonakis I (2013)
1660 Structural analysis of the G-box domain of the microcephaly protein CPAP suggests a role in
1661 centriole architecture. *Structure* 21: 2069-77
- 1662 Hemsley A, Arnheim N, Toney MD, Cortopassi G, Galas DJ (1989) A simple method for site-
1663 directed mutagenesis using the polymerase chain reaction. *Nucleic Acids Res* 17: 6545-51
- 1664 Holm L, Laakso LM (2016) Dali server update. *Nucleic Acids Res* 44: W351-5
- 1665 Holm L, Rosenstrom P (2010) Dali server: conservation mapping in 3D. *Nucleic Acids Res*
1666 38: W545-9

- 1667 Hu K (2008) Organizational changes of the daughter basal complex during the parasite
1668 replication of *Toxoplasma gondii*. *PLoS Pathog* 4: e10
- 1669 Hutchinson EG, Thornton JM (1994) A revised set of potentials for beta-turn formation in
1670 proteins. *Protein Sci* 3: 2207-16
- 1671 Im YJ, Davis AJ, Perera IY, Johannes E, Allen NS, Boss WF (2007) The N-terminal
1672 membrane occupation and recognition nexus domain of Arabidopsis phosphatidylinositol
1673 phosphate kinase 1 regulates enzyme activity. *J Biol Chem* 282: 5443-52
- 1674 Jacobs SA, Harp JM, Devarakonda S, Kim Y, Rastinejad F, Khorasanizadeh S (2002) The
1675 active site of the SET domain is constructed on a knot. *Nat Struct Biol* 9: 833-8
- 1676 Jayasinghe I, Clowsley AH, Lin R, Lutz T, Harrison C, Green E, Baddeley D, Di Michele L,
1677 Soeller C (2018) True Molecular Scale Visualization of Variable Clustering Properties of
1678 Ryanodine Receptors. *Cell Rep* 22: 557-567
- 1679 Jiang M, Hu J, White FKH, Williamson J, Klymchenko AS, Murthy A, Workman SW, Tseng
1680 GN (2019) S-Palmitoylation of junctophilin-2 is critical for its role in tethering the
1681 sarcoplasmic reticulum to the plasma membrane. *J Biol Chem* 294: 13487-13501
- 1682 Joosten RP, Long F, Murshudov GN, Perrakis A (2014) The PDB_REDO server for
1683 macromolecular structure model optimization. *IUCrJ* 1: 213-20
- 1684 Kabsch W (2010) Xds. *Acta Crystallogr D Biol Crystallogr* 66: 125-32
- 1685 Kelly SM, Jess TJ, Price NC (2005) How to study proteins by circular dichroism. *Biochim*
1686 *Biophys Acta* 1751: 119-39
- 1687 Kohl L, Sherwin T, Gull K (1999) Assembly of the paraflagellar rod and the flagellum
1688 attachment zone complex during the *Trypanosoma brucei* cell cycle. *J Eukaryot Microbiol*
1689 46: 105-9
- 1690 Krissinel E, Henrick K (2007) Inference of macromolecular assemblies from crystalline state.
1691 *J Mol Biol* 372: 774-97
- 1692 Kunita R, Otomo A, Mizumura H, Suzuki K, Showguchi-Miyata J, Yanagisawa Y, Hadano S,
1693 Ikeda JE (2004) Homo-oligomerization of ALS2 through its unique carboxyl-terminal regions
1694 is essential for the ALS2-associated Rab5 guanine nucleotide exchange activity and its
1695 regulatory function on endosome trafficking. *J Biol Chem* 279: 38626-35
- 1696 Lacomble S, Vaughan S, Gadelha C, Morphew MK, Shaw MK, McIntosh JR, Gull K (2009)
1697 Three-dimensional cellular architecture of the flagellar pocket and associated cytoskeleton in
1698 trypanosomes revealed by electron microscope tomography. *Journal of cell science* 122:
1699 1081-90
- 1700 Li J, Liu H, Raval MH, Wan J, Yengo CM, Liu W, Zhang M (2019) Structure of the
1701 MORN4/Myo3a Tail Complex Reveals MORN Repeats as Protein Binding Modules.
1702 *Structure*
- 1703 Li MZ, Elledge SJ (2012) SLIC: a method for sequence- and ligation-independent cloning.
1704 *Methods Mol Biol* 852: 51-9

- 1705 Ma H, Lou Y, Lin WH, Xue HW (2006) MORN motifs in plant PIPKs are involved in the
1706 regulation of subcellular localization and phospholipid binding. *Cell Res* 16: 466-78
- 1707 McCoy AJ, Grosse-Kunstleve RW, Adams PD, Winn MD, Storoni LC, Read RJ (2007)
1708 Phaser crystallographic software. *J Appl Crystallogr* 40: 658-674
- 1709 Mecklenburg KL (2007) Drosophila retinophilin contains MORN repeats and is conserved in
1710 humans. *Mol Genet Genomics* 277: 481-9
- 1711 Micsonai A, Wien F, Bulyaki E, Kun J, Moussong E, Lee YH, Goto Y, Refregiers M, Kardos J
1712 (2018) BeStSel: a web server for accurate protein secondary structure prediction and fold
1713 recognition from the circular dichroism spectra. *Nucleic Acids Res* 46: W315-W322
- 1714 Micsonai A, Wien F, Kernya L, Lee YH, Goto Y, Refregiers M, Kardos J (2015) Accurate
1715 secondary structure prediction and fold recognition for circular dichroism spectroscopy. *Proc
1716 Natl Acad Sci U S A* 112: E3095-103
- 1717 Mikami K, Saavedra L, Sommarin M (2010) Is membrane occupation and recognition nexus
1718 domain functional in plant phosphatidylinositol phosphate kinases? *Plant Signal Behav* 5:
1719 1241-4
- 1720 Molla-Herman A, Ghossoub R, Blisnick T, Meunier A, Serres C, Silbermann F, Emmerson C,
1721 Romeo K, Bourdoncle P, Schmitt A, Saunier S, Spassky N, Bastin P, Benmerah A (2010)
1722 The ciliary pocket: an endocytic membrane domain at the base of primary and motile cilia. *J
1723 Cell Sci* 123: 1785-95
- 1724 Morriswood B, Havlicek K, Demmel L, Yavuz S, Sealey-Cardona M, Vidilaseris K, Anrather
1725 D, Kostan J, Djinicovic-Carugo K, Roux KJ, Warren G (2013) Novel Bilobe Components in
1726 Trypanosoma brucei Identified Using Proximity-Dependent Biotinylation. *Eukaryot Cell* 12:
1727 356-67
- 1728 Morriswood B, He CY, Sealey-Cardona M, Yelinek J, Pypaert M, Warren G (2009) The
1729 bilobe structure of Trypanosoma brucei contains a MORN-repeat protein. *Mol Biochem
1730 Parasitol* 167: 95-103
- 1731 Morriswood B, Schmidt K (2015) A MORN-repeat protein facilitates protein entry into the
1732 flagellar pocket of Trypanosoma brucei. *Eukaryot Cell*
- 1733 Munro ML, Jayasinghe ID, Wang Q, Quick A, Wang W, Baddeley D, Wehrens XH, Soeller C
1734 (2016) Junctophilin-2 in the nanoscale organisation and functional signalling of ryanodine
1735 receptor clusters in cardiomyocytes. *J Cell Sci* 129: 4388-4398
- 1736 Murshudov GN, Vagin AA, Dodson EJ (1997) Refinement of macromolecular structures by
1737 the maximum-likelihood method. *Acta Crystallogr D Biol Crystallogr* 53: 240-55
- 1738 Nakada T, Kashiwara T, Komatsu M, Kojima K, Takeshita T, Yamada M (2018) Physical
1739 interaction of junctophilin and the CaV1.1 C terminus is crucial for skeletal muscle
1740 contraction. *Proc Natl Acad Sci U S A* 115: 4507-4512
- 1741 Otomo A, Hadano S, Okada T, Mizumura H, Kunita R, Nishijima H, Showguchi-Miyata J,
1742 Yanagisawa Y, Kohiki E, Suga E, Yasuda M, Osuga H, Nishimoto T, Narumiya S, Ikeda JE
1743 (2003) ALS2, a novel guanine nucleotide exchange factor for the small GTPase Rab5, is
1744 implicated in endosomal dynamics. *Hum Mol Genet* 12: 1671-87

- 1745 Panjkovich A, Svergun DI (2018) CHROMIXS: automatic and interactive analysis of
1746 chromatography-coupled small-angle X-ray scattering data. *Bioinformatics* 34: 1944-1946
- 1747 Pelletier L, Stern CA, Pypaert M, Sheff D, Ngo HM, Roper N, He CY, Hu K, Toomre D,
1748 Coppens I, Roos DS, Joiner KA, Warren G (2002) Golgi biogenesis in *Toxoplasma gondii*.
1749 *Nature* 418: 548-52
- 1750 Perni S, Lavorato M, Beam KG (2017) De novo reconstitution reveals the proteins required
1751 for skeletal muscle voltage-induced Ca(2+) release. *Proc Natl Acad Sci U S A* 114: 13822-
1752 13827
- 1753 Pernot P, Round A, Barrett R, De Maria Antolinos A, Gobbo A, Gordon E, Huet J, Kieffer J,
1754 Lentini M, Mattenet M, Morawe C, Mueller-Dieckmann C, Ohlsson S, Schmid W, Surr J,
1755 Theveneau P, Zerrad L, McSweeney S (2013) Upgraded ESRF BM29 beamline for SAXS
1756 on macromolecules in solution. *J Synchrotron Radiat* 20: 660-4
- 1757 Porod G (1951) Die Röntgenkleinwinkelstreuung Von Dichtgepackten Kolloiden Systemen
1758 .1. *Kolloid Z Z Polym* 124: 83-114
- 1759 Pramanik J, Keasling JD (1997) Stoichiometric model of *Escherichia coli* metabolism:
1760 incorporation of growth-rate dependent biomass composition and mechanistic energy
1761 requirements. *Biotechnol Bioeng* 56: 398-421
- 1762 Rao VD, Misra S, Boronenkov IV, Anderson RA, Hurley JH (1998) Structure of type II beta
1763 phosphatidylinositol phosphate kinase: a protein kinase fold flattened for interfacial
1764 phosphorylation. *Cell* 94: 829-39
- 1765 Rappsilber J, Mann M, Ishihama Y (2007) Protocol for micro-purification, enrichment, pre-
1766 fractionation and storage of peptides for proteomics using StageTips. *Nat Protoc* 2: 1896-
1767 906
- 1768 Receveur-Brechot V, Durand D (2012) How random are intrinsically disordered proteins? A
1769 small angle scattering perspective. *Curr Protein Pept Sci* 13: 55-75
- 1770 Richmond GS, Gibellini F, Young SA, Major L, Denton H, Lilley A, Smith TK (2010)
1771 Lipidomic analysis of bloodstream and procyclic form *Trypanosoma brucei*. *Parasitology*
1772 137: 1357-92
- 1773 Rossi D, Scarcella AM, Liguori E, Lorenzini S, Pierantozzi E, Kutchukian C, Jacquemond V,
1774 Messa M, De Camilli P, Sorrentino V (2019) Molecular determinants of homo- and
1775 heteromeric interactions of Junctophilin-1 at triads in adult skeletal muscle fibers. *Proc Natl*
1776 *Acad Sci U S A* 116: 15716-15724
- 1777 Saliba AE, Vonkova I, Ceschia S, Findlay GM, Maeda K, Tischer C, Deghou S, van Noort V,
1778 Bork P, Pawson T, Ellenberg J, Gavin AC (2014) A quantitative liposome microarray to
1779 systematically characterize protein-lipid interactions. *Nat Methods* 11: 47-50
- 1780 Saliba AE, Vonkova I, Deghou S, Ceschia S, Tischer C, Kugler KG, Bork P, Ellenberg J,
1781 Gavin AC (2016) A protocol for the systematic and quantitative measurement of protein-lipid
1782 interactions using the liposome-microarray-based assay. *Nat Protoc* 11: 1021-38
- 1783 Salzer U, Kostan J, Djinovic-Carugo K (2017) Deciphering the BAR code of membrane
1784 modulators. *Cell Mol Life Sci* 74: 2413-2438

- 1785 Scholz J, Besir H, Strasser C, Suppmann S (2013) A new method to customize protein
1786 expression vectors for fast, efficient and background free parallel cloning. *BMC Biotechnol*
1787 13: 12
- 1788 Schumann Burkard G, Jutzi P, Roditi I (2011) Genome-wide RNAi screens in bloodstream
1789 form trypanosomes identify drug transporters. *Mol Biochem Parasitol* 175: 91-4
- 1790 Studier FW (2005) Protein production by auto-induction in high density shaking cultures.
1791 *Protein Expr Purif* 41: 207-34
- 1792 Svergun D, Barberato C, Koch MHJ (1995) CRY SOL - A program to evaluate x-ray solution
1793 scattering of biological macromolecules from atomic coordinates. *Journal of Applied*
1794 *Crystallography* 28: 768-773
- 1795 Svergun DI (1992) Determination of the Regularization Parameter in Indirect-Transform
1796 Methods Using Perceptual Criteria. *Journal of Applied Crystallography* 25: 495-503
- 1797 Svergun DI (1999) Restoring low resolution structure of biological macromolecules from
1798 solution scattering using simulated annealing. *Biophys J* 76: 2879-86
- 1799 Takeshima H, Komazaki S, Nishi M, Iino M, Kangawa K (2000) Juncophilins: a novel family
1800 of junctional membrane complex proteins. *Mol Cell* 6: 11-22
- 1801 Tsuchida J, Nishina Y, Wakabayashi N, Nozaki M, Sakai Y, Nishimune Y (1998) Molecular
1802 cloning and characterization of meichroacidin (male meiotic metaphase chromosome-
1803 associated acidic protein). *Dev Biol* 197: 67-76
- 1804 Tyanova S, Temu T, Cox J (2016) The MaxQuant computational platform for mass
1805 spectrometry-based shotgun proteomics. *Nat Protoc* 11: 2301-2319
- 1806 Valentini E, Kikhney AG, Previtali G, Jeffries CM, Svergun DI (2015) SASBDB, a repository
1807 for biological small-angle scattering data. *Nucleic Acids Res* 43: D357-63
- 1808 Volkov VV, Svergun DI (2003) Uniqueness of ab initio shape determination in small-angle
1809 scattering. *Journal of Applied Crystallography* 36: 860-864
- 1810 Walter TS, Meier C, Assenberg R, Au KF, Ren J, Verma A, Nettleship JE, Owens RJ, Stuart
1811 DI, Grimes JM (2006) Lysine methylation as a routine rescue strategy for protein
1812 crystallization. *Structure* 14: 1617-22
- 1813 Wilson JR, Jing C, Walker PA, Martin SR, Howell SA, Blackburn GM, Gamblin SJ, Xiao B
1814 (2002) Crystal structure and functional analysis of the histone methyltransferase SET7/9.
1815 *Cell* 111: 105-15
- 1816 Winn MD, Ballard CC, Cowtan KD, Dodson EJ, Emsley P, Evans PR, Keegan RM, Krissinel
1817 EB, Leslie AG, McCoy A, McNicholas SJ, Murshudov GN, Pannu NS, Potterton EA, Powell
1818 HR, Read RJ, Vagin A, Wilson KS (2011) Overview of the CCP4 suite and current
1819 developments. *Acta Crystallogr D Biol Crystallogr* 67: 235-42
- 1820 Wirtz E, Leal S, Ochatt C, Cross GA (1999) A tightly regulated inducible expression system
1821 for conditional gene knock-outs and dominant-negative genetics in *Trypanosoma brucei*. *Mol*
1822 *Biochem Parasitol* 99: 89-101

- 1823 Woo JS, Srikanth S, Nishi M, Ping P, Takeshima H, Gwack Y (2016) Junctophilin-4, a
1824 component of the endoplasmic reticulum-plasma membrane junctions, regulates Ca²⁺
1825 dynamics in T cells. *Proc Natl Acad Sci U S A* 113: 2762-7
- 1826 Xiao B, Jing C, Wilson JR, Walker PA, Vasisht N, Kelly G, Howell S, Taylor IA, Blackburn
1827 GM, Gamblin SJ (2003) Structure and catalytic mechanism of the human histone
1828 methyltransferase SET7/9. *Nature* 421: 652-6
- 1829 Yamanaka K, Vande Velde C, Eymard-Pierre E, Bertini E, Boespflug-Tanguy O, Cleveland
1830 DW (2003) Unstable mutants in the peripheral endosomal membrane component ALS2
1831 cause early-onset motor neuron disease. *Proc Natl Acad Sci U S A* 100: 16041-6
- 1832 Yang B, Wu YJ, Zhu M, Fan SB, Lin J, Zhang K, Li S, Chi H, Li YX, Chen HF, Luo SK, Ding
1833 YH, Wang LH, Hao Z, Xiu LY, Chen S, Ye K, He SM, Dong MQ (2012) Identification of
1834 cross-linked peptides from complex samples. *Nat Methods* 9: 904-6
- 1835 Yuan ZF, Liu C, Wang HP, Sun RX, Fu Y, Zhang JF, Wang LH, Chi H, Li Y, Xiu LY, Wang
1836 WP, He SM (2012) pParse: a method for accurate determination of monoisotopic peaks in
1837 high-resolution mass spectra. *Proteomics* 12: 226-35
1838

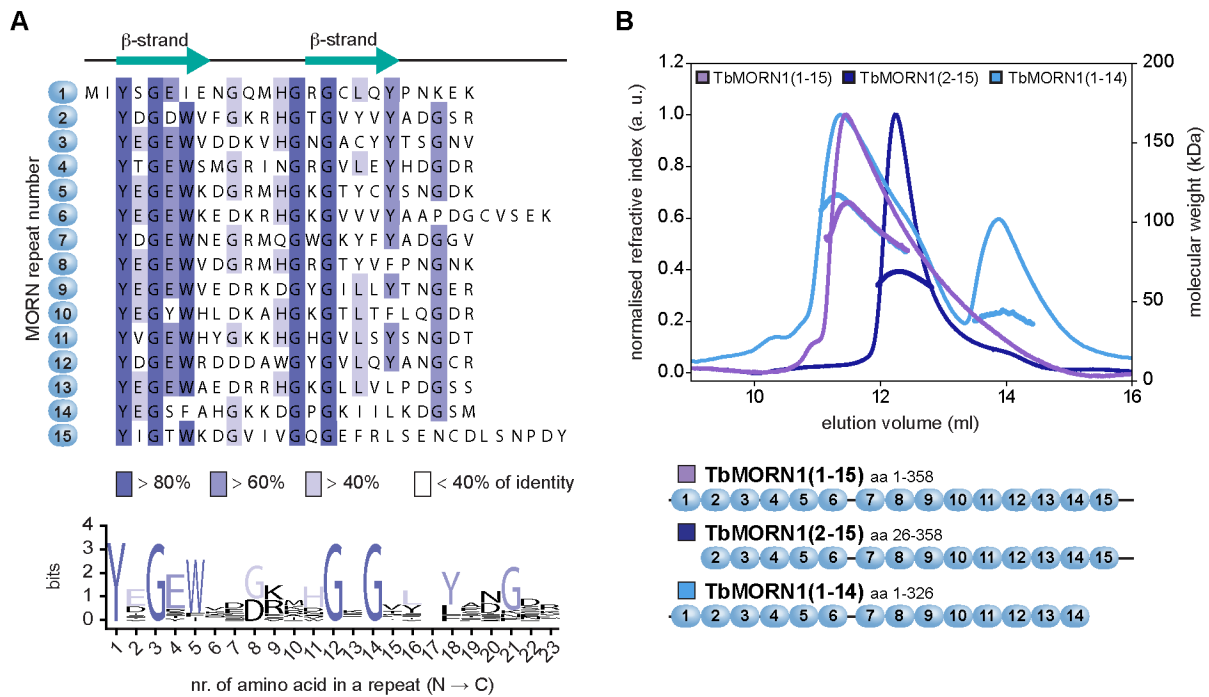


Figure 1. TbMORN1 primary structure and dimerisation. (A) Primary structure of TbMORN1, with individual MORN repeats shown in alignment, and coloured according to amino acid conservation. A schematic of the predicted secondary structure of each repeat is shown above the alignment. A consensus amino acid sequence of the individual MORN repeats from TbMORN1 based on the alignment is shown in the sequence logo. (B) TbMORN1 dimerises via its C-terminus. SEC-MALS profiles of TbMORN1(1-15), TbMORN1(2-15), and TbMORN1(1-14). Schematics are shown underneath. TbMORN1(1-15) tended to form high-order assemblies, whereas removal of the first MORN repeat resulted in a monodisperse dimer. Removal of the last MORN repeat in TbMORN1(1-14) resulted in a polydisperse mixture of higher-order assemblies, dimers, and monomers.

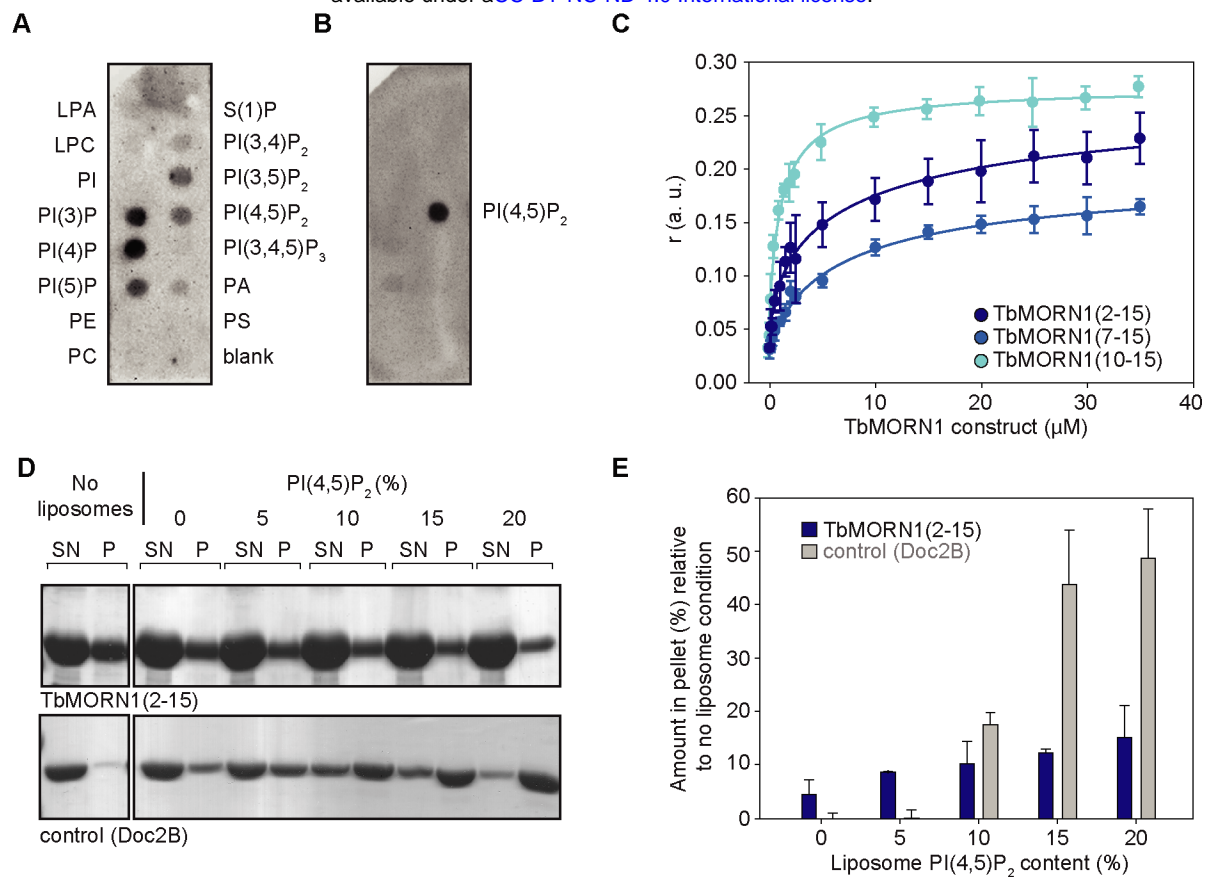


Figure 2. TbMORN1 interacts with phospholipids but not liposomes. (A) Purified recombinant TbMORN1 binds to multiple phospholipid species in protein-lipid overlay assays. PIP strips were incubated with purified recombinant TbMORN1(1-15) protein, and bound proteins were detected by immunoblotting with an anti-His tag antibody. Abbreviations: PI(n)P, phosphatidylinositol (n) phosphate; PA, phosphatidic acid; LPA, lysophosphatidic acid; LPC, lysophosphatidylcholine; PI, phosphatidylinositol; PE, phosphatidylethanolamine; PC, phosphatidylcholine; S(1)P, sphingosine-1-phosphate; PS, phosphatidylserine. Data were obtained from 3 independent experiments using 2 biological replicates; an exemplary blot is shown. (B) PIP strip overlaid with the PH domain of PLC δ , a positive control for PI(4,5)P₂ binding. Data were obtained from 3 independent experiments using 2 biological replicates; an exemplary blot is shown. The PIP strips presented here were exposed to the light source for the same time. (C) Fluorescence anisotropy measurements of 0.1 μM BODIPY TMR-PI(4,5)P₂ in the presence of TbMORN1(2-15), (7-15) and (10-15). All three truncations of TbMORN1 interacted with PI(4,5)P₂ with binding affinities in the low micromolar range. Data obtained from 3 independent experiments using 3 biological replicates, with 10 technical replicates for each experiment. Traces show mean values, bars are s.e.m. (D) Liposome co-sedimentation assay. POPC liposomes containing 0, 5, 10, 15 and 20% of porcine brain PI(4,5)P₂ were incubated with 10 μM TbMORN1(2-15). TbMORN1(2-15) was found in both pellet (P) and supernatant (SN) fractions but did not increase proportionally to PI(4,5)P₂ concentration. The positive control, Doc2B, bound PI(4,5)P₂ in a concentration-dependent manner, with a shift from SN to P fractions proportional to the increase in % of PI(4,5)P₂ present in the liposomes. Data were obtained from 2 independent experiments using 2 biological replicates; an exemplary blot is shown. (E) Quantification of the liposome pelleting assays. The amount of protein in the pellet fraction is presented relative to the amount present in the pellet fraction of the no liposome condition.

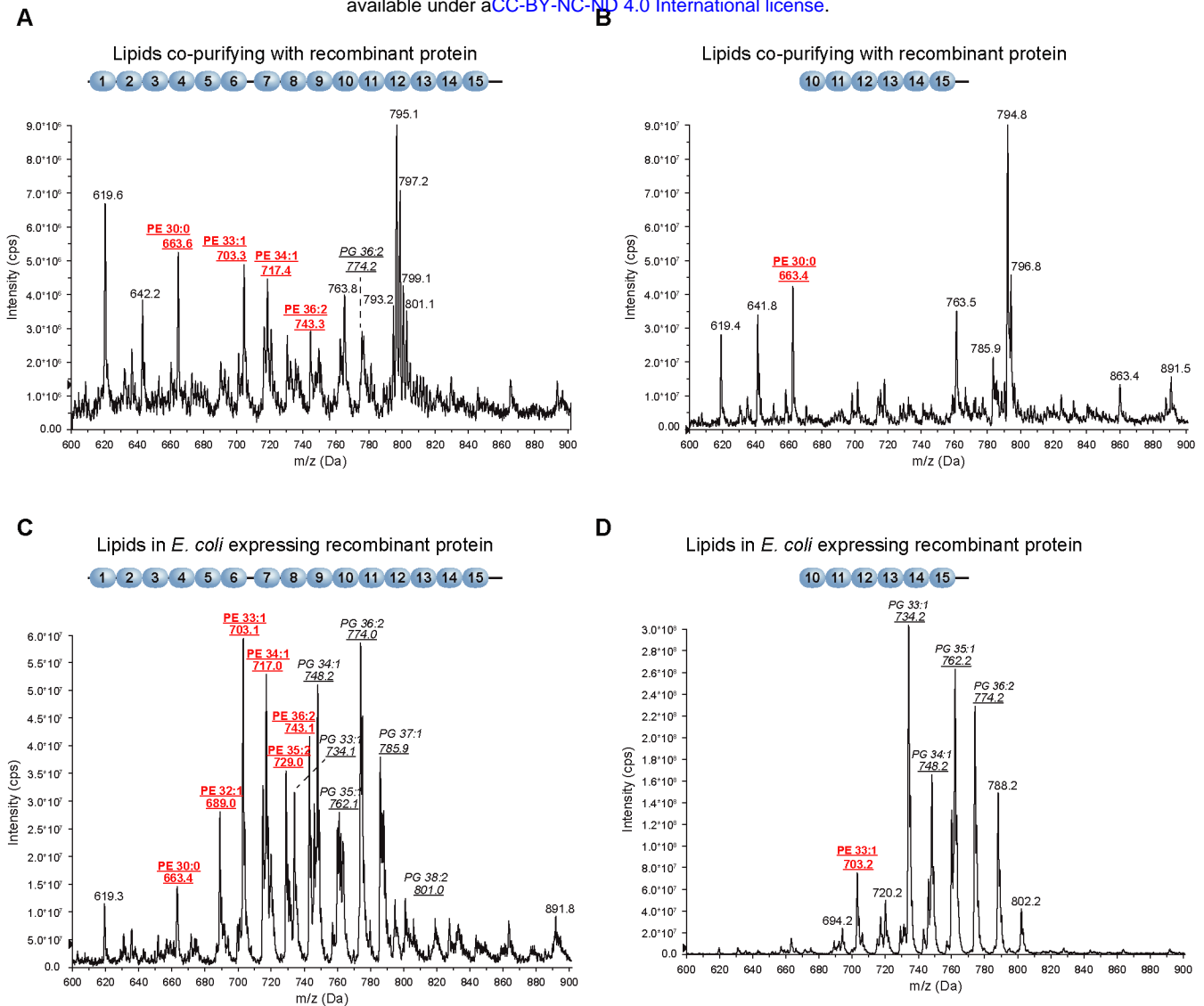


Figure 3. Recombinant TbMORN1 co-purifies with PE and increases *E. coli* PE levels. Negative ion mode survey scan (600-900 m/z) of lipid extracts from the indicated conditions. (A,B) Lipid extracts from purified recombinant TbMORN1(1-15) (A) and TbMORN1(10-15) (B). A large amount of PE co-purified with TbMORN1(1-15) but very little was associated with TbMORN1(10-15). (C,D) Lipid extracts from *E. coli* cells expressing the indicated constructs. (C) Cells expressing TbMORN1(1-15) had elevated PE levels. (D) Cells expressing TbMORN1(10-15) showed no changes to cellular lipid ratios compared to wild-type (empty vector control). In all cases, phospholipid identity was confirmed by daughter fragmentation and reported here. Schematics of the recombinant TbMORN1 constructs are shown above the traces.

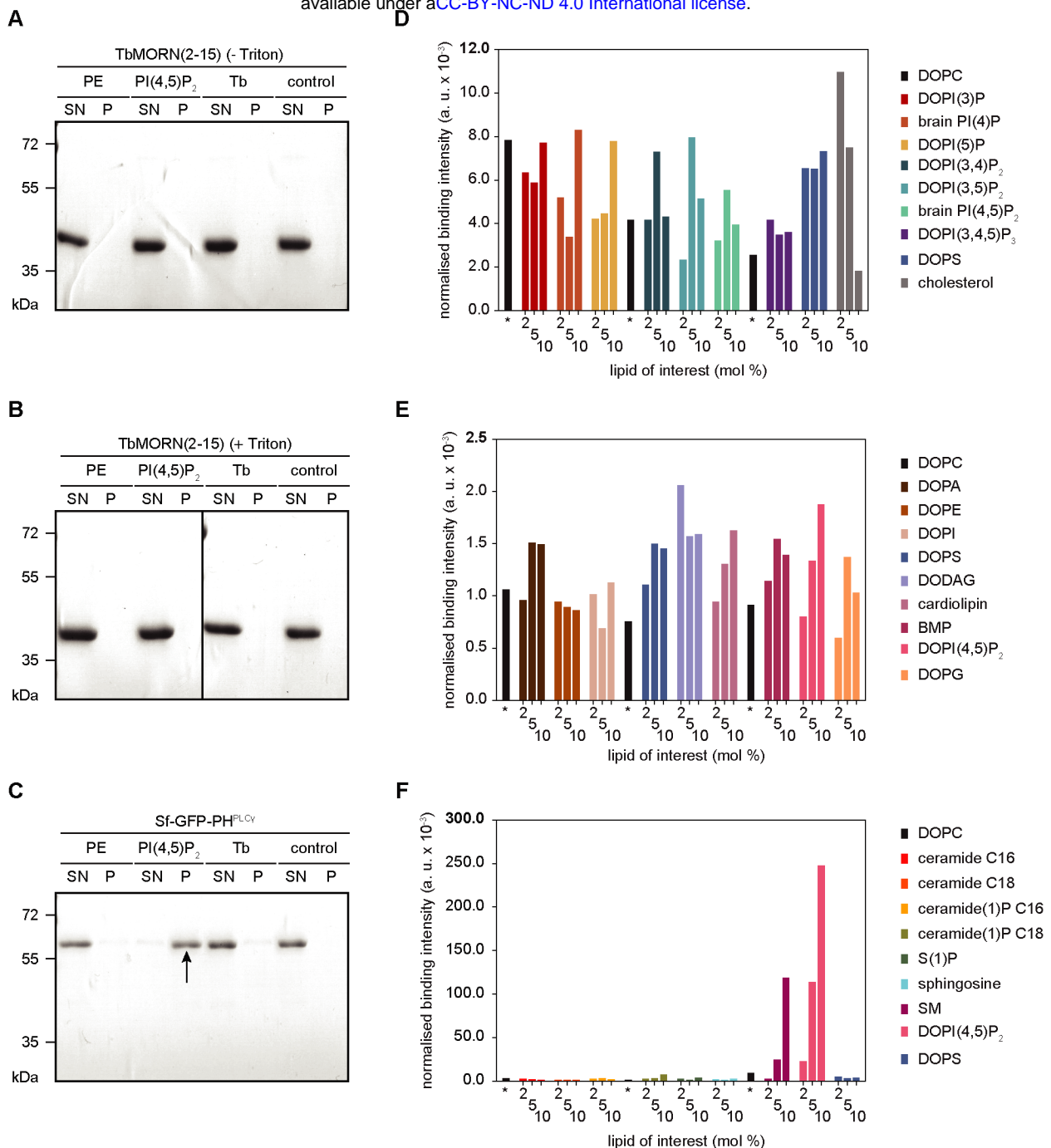


Figure 4. TbMORN1(2-15) does not bind to liposomes in vitro. (A-C) Liposome pelleting assays using sucrose-loaded vesicles (SLVs). His-TbMORN1(2-15) was purified in the absence (A) or presence (B) of Triton X-100 in the lysis buffer. The purified proteins were incubated with SLVs, which were then pelleted by centrifugation. Supernatant (SN) and pellet (P) fractions were analysed by SDS-PAGE using Coomassie staining. The SLVs were made from commercial lipids with an excess of either PE or PI(4,5)P₂, and also reconstituted from purified whole-cell trypanosome lipids (Tb). A no-SLV condition was included as an additional negative control. (C) The PH domains of PLC γ was used as a positive control for PI(4,5)P₂ binding. As expected, the PLC γ PH domain co-sedimented with PI(4,5)P₂-containing SLVs and was entirely present in the P fraction in this condition (arrow). The recombinant TbMORN1 proteins remained in the SN fraction in all conditions. (D-F) Liposome microarray analysis. Microchips carrying giant unilamellar vesicles (GUVs) with lipids of interest at three different concentrations (2, 5 and 10 mol %) were incubated with purified recombinant EGFP-TbMORN1(2-15). No significant binding was observed. (D) n (independent replicates) = 7; (E) n (independent replicates) = 3. (F) Microchip incubated with PLC- δ 1 PH domain. A specific and concentration-dependent binding between the PLC- δ 1 PH domain and DOPI(4,5)P₂ and SM was observed. DOPC, a carrier lipid, was used as an internal negative control of binding, as well as a marker for tracking positions of liposomes on a given microarray. n (independent replicates) = 1. Note the different scales on the y-axes of the three charts.

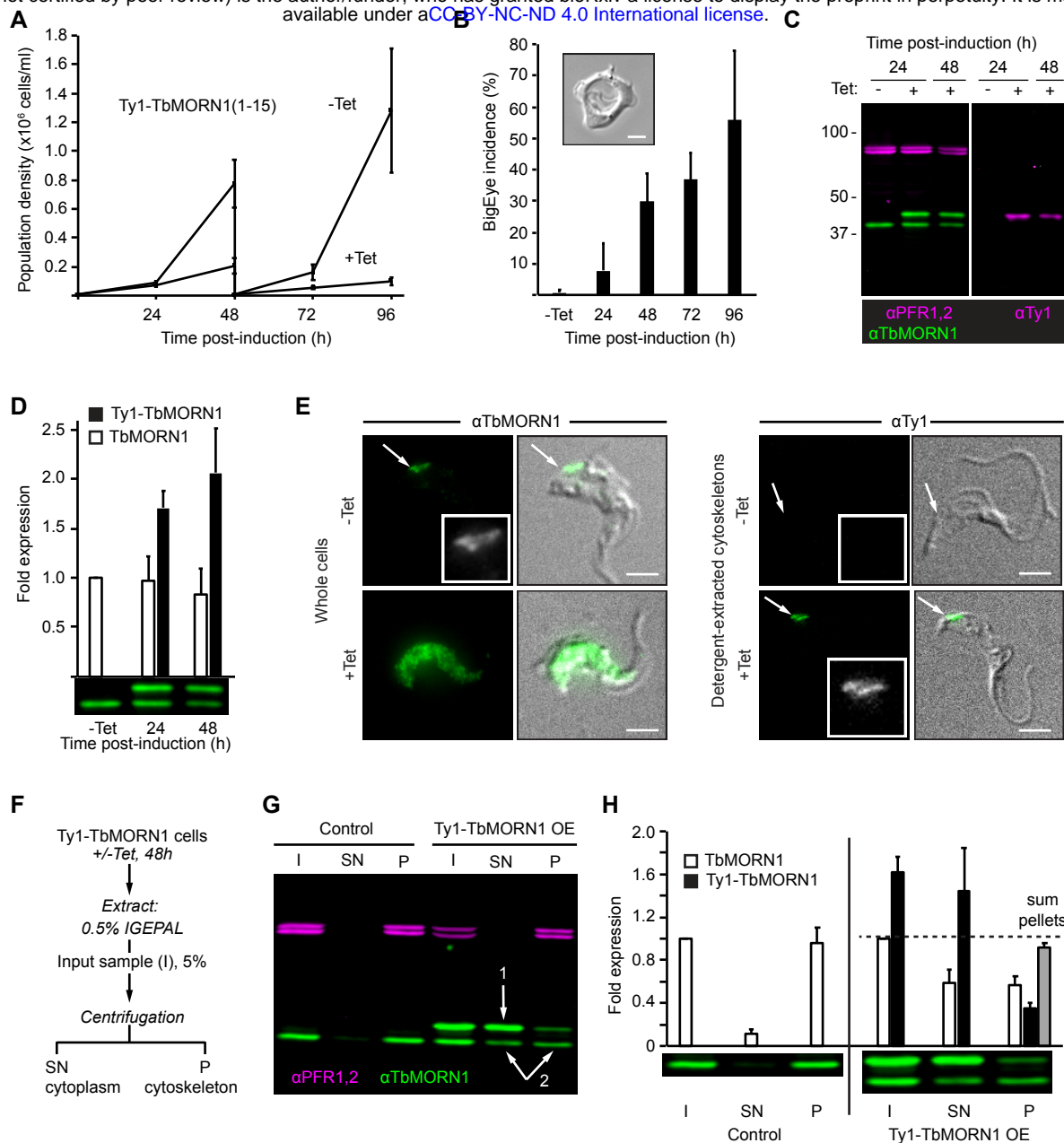


Figure 5. Overexpression of Ty1-tagged TbMORN1 causes a dominant negative phenotype. (A) Overexpression of Ty1-TbMORN1 is deleterious. Growth curves of control (-Tet) cells, and cells inducibly expressing Ty1-TbMORN1(1-15) (+Tet). Population density was measured every 24h, and the cultures split and reseeded at 48h. Data were compiled from 3 separate clones, each induced in 3 independent experiments; bars show mean \pm SD. (B) Overexpression of Ty1-TbMORN1 produces a BigEye phenotype. The incidence of BigEye cells was counted in control (-Tet) and Ty1-TbMORN1-expressing cells at the indicated timepoints. Data were compiled from 3 separate clones, each induced in 3 independent experiments; bars show mean \pm SD. The inset shows an example BigEye cell. Scale bar, 2 μ m. (C) Tight induction of Ty1-TbMORN1 expression. Whole-cell lysates were harvested from control (-Tet) and Ty1-TbMORN1-expressing cells (+Tet) at the indicated timepoints and probed with anti-TbMORN1 and anti-Ty1 antibodies. PFR1,2 were used as a loading control. At least three independent inductions were carried out for each clone; an exemplary blot is shown. (D) Quantification of overexpression. The levels of endogenous TbMORN1 and ectopic Ty1-TbMORN1 in immunoblots were normalised relative to the PFR1,2 signal. Data were compiled using 3 separate clones, each induced in at least two independent experiments; bars show mean \pm SD. (E) Ty1-TbMORN1 can localise correctly to the cytoskeleton. Whole cells or detergent-extracted cytoskeletons were fixed and labelled with anti-TbMORN1 or anti-Ty1 antibodies. The fluorescence signal is shown with the transmitted light image of the cell overlaid; inset shows the fluorescence signal from the antibody in greyscale. Results confirmed for 3 separate clones, exemplary images are shown. Scale bars, 2 μ m. (F) Schematic of the fractionation protocol. (G) Overexpression of Ty1-TbMORN1 displaces the endogenous protein from the cytoskeleton. Control and Ty1-TbMORN1-expressing cells were fractionated as shown in panel F and the I, SN, and P fractions were blotted. PFR1,2 was used as a marker for the cytoskeleton. Expression of Ty1-TbMORN1 was accompanied by a displacement of endogenous TbMORN1 from the insoluble (P) fraction into the soluble (SN) fraction (arrows 1,2). Equal fractions (5%) were loaded in each lane. 3 independent experiments using 3 separate clones were carried out; an exemplary blot is shown. (H) Quantification of the fractionation data. Bars show mean \pm SD.

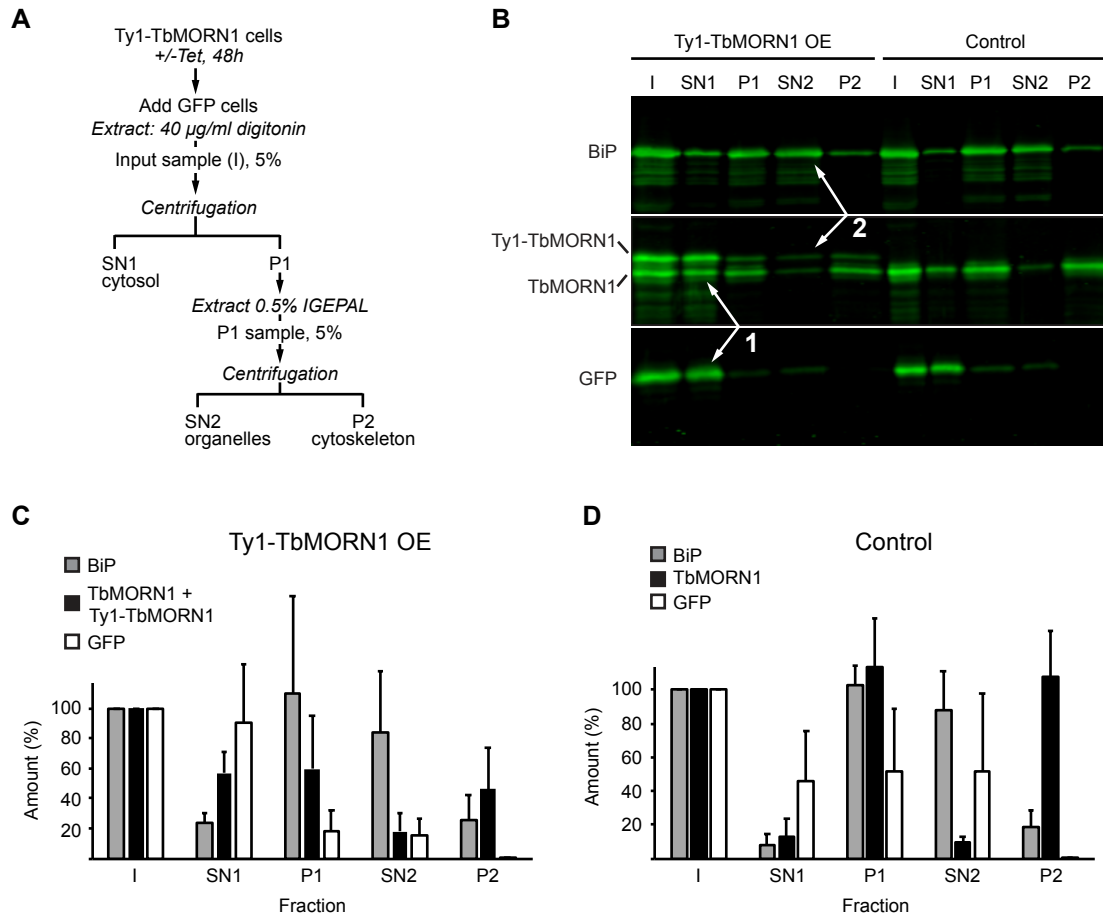


Figure 6. Overexpressed Ty1-TbMORN1 is predominantly cytosolic. (A) Schematic of the two-step fractionation scheme. (B) Immunoblots of fractions taken from control and Ty1-TbMORN1 overexpressing cells, using anti-BiP, anti-TbMORN1 and anti-GFP antibodies. Note that the membrane was cut into three strips for the immunoblot. Equal fractions (5%) were loaded in each lane. The overexpressed Ty1-TbMORN1 was predominantly extracted by digitonin and partitioned with the cytosolic GFP into the SN1 fraction (arrows 1). Very little of the remainder was subsequently extracted with non-ionic detergent into the SN2 fraction (arrows 2), with most partitioning into the cytoskeleton-associated P2 fraction. Three independent experiments were carried out using cells from three clones pooled together; an exemplary blot is shown. (C,D) Quantification of the immunoblots of the two-step fractionation. Data were compiled from three independent experiments, each using cells pooled from three separate clones. Bars show mean values + SD.

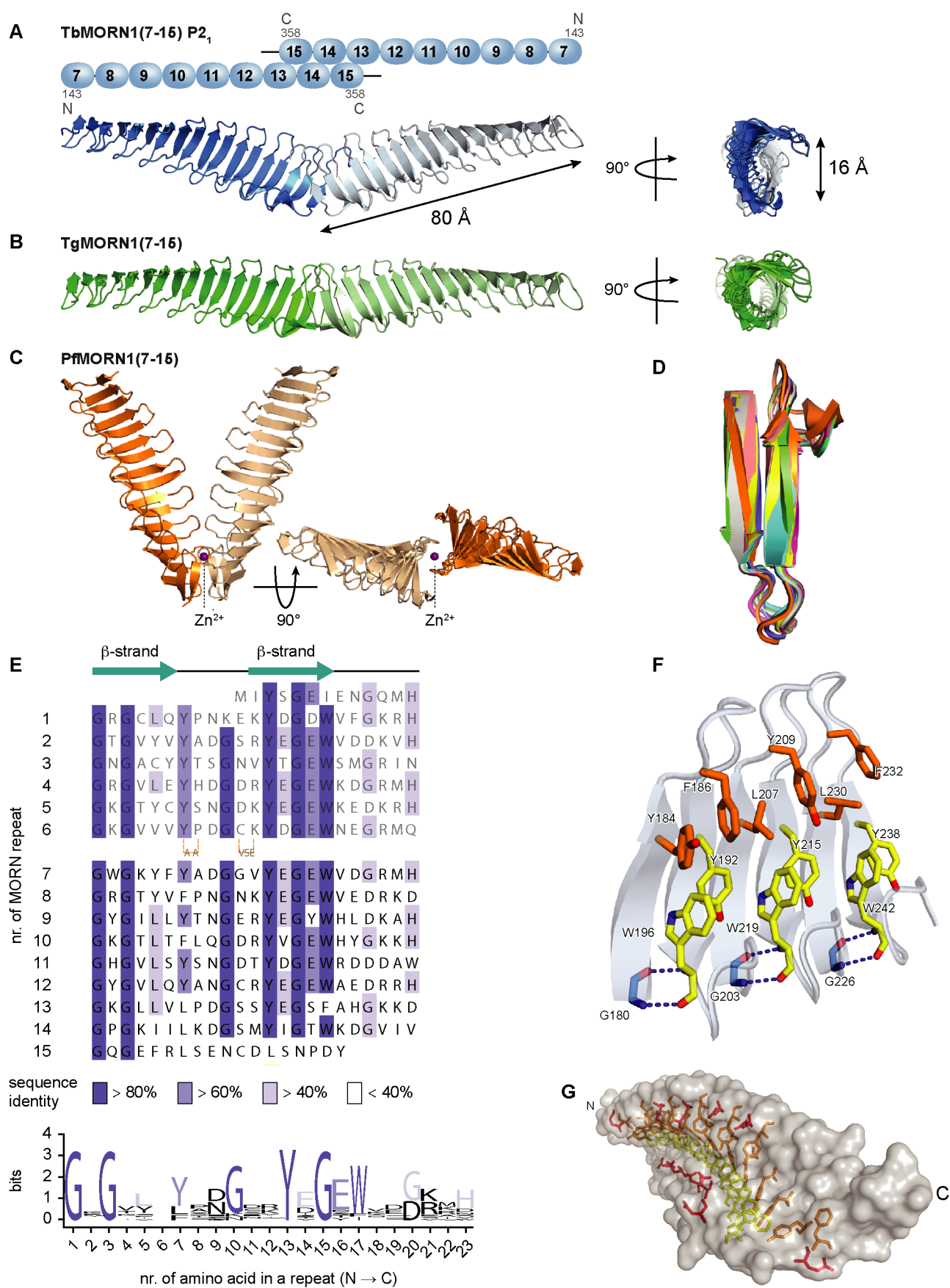


Figure 7. High-resolution structures of MORN repeat proteins and a structural redefinition of the MORN repeat. (A) Schematic depiction and crystal structure of the TbMORN1(7-15) dimer in its P21 crystal form. Amino acid numbers and N- and C-termini are indicated in the schematic. The crystal structure is shown in two orientations, with main dimensions indicated in Å. The structure contains 2 x 9 MORN repeats, and is an antiparallel homodimer with the subunits arranged in a splayed tail-to-tail configuration. The secondary structure consists of exclusively antiparallel beta-strands and peripherally positioned loops, which together form a longitudinal gutter through the middle of the protein. (B) Crystal structure of TgMORN1(7-15) shown in two orientations. The number of MORN repeats and the configuration is the same as for TbMORN1(7-15) in panel A. (C) Crystal structure of PfMORN1(7-15) shown in two orientations. The bound zinc ion is labelled. The structure contains 2x 9 MORN repeats, again in tail-to-tail configuration but with an overall V-shaped arrangement. (D) Alignment of all 9 TbMORN1(7-15) MORN repeats in the crystal structure reveals a high level of structural conservation. (E) A revised consensus MORN repeat sequence, based on the crystal structures. A new alignment of the MORN repeats in TbMORN1 is shown. Repeats 7-15 are present in the crystal structure; repeats 1-6 are inferred. Conservation of sequence identity is indicated by colour intensity. Each MORN repeat consists of a β -hairpin, built up of two 6-residue β -strands connected by a 5-residue loop. The β -hairpin is followed by a 6-residue loop that connects to the next MORN repeat. The new 23-residues long consensus MORN repeat starts with the GxG motif. (F) The tertiary structure of individual MORN repeats is stabilised by hydrogen bonds between the first G of the GxG motif and the W from the YEGEW motif. MORN repeat arrays are further stabilised by aromatic stacking between the highly conserved aromatic residues in the YEGEW and LxY motifs, and by T-shaped π -stacking interactions of the highly conserved Y of the YEGEW motif, which is sandwiched between the W residue of its own motif, and the W residue in the next YEGEW motif. (G) A single TbMORN1(7-15) subunit viewed at an oblique angle. The residues of the YEGEW and LxY motifs involved in aromatic stacking line the surface of the longitudinal gutter running through the middle of the protein.

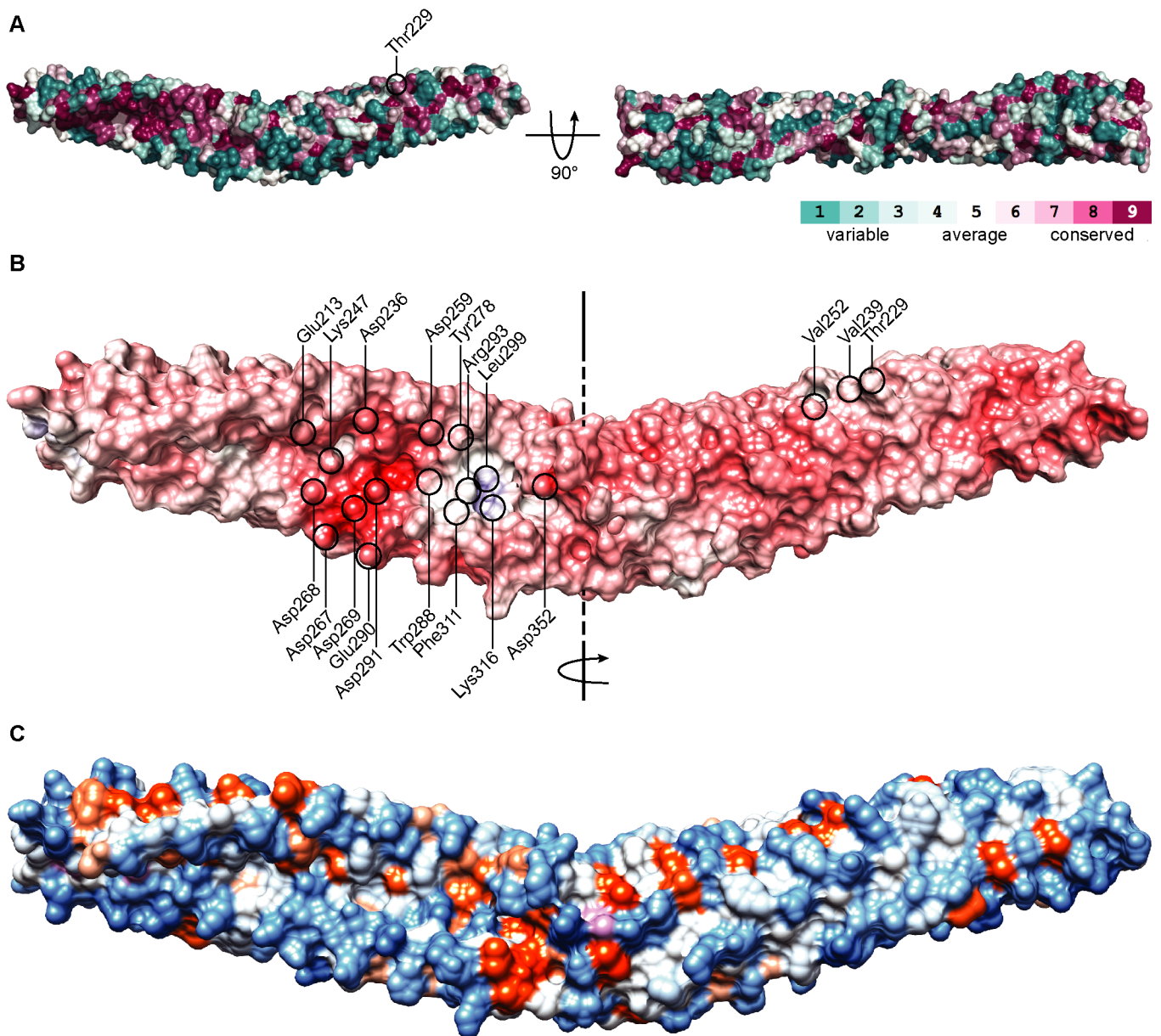
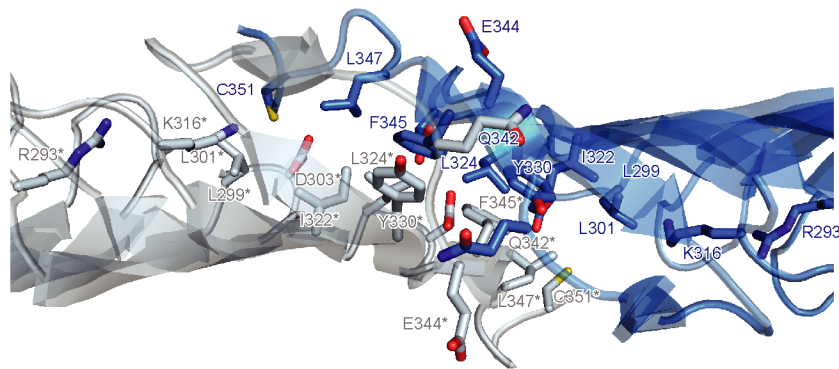
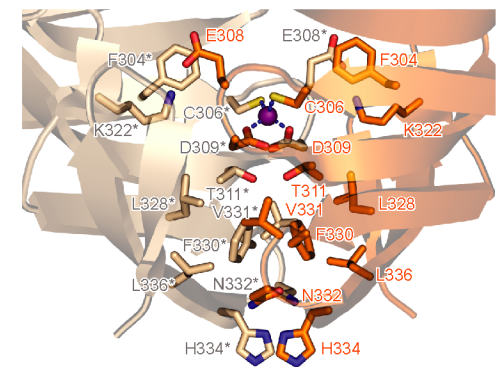


Figure 8. Conservation and properties of residues in TbMORN1(7-15). (A) Conservation map of the TbMORN1(7-15) P₂₁ crystal structure reveals a highly conserved stretch of residues along the gutter. The structure is shown in two orientations, with residues colour-coded according to the level of conservation. (B) An electrostatic map of TbMORN1(7-15) P₂₁. Colour scale: red = -13 kT; blue = +13 kT. Individual residues contributing to its surface electrostatics are labelled, namely those of the two negatively-charged loops building up a negative patch inside the gutter, and the residues contributing to a small positively-charged region close to the dimer interface. (C) Hydrophobic map of TbMORN1(7-15) P₂₁. Colour scale: blue = hydrophilic; orange = hydrophobic, pink = methionine residues.

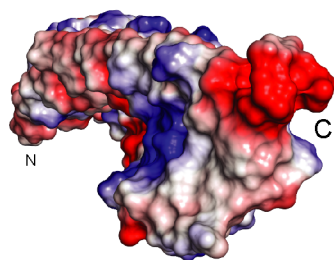
A TbMORN1(7-15) P2₁



B PfMORN1(7-15)



C TbMORN1(7-15)



TbMORN1(7-15) with K316A, R293A

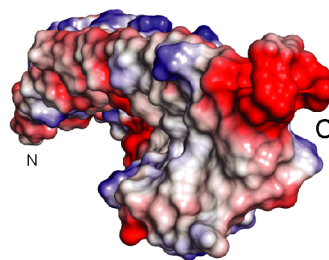


Figure 9. Dimerisation interfaces of TbMORN1(7-15) and PfMORN1(7-15). (A) The dimerisation interface of TbMORN1(7-15) P2₁ involves residues from MORN repeats 12-15, which stabilised the interface via aromatic π -stacking (Tyr330 and Phe345 from the respective subunits), hydrophobic interactions (Leu301, Leu347, Ile339, Ile322, Leu324), and additionally via hydrogen bonding interactions at the edges of the dimer interface. In comparison to the TbMORN1(7-15) C2 crystal structure, there are no disulphide bridges stabilising the dimerisation interface of TbMORN1(7-15) P2₁. (B) The dimerisation interface of the V-shaped PfMORN1(7-15) dimer is smaller and is additionally stabilised by the incorporation of a structural Zn²⁺ ion, which is tetrahedrally coordinated by Cys306 and Asp309 residues from each respective subunit. Thr311 holds the side chain of Asp309 in the appropriate orientation. The dimer interface is additionally stabilised by symmetric hydrogen bonding between the Thr311 pair, aromatic stacking between the Phe330 pair, a hydrophobic cluster formed by Leu328, Val331 and Leu336, two salt bridges between Lys322 and Glu308 from the respective subunits, anion- π interaction of a side chain of Glu308 with Phe304, and a combination of aromatic stacking (His334 pair) and polar interactions (His334, Asn332) at the vertex of the dimer. (C) An electrostatic map calculated for a single subunit of TbMORN1(7-15). The structure on the right shows the predicted effect of two point mutations, R293A from MORN repeat 13, and K316A from MORN repeat 14. The mutations are expected to result in the loss of a positively-charged patch close to the dimer interface, and consequently disrupt the dimerisation of the TbMORN1(2-15) constructs.

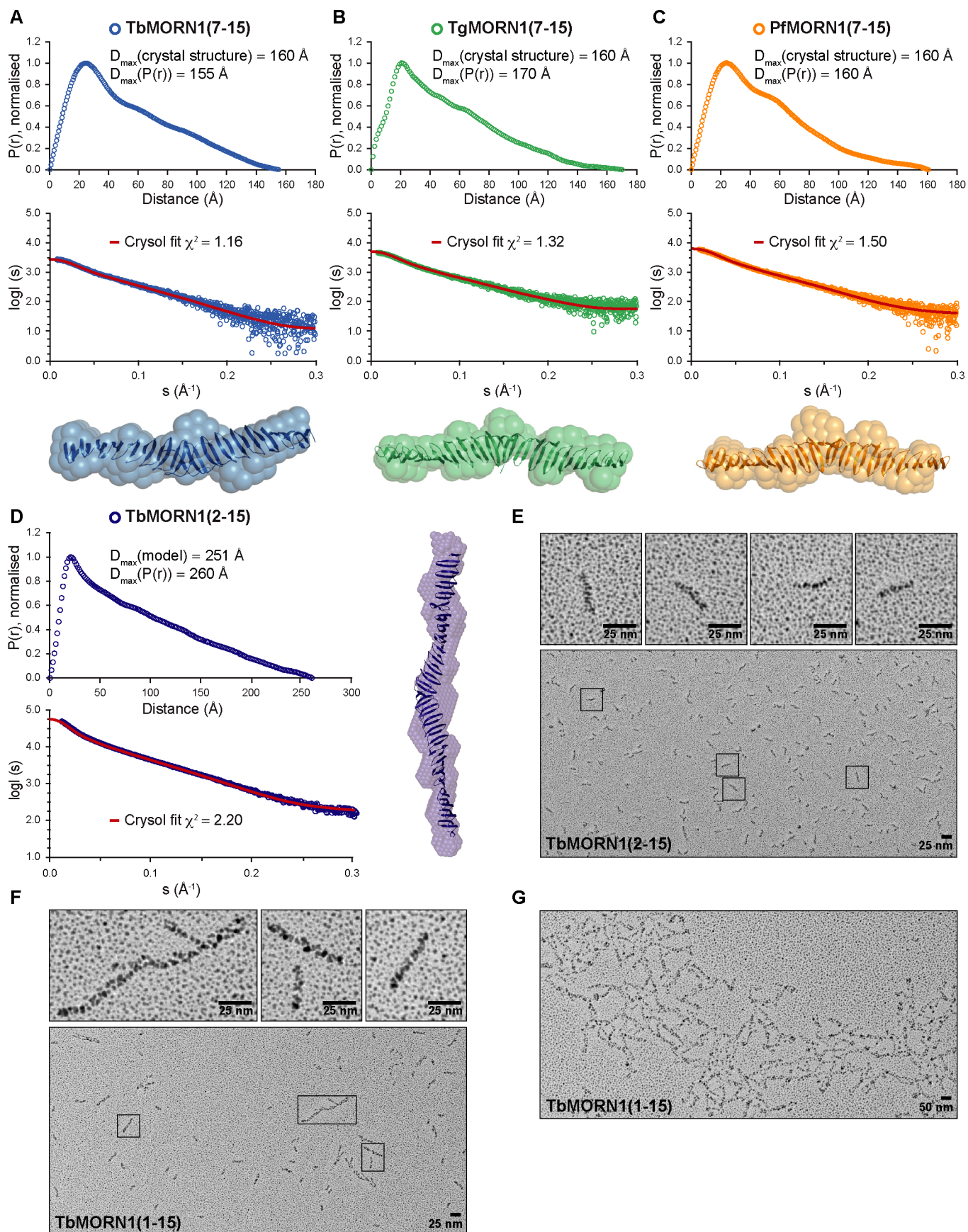


Figure 10. MORN1 proteins form extended dimers in solution. (A-D) SAXS experiments on TbMORN1(7-15) (A), TgMORN1(7-15) (B), PfMORN1(7-15) (C), and TbMORN1(2-15) (D). For each respective protein, the results include a $P(r)$ plot with derived experimental D_{max} value compared with a D_{max} value derived from the structure, an experimental SAXS scattering data with a fit calculated by the Crysol programme, and a SAXS-based ab initio molecular envelope. In the case of TbMORN1(2-15), the theoretical D_{max} value was derived from a structural model, which was generated by spiking the TbMORN1(7-15) structure with additional structures of individual TbMORN1(7-15) subunits. (E-G) EM with rotary shadowing of TbMORN1(2-15) and full-length TbMORN1. (E) TbMORN1(2-15) forms a homogenous population of extended dimers of approximately 25 nm in length (see insets for individual examples). (F) Full-length TbMORN1 is heterogeneous and includes rare filaments of 175-200 nm in length (first inset) and individual dimers (second and third inset). (G) Large oligomers of full-length TbMORN1 assembled in a mesh-like structure. Magnification, 71,000x; scale bars, 25 nm, 50 nm as indicated. n (independent replicates) = 2, n (biological replicates) = 2.

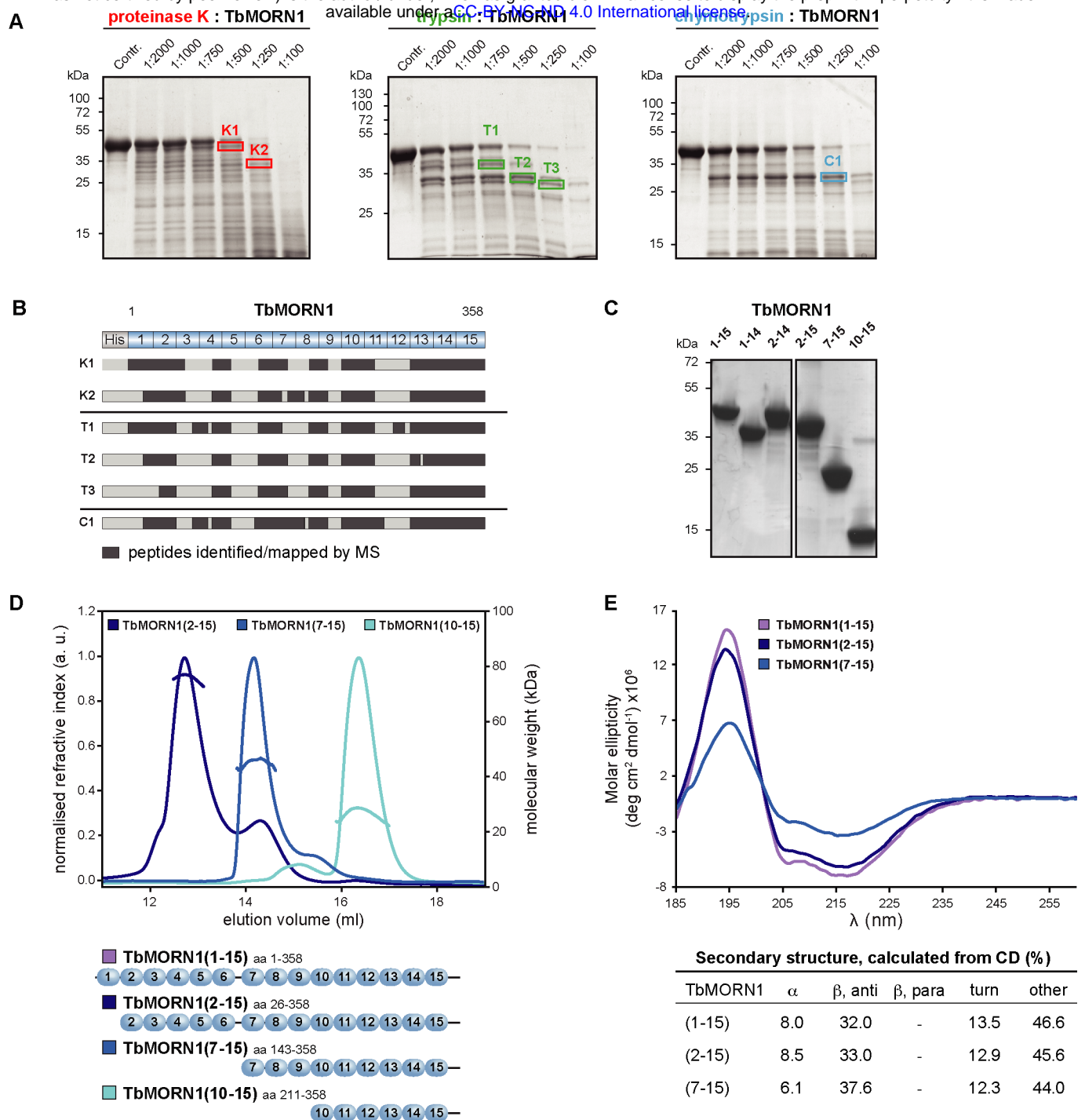


Figure S1. Low-resolution structural analysis of TbMORN1. (A) Full-length TbMORN1 with an N-terminal HisTag was subjected to limited proteolysis using proteinase K (red), trypsin (green), and chymotrypsin (cyan) at protease:protein ratios (w/w) as indicated on each panel. Samples were resolved by SDS-PAGE and selected bands (labelled boxes) corresponding to proteolytic products were excised and analysed by mass spectrometry. Control (Contr.) corresponds to protein without protease treatment. (B) Mass spectrometry analysis of the excised proteolytic products indicated in panel A. Peptides identified and mapped by mass spectrometry are shown as dark grey boxes; a schematic of the full-length construct is shown above, with individual MORN repeats labelled. Note that the proteolytic products show progressive degradation from their N-termini, while the C-terminal part is stable. (C) Coomassie-stained SDS-PAGE gel showing purified recombinant TbMORN1 truncations. (D) SEC-MALS traces of TbMORN1 (2-15), (7-15), and (10-15). Chromatographic separation was done using a Superdex 200 Increase 10/300 GL column. The three proteins all eluted as dimers. Schematics are shown underneath. (E) Far-UV CD profiles of TbMORN1, TbMORN1(2-15) and (10-15). A positive peak at 195 nm and a negative one at 218 nm demonstrated that the constructs are all β -proteins. The secondary structure content predictions for each construct were calculated in BeStSel and are shown below the CD graph.

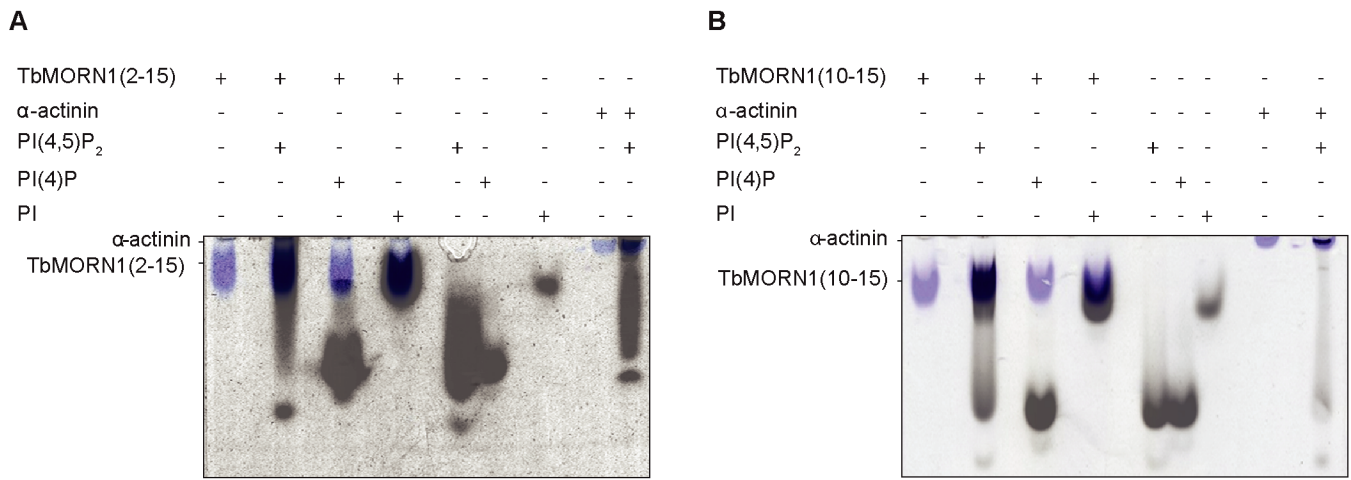


Figure S2. TbMORN1 interacts with PI(4,5)P₂ in native gel bandshift assays. (A) Native gel electrophoresis of TbMORN1(2-15) and (B) TbMORN1(10-15) in the presence and absence of PI(4,5)P₂, PI(4)P and PI, all labelled with Bodipy TMR fluorescent dye. α -actinin served as a positive control of PI(4,5)P₂ binding. Data obtained from two independent experiments, each using a different biological replicates.

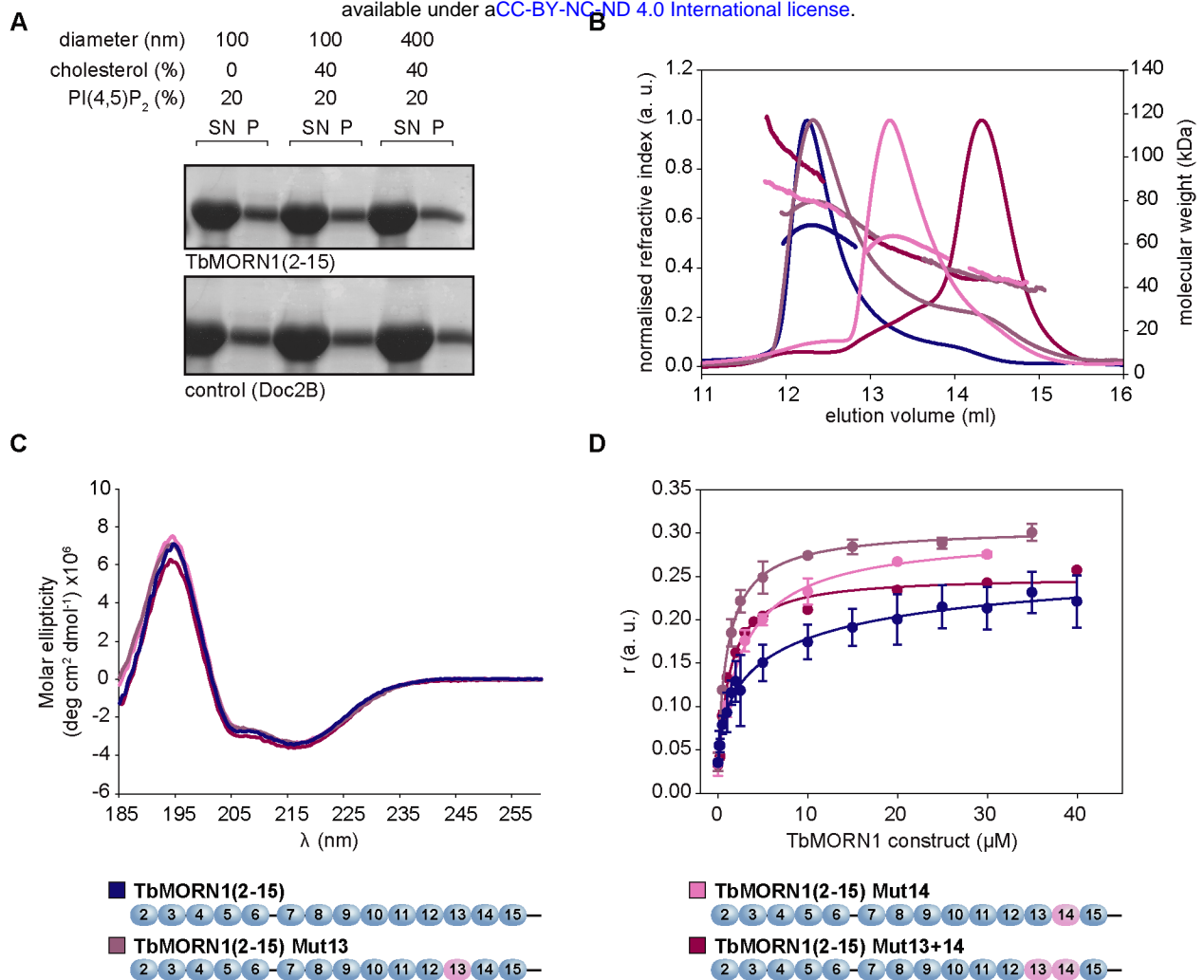
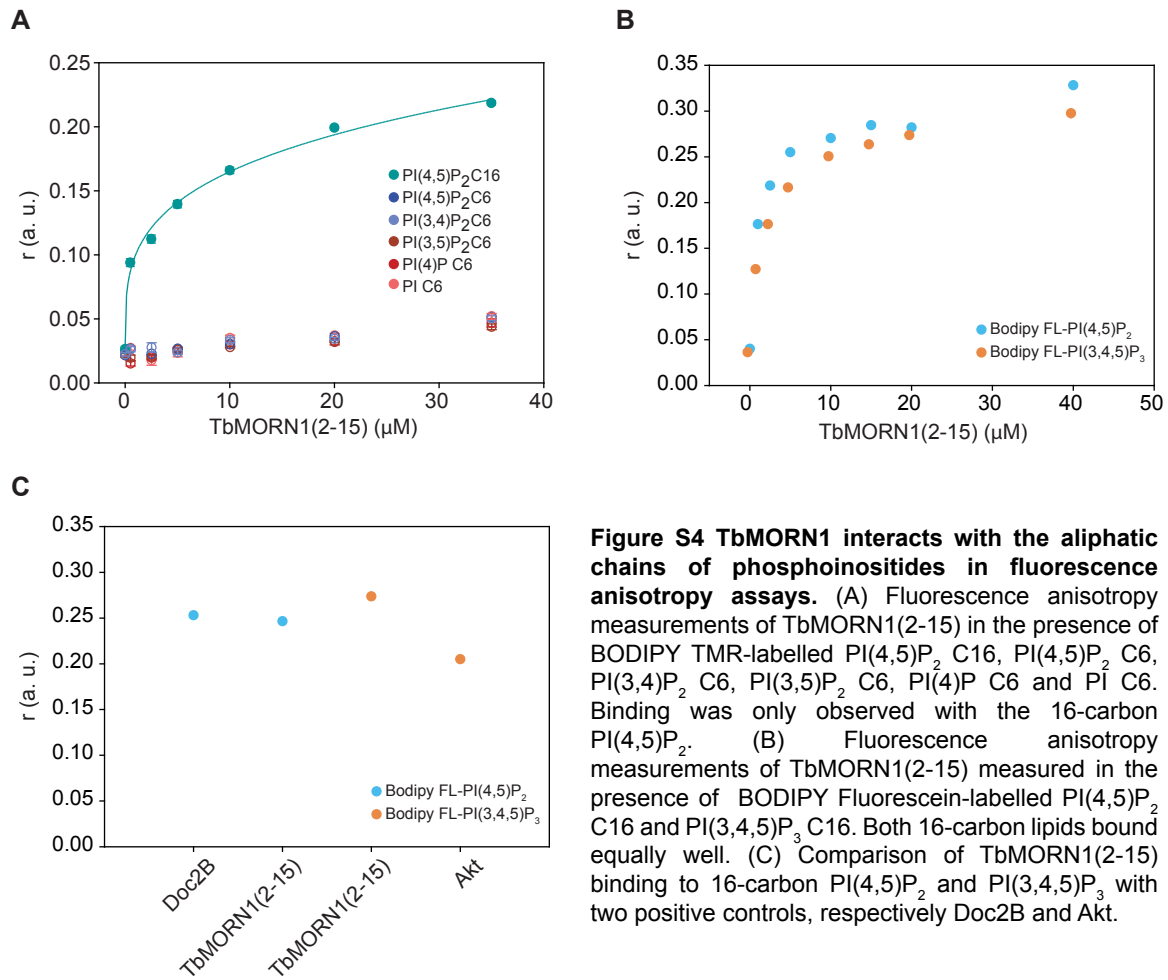


Figure S3. Mutagenesis of putative PI(4,5)P₂ binding sites in TbMORN1 has no effect on binding. (A) Liposome co-sedimentation assay performed on TbMORN1(2-15) in the presence of POPC liposomes containing 20% of porcine brain PI(4,5)P₂ and 0 or 40% cholesterol. The excess cholesterol was expected to promote local high concentrations of PI(4,5)P₂ on the surface of the liposomes. To assay for the effect of curvature, two batches of liposomes containing 20% PI(4,5)P₂ and 40% of cholesterol were tested, with the diameter of the liposomes being either 100 or 400 nm. No significant co-sedimentation of TbMORN1(2-15) and PI(4,5)P₂-containing liposomes was observed. The positive control, 10 μM Doc2B was predominantly found in the pellet (P) fractions. (B) SEC-MALS profiles of TbMORN1(2-15) and its mutagenised variants. Residues comprising the putative PI(4,5)P₂-binding sites in MORN repeats 13 and 14 were mutated to alanines. Mutagenesis of repeat 13 (Mut13) did not result in any change to the dimeric status of the protein. However, mutagenesis of repeat 14 (Mut14) resulted in a mixture of monomers and dimers being eluted, while mutagenesis of both repeats (Mut13+14) resulted in monomeric protein. (C) Far-UV CD profiles of TbMORN1(2-15) and its putative PI(4,5)P₂-binding mutants. The constructs remained β-proteins despite the site-directed mutagenesis. (D) Fluorescence anisotropy measurements of TbMORN1(2-15) and its putative PI(4,5)P₂-binding mutants, measured in the presence of 0.1 μM BODIPY TMR-PI(4,5)P₂. All constructs showed good interaction with the fluorophore-conjugated PI(4,5)P₂.



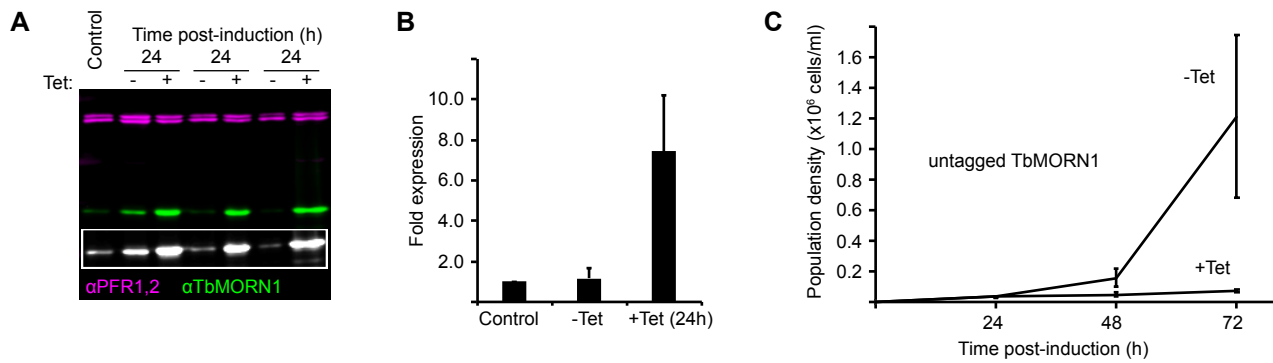


Figure S5. Overexpression of untagged TbMORN1 causes a dominant negative phenotype. (A) Inducible overexpression of untagged TbMORN1. Immunoblot of whole-cell lysates from three separate clones overexpressing untagged TbMORN1 from an ectopic locus. TbMORN1 was detected using anti-TbMORN1 antibodies; anti-PFR1,2 antibodies were used as a loading control. Inset shows a greyscale image of the TbMORN1 channel with enhanced levels so the endogenous protein is visible. Three separate clones were assayed, each in three independent experiments; an exemplary blot is shown. One of the three clones appeared to have slightly leaky expression, with TbMORN1 levels in the -Tet condition being higher than controls. (B) Quantification of overexpression. TbMORN1 levels in control, uninduced (-Tet) and induced (+Tet) were normalised relative to the loading control and expressed relative to the control cells. Approximately 7-fold overexpression was achieved relative to control cells. Data were obtained from blots using 3 separate clones, each induced in 3 independent experiments. Bars show mean + SD. (C) Overexpression of untagged TbMORN1 is deleterious. Uninduced (-Tet) and TbMORN1 overexpressing (+Tet) cells were assayed at 24 h intervals in a 3-day timecourse. Data were obtained from blots using 3 separate clones, each induced in 3 independent experiments. Mean +/- SD.

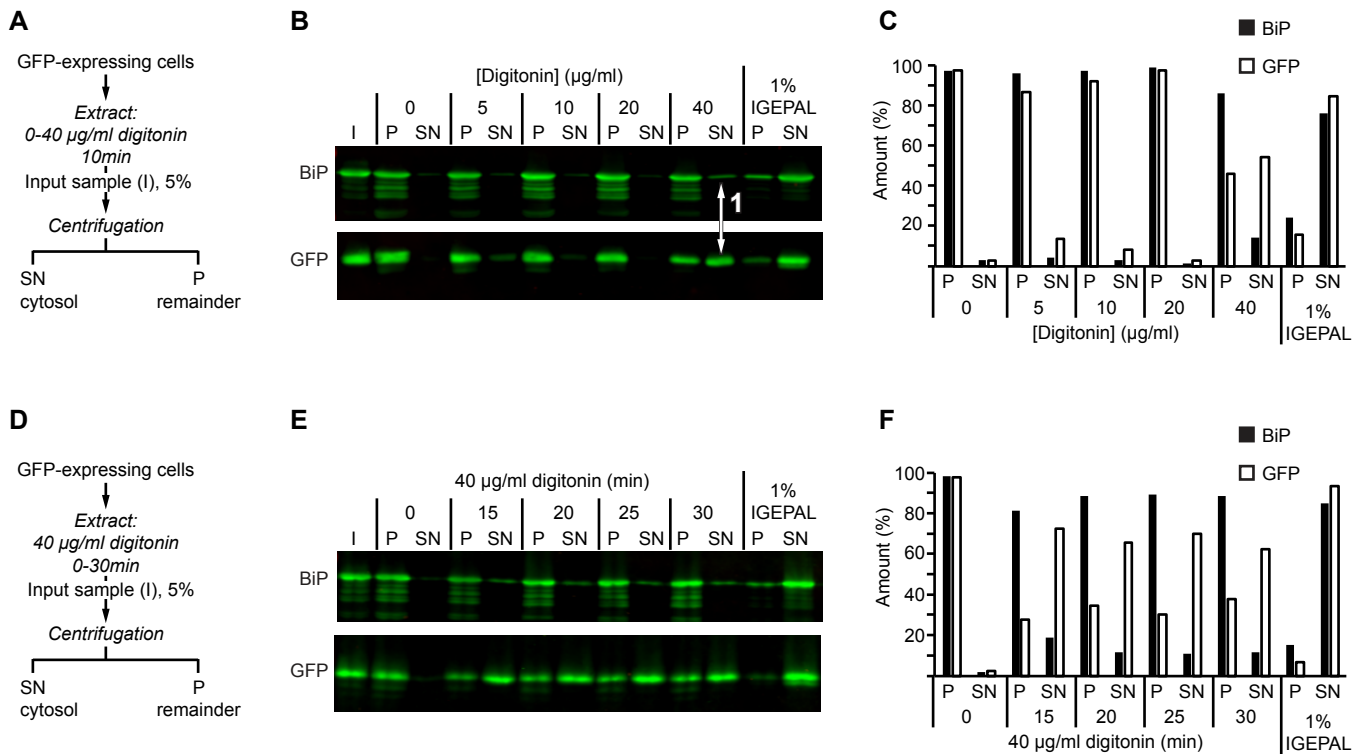
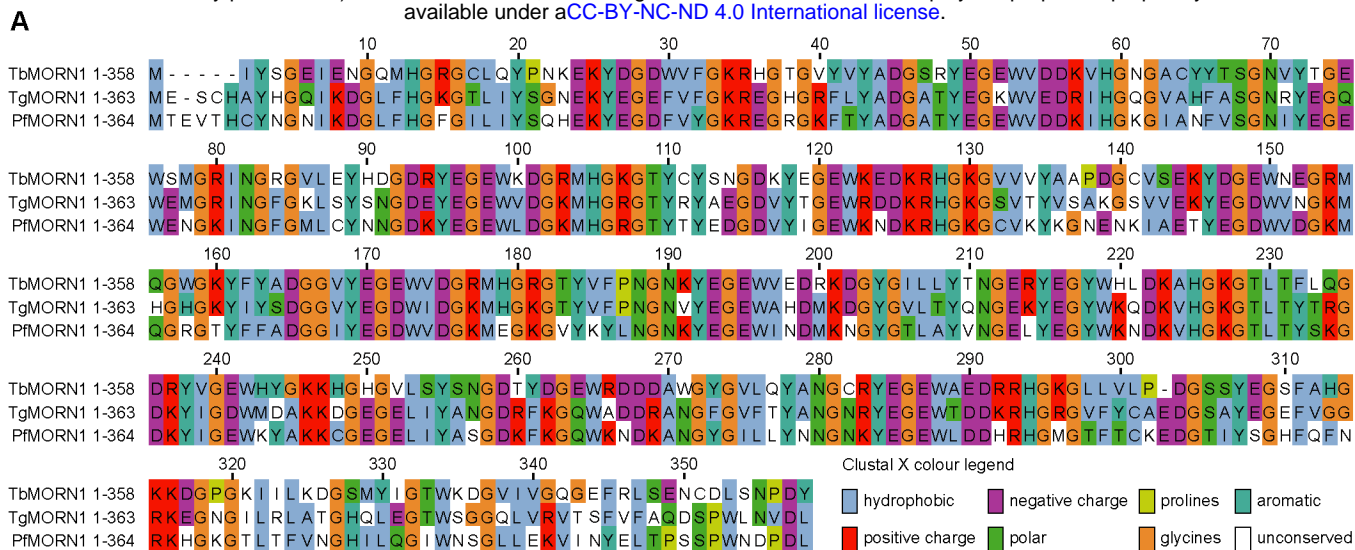
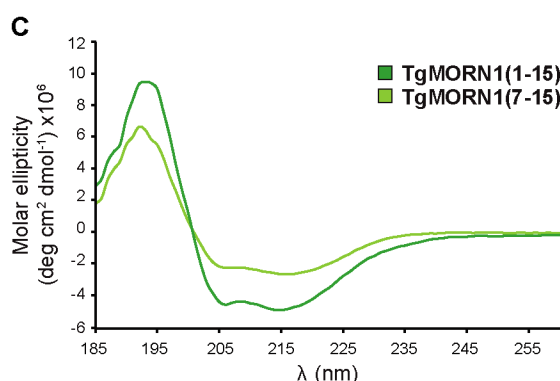


Figure S6. Optimisation of digitonin fractionation. (A) Schematic of the one-step fractionation scheme. Cells expressing cytosolic GFP were incubated in increasing concentrations of digitonin for 10 min prior to separation of fractions by centrifugation. Equal fractions (5%) were then blotted with antibodies specific for GFP and the endoplasmic reticulum chaperone BiP. (B) At 40 µg/ml digitonin, good solubilisation of GFP is achieved with only negligible solubilisation of BiP (arrow 1). Both proteins are efficiently solubilised using 1% IGEPAL as a positive control. Multiple independent experiments were carried out; an exemplary blot is shown. Note that the membrane was cut into strips prior to blotting, but the samples shown are from the same experiment. (C) Quantification of the immunoblot shown in B. (D, E, F) As per panels A-C, but with a constant 40 µg/ml digitonin concentration and considering the effect of varying incubation time (0-30 min).



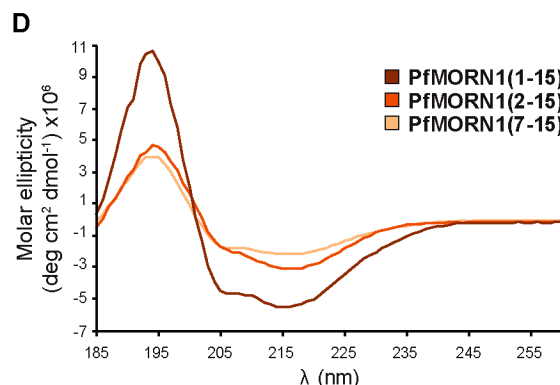
B
Comparison of MORN1 proteins and % of their sequence identity

<i>T. brucei</i> / <i>P. falciparum</i>	54
<i>T. brucei</i> / <i>T. gondii</i>	57
<i>P. falciparum</i> / <i>T. gondii</i>	65



Secondary structure, calculated from CD (%)

TgMORN1	α	β, anti	β, para	turn	other
(1-15)	5.3	30.8	0.8	13.0	50.1
(7-15)	4.8	42.3	-	11.8	41.1



Secondary structure, calculated from CD (%)

PfMORN1	α	β, anti	β, para	turn	other
(1-15)	6.4	29.8	1.9	13.8	48.1
(2-15)	6.2	35.7	-	13.4	44.7
(7-15)	6.6	32.6	1.0	12.0	47.8

Figure S7. Comparison of MORN1 proteins, and secondary structure analysis of apicomplexan MORN1s. (A) Amino acid sequence alignment of MORN1 proteins from *Trypanosoma brucei*, *Toxoplasma gondii* and *Plasmodium falciparum*. The number of amino acids in each protein is indicated, amino acid numbers in the alignment are those for TbMORN1. The alignment is coloured according to the amino acid properties. (B) Pairwise comparison of percentage sequence identity between the three proteins. (C) Far-UV CD measurements obtained for TgMORN1(1-15) and TgMORN1(7-15). The secondary structure content predictions for each of the measured proteins were calculated in BeStSel and are shown below the CD graph. (D) As (C), but PfMORN1(1-15), (2-15) and (7-15). Like TbMORN1, TgMORN1 and PfMORN1 are also all-β proteins.

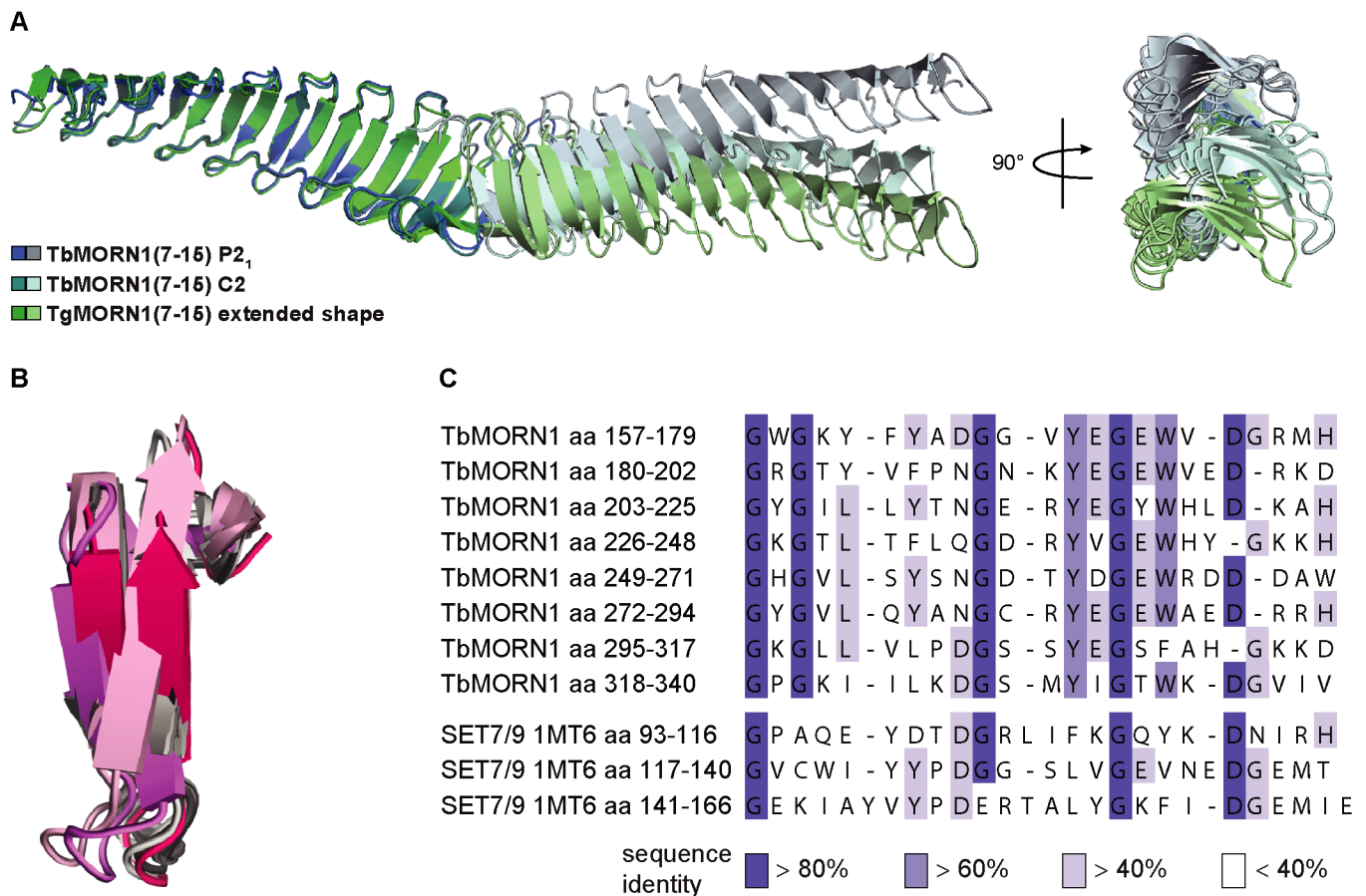
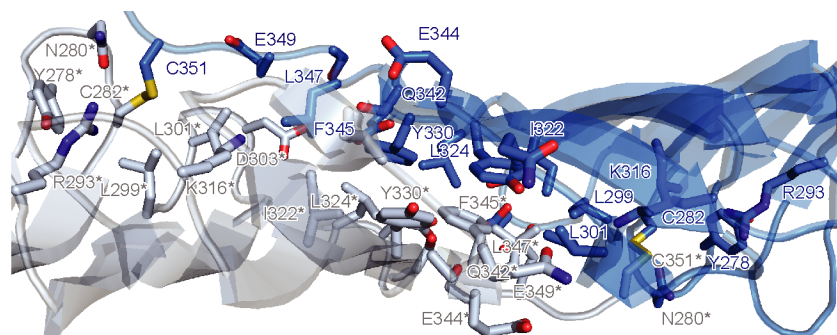
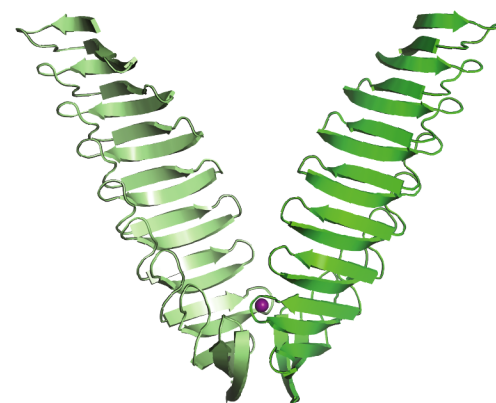


Figure S8. Comparison of MORN1 extended dimers, and with SETD7. (A) TbMORN1(7-15) P₂₁, TbMORN1(7-15) C₂, and TgMORN1(7-15) extended dimers superimposed on each other, and displayed in two orientations. In contrast to the other two proteins, the P₂₁ crystal structure of TbMORN1(7-15) displays a bend of approximately 30° among the subunits. (B) TbMORN1(7-15) MORN repeats superimposed on three MORN repeats from SETD7 (SET7/9). Alignment of the three MORN repeats from SETD7 with MORN repeat 7 from the TbMORN1(7-15) crystal structure over 22-23 aligned C-atoms yielded rmsd values of 2.3, 1.5 and 1.9 Å respectively. (C) Sequence alignment of MORN repeats from the TbMORN1(7-15) crystal structure with three MORN repeats from SETD7. The first Gly residue is conserved in all MORN repeats of TbMORN1(7-15) and SETD7 structures.

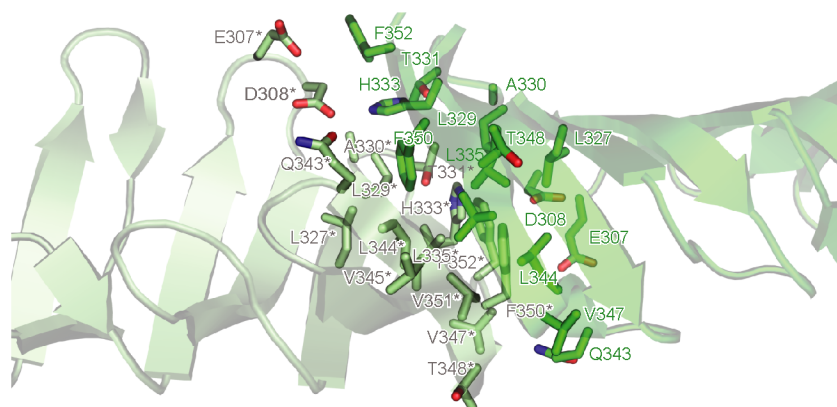
A TbMORN1(7-15) C2



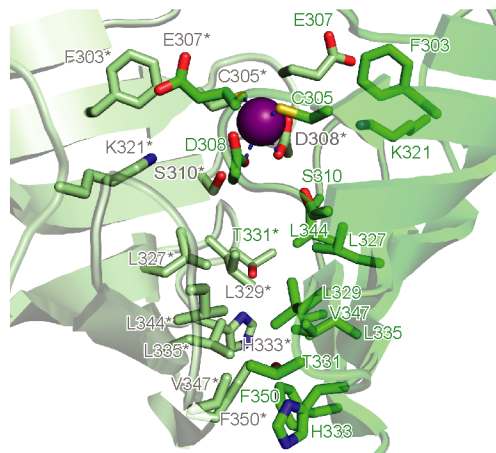
B TgMORN1(7-15)



C TgMORN1(7-15) extended dimer



D TgMORN1(7-15) V-shaped dimer



E SAXS - Kratky plots

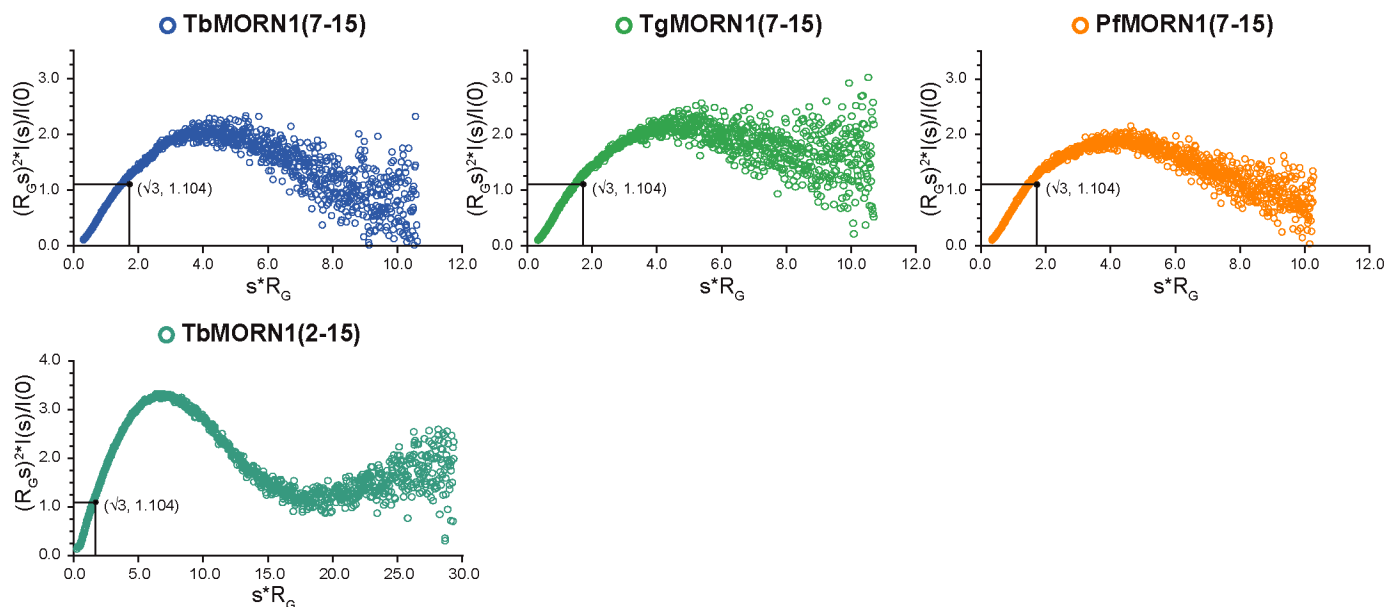


Figure S9. MORN dimer interfaces and SAXS analysis of proteins in solution. (A) Dimer interface of TbMORN1(7-15) C2 crystal form. In comparison to the P2₁ form, the dimer interface of C2 structure is broader, and is additionally stabilised by two disulphide bridges formed between Cys351 at the C-terminus of repeat 15 and Cys282 from the β -hairpin loop of repeat 12. (B) Crystal structure of the TgMORN1(7-15) V-shaped dimer, incorporating Zn²⁺ in its dimerisation interface. (C) Dimer interface of the TgMORN1(7-15) extended dimer, which utilises residues from MORN repeats 13-15. In contrast to TbMORN1(7-15), where the dimerisation interface is centred around aromatic stacking, a hydrophobic core plays a crucial role in the dimer interface of extended TgMORN1(7-15). Leu327, Leu329, Leu335, Leu344, Val345, Val347, Phe350 and Phe352 are part of this hydrophobic core. The dimer is stabilised by a single salt bridge formed between Asp308 of one, and His333 of the second subunit. This salt bridge is further stabilised by two hydrogen bonds between the main-chain nitrogen of Val345 and a carbonyl oxygen of Val347 of respective subunits. (D) Dimer interface of the TgMORN1(7-15) V-shaped dimer. Cys305 and Asp308 incorporate a structural Zn²⁺ ion, which stabilises the somewhat smaller dimerisation interface of this protein. Although its dimerisation interface is very similar to that of PfmORN1(7-15), it lacks the aromatic core of PfmORN1(7-15). The latter is replaced by a series of unique aromatic stacking interactions at the protein's vertex, these being contributed by a pair of Phe350 residues, sandwiched between a pair of His333 residues. (E) Kratky plots derived from SAXS analysis of TbMORN1(7-15), TgMORN1(7-15), PfmORN1(7-15), and TbMORN1(2-15). The shape of the plots suggests an elongated shape of the dimers in solution.

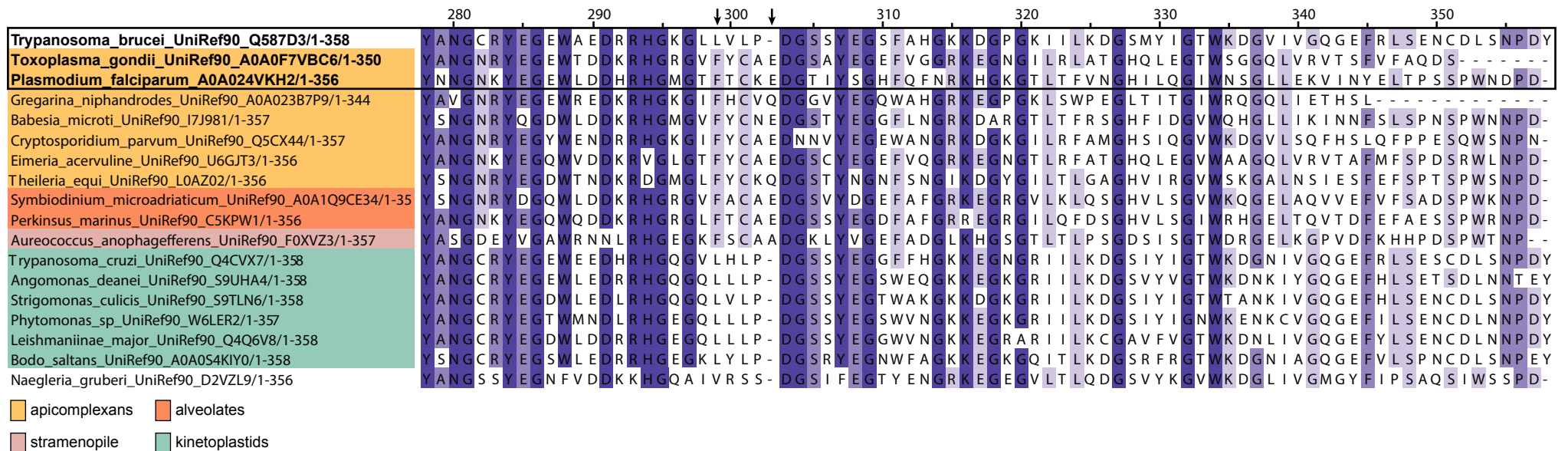


Figure S10. Conservation of residues for formation of V-shaped dimers in Apicomplexa and related clades. Amino acid sequence alignment of the C-termini of TbMORN1, TgMORN1, PfmORN1, and fifteen other MORN repeat-containing proteins from related taxa. Amino acid numbers are given according to the TbMORN1 protein, and the three proteins with experimentally-determined high-resolution structures are shown in bold within the black box. Essential for formation of a V-shaped dimer are a coordinating Cys residues and an anion- π interaction pair. In TbMORN1, the coordinating Cys residue has been substituted for Leu (Leu 301). Similarly the Phe and Glu residues of the anion- π interaction pair (indicated with black arrows) have been substituted for Leu (Leu299) and are not present (deletion after Pro302) respectively. This supports the conclusion that TbMORN1 exists only in the extended form, while the apicomplexan proteins and those from related clades are probably capable of adopting both extended and V-shaped conformations.

Table 1. X-ray data collection statistics

	PfMORN (SMet)	PfMORN	TbMORN	TbMORN	TgMORN	TgMORN (V-shape)
Source	ID29	ID29	ESRF ID23-1	ESRF ID23-1	ESRF ID30B	ESRF ID30B
Wavelength (Å)	0.979	0.976	0.979	1.89	0.967	1.0
Resolution (Å)	47.47-2.5 (2.59-2.5)	46.3-2.14 (2.2-2.14)	48.28-2.35 (2.43-2.35)	48.14-2.53 (2.65-2.53)	48.92-2.90 (3.08-2.90)	49.45-2.50 (2.60-2.50)
Space group	<i>C222₁</i>	<i>C222₁</i>	<i>P2₁</i>	<i>C2</i>	<i>P4₃2₁2</i>	<i>P6₂22</i>
Unit cell (Å, °)	a=57.33, b=79.18, c=94.42	a=57.33, b=79.18, c=94.42	a=69.04, b=27.63, c=114.54; β=101.83	a=192.88, b=49.74, c=41.98	a=b=53.92, c=348.85	a=b=205.86, c=40.58
Molecules (a.u.)	1	1	2	2	2	1
Unique reflections	7832(762)	12148 (974)	17460 (1247)	12419(975)	12331 (1819)	18162 (1960)
Completeness (%)	99.5(98.3)	99.6(98.1)	95.4 (71.5)	93.1(60.0)	99.1 (95.4)	99.7 (97.9)
R_{merge}^b	0.059(0.301)	0.037 (1.283)	0.092 (0.466)	0.116 (1.365)	0.140 (2.252)	0.198 (2.116)
R_{meas}^c	0.062(0.314)	0.042 (1.510)	0.100 (0.532)	0.146 (1.893)	0.158 (2.536)	0.204 (2.177)
CC(1/2)	0.999(0.983)	1.000 (0.467)	0.998 (0.897)	0.995 (0.303)	0.999 (0.772)	0.999 (0.426)
Multiplicity	13.0 (12.9)	4.2 (3.2)	6.1 (4.1)	6.2 (3.7)	8.4 (8.0)	17.9 (18.1)
$I/\sigma(I)$	30.3 (8.1)	17.5 (0.8)	13.4 (2.8)	9.3 (0.9)	11.8 (0.5)	14.6 (1.6)
B_{Wilson} (Å ²)	57.3	58.0	18.74	36.7	22.97	42.3
$R_{\text{work}}^e/R_{\text{free}}^f$		23.0/26.4	23.2/25.6	22.5/28.2	31.8/33.8	20.1/23.9
r.m.s.d. bonds (Å)		0.003	0.004	0.011	0.0084	0.007
r.m.s.d. angles (°)		0.6	1.24	1.612	1.417	0.811

^a Values in parentheses are for the highest resolution shell.

$${}^b R_{merge} = \frac{\sum_{hkl} \sum_{i=1}^N |I_{i(hkl)} - \bar{I}_{(hkl)}|}{\sum_{hkl} \sum_{i=1}^N I_{i(hkl)}}$$

$${}^c R_{meas} = \frac{\sum_{hkl} \sqrt{N/(N-1)} \sum_{i=1}^N |I_{i(hkl)} - \bar{I}_{(hkl)}|}{\sum_{hkl} \sum_{i=1}^N I_{i(hkl)}}$$

where $\bar{I}_{(hkl)}$ is the mean intensity of multiple $I_{i(hkl)}$ observations of the symmetry-related reflections, N is the redundancy

$${}^e R_{work} = \frac{\sum ||F_{obs}| - |F_{calc}||}{\sum |F_{obs}|}$$

${}^f R_{free}$ is the cross-validation R_{factor} computed for the test set of reflections (5%) which are omitted in the refinement process.

Intermolecular cross-links in TbMORN1

chemical cross-linking agent	cross-linked amino acids and respective MORN repeats	best e-value	number of PSMs in the dimer
BS ³ (spacer arm length 11.4 Å)	aa 100 x aa 123 (repeat 5 x repeat 6)	7.5×10^{-13}	4
	aa 223 x aa 246 (repeat 10 x repeat 11)	5.7×10^{-22}	7
	aa 296 x aa 321 (repeat 13 x repeat 14)	1.8×10^{-11}	56
	aa 321 x aa 321 (repeat 14 x repeat 14)	6.4×10^{-5}	1
EDC (spacer arm length 0 Å)	aa 308 x aa 321 (repeat 14 x repeat 14)	1.1×10^{-8}	5
	aa 321 x aa 326 (repeat 14 x repeat 15)	1.9×10^{-9}	3

Table S1. Intermolecular contacts in TbMORN1. A summary of intermolecular cross-links in the TbMORN1 dimer as a result of chemical cross-linking with either BS³ or EDC followed by mass spectrometry analysis. To remove low quality peptide-spectrum matches (PSMs), an additional e-Value cutoff of < 0.001 was applied. In order to distinguish intra- from inter-molecular chemical cross-links, results from monomers and dimers were compared. Cross-links were scored as intermolecular when there were: (1) minimally 3 peptide PSMs in dimer and (2) minimally 3-times more PSMs in dimer than in monomer. Results compiled from two independent experiments.

<u>Thermostability</u>	
TbMORN1 construct	T _m (°C) (DSF)
2-15	44.2 ± 0.3
2-15 ^{Mut13}	43.8 ± 0.3
2-15 ^{Mut14}	41.4 ± 0.5
2-15 ^{Mut13+14}	41.7 ± 0.3

Table S2: Analysis of TbMORN1(2-15) mutagenesis constructs. Thermostability of TbMORN1(2-15) and its mutagenised derivatives with mutations in MORN repeats 13 and 14 was measured by differential scanning fluorimetry (DSF), given here as melting temperature (T_m) values (°C).

Data collection parameters				
Radiation source	Petra III (DESY, Hamburg, Germany)		ESRF (Grenoble, France)	
Beamline	EMBL P12		BM29	
Detector	Pilatus 2M		Pilatus 1M	
Beam geometry (mm, FWHM)	0.12 x 0.20		0.10 x 0.20	
Wavelength (nm)	0.12		0.099	
Sample-detector distance (m)	3.1		2.867	
Momentum transfer s range (nm ⁻¹)	0.01 – 4.0		0.04 – 5.0	
Exposure time (s)	1 sec (SEC-SAXS mode) 0.05 sec (Batch mode)		1 sec (SEC-SAXS mode)	
Overall Parameters				
	TbMORN1 (7-15)	TgMORN1 (7-15)	PfMORN1 (7-15)	TbMORN1 (2-15)
Buffer	Buffer 1*	Buffer 2**	Buffer 2**	Buffer 2**
Temperature (°C)	20	20	10	20
Working concentration (mg/ml)	n.a.	n.a.	1	n.a.
Concentration range measured			1-8	
R _g from Guinier approximation (nm)	4.1±0.04	4.0±0.03	3.8±0.1	6.5±0.6
R _g from PDDF (nm)	4.4±0.02	4.3±0.04	4.2±0.03	7.2±0.05
D _{max} (nm)	155	17.0	16.0	260
Molecular weight, I(0) (kDa)	n.a.	n.a.	52 ±5	n.a.
Molecular weight, offline RALS (kDa)	46±5	50±5	32±5	74±5
Molecular weight from DATMOV, (kDa)	60±5	58±5	46±5	71±5
Molecular weight from sequence (dimer, kDa)	52	49	46	70
Software employed				
Primary data reduction	SASFLOW		ESRF EDNA pipeline	
Data processing	PRIMUS/Chromixs			
Calculation of theoretical data	Crysol			
<i>Ab initio</i> modelling	DAMMIN		DAMMIF	
SASBDB accession code	SASDGA7	SASDGB7	SASDGC7	SASDG97

Buffer 1* 20 mM Tris, 200 mM NaCl, 2% glycerol, 0.5 mM DTT

Buffer 2** 20 mM Tris-HCl pH 7.5, 100 mM NaCl

Table S3. SAXS data collection summary.